Small-Angle X-ray Scattering of Polymers

Benjamin Chu* and Benjamin S. Hsiao

Department of Chemistry, State University of New York at Stony Brook, Stony Brook, New York 11794-3400

Received October 16, 2000

Contents

I. Introduction

A. Aim and Scope

This review will cover small-angle X-ray scattering of polymers, especially with the use of synchrotron radiation. By nature, small-angle X-ray scattering (SAXS) probes relatively large-scale structures, in contrast to wide-angle X-ray diffraction (WAXD) that deals mainly with the atomic structure of crystals. SAXS includes not only the diffraction of large lattice spacing, of the order of tens, hundreds, or even thousands of interatomic distances, but also the scattering by perturbed or nonperiodic structures of amorphous and mesormorphic materials. While the fundamental relation describing WAXD remains to be the Bragg equation, $n\lambda = 2d \sin(\theta/2)$ [with θ being the scattering angle (we note that θ is used in this review instead of 2θ in order to be consistent with light scattering); λ is the X-ray wavelength; and d is the lattice spacing], the scattering (or diffraction) of semicrystalline or amorphous materials is often described in terms of electron density at point $\boldsymbol{x}$, $\rho(\boldsymbol{x})$, in reciprocal or Fourier space. Polymer chains can form semicrystalline, mesormorphic, or amorphous structures. Therefore, a proper structure and morphology analysis of many polymers requires information using a combination of SAXS and WAXD, even though the WAXD measurements can appear in the normal SAXS q range because of larger lattice spacing. Here, q [$=(4\pi/\lambda)\sin(\theta/2)$] is the magnitude of the scattering wave vector.

Polymers are molecules made up of many monomer segments. If all the monomer segments are of the same type, these are homopolymers. If the segments are made up of two (or more) monomer types, these are copolymers. Copolymers can have star, random, graft, block, and branched architectures. Polymers can also be neutral or charged macromolecules, such as biopolymers. In fact, a vast number of SAXS experiments were reported on biological macromolecules in solution, before synchrotron facilities had become available. However, as time-resolved protein folding and protein dynamics are covered

10.1021/cr9900376 CCC: $36.00
Published on Web 05/19/2001

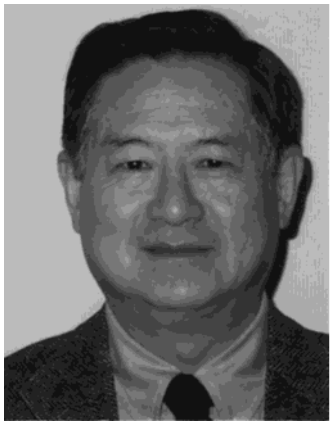

Benjamin Chu obtained his B.S. degree, magna cum laude, from St. Norbert College and his Ph.D. degree in Physical Chemistry from Cornell University. He was a postdoctoral student with the late Professor Peter J. W. Debye for four years before he started his academic career at the University of Kansas. In 1968, he moved to the State University of New York at Stony Brook, where he is now a Distinguished Professor.

Benjamin Hsiao obtained his B.S. degree from National Taiwan University and his Ph.D. degree from the University of Connecticut. He was a Postdoctoral Fellow with Professors Richard S. Stein and H. Henning Winter at the University of Massachusetts, Amherst, from 1987 to 1989. He was a Staff Scientist and then a Senior Scientist with DuPont Fibers and DuPont Central Research & Development, respectively, from 1989 to 1997. He was also an Adjunct Associate Professor, Materials Science, University of Delaware, from 1994 to 1997. In 1997 he moved to the State University of New York at Stony Brook, where he is currently an Associate Professor in the Chemistry Department.

elsewhere in this special issue, the review on the biological systems will be cursory in nature, emphasizing mainly on the similarity between the often complex biopolymers and the simpler synthetic polymers. Russell[1] reviewed the topic of synchrotron SAXS studies for polymers with extensive theories and references. The present review will emphasize experiments performed after his review. Some fundamental equations are, nevertheless, introduced for the convenience of the reader.

In this review, we have intentionally missed two exciting recent developments related to the technique of synchrotron SAXS. One is the microfocus synchrotron SAXS technique, and the other is the coherent scattering or photon correlation studies using high-intensity SAXS (for example, Sector 8 at the APS will be devoted for this purpose) to investigate dynamic processes in polymers. Each of these subjects is under rapid development, which may deserve an independent review later. The scope of this article is mainly intended to cover the more "conventional" applications of synchrotron SAXS.

B. Short History

Wilhelm Conrad Röntgen received the first Nobel Prize in Physics for discovering X-rays. P. Krishnamurti reported the first SAXS observations on amorphous materials including colloidal solutions and liquid mixtures in the late 1920s.[2] In the next 40 years or so it was not a trivial task to make SAXS measurements using conventional X-ray sources, especially on polymer solutions. The primary difficulty is associated with the fact that the scattering measurements have to be done so very close to the incident X-ray beam. For example, with Cu Kα radiation of 0.154 nm and a spacing d of 10 nm, the scattering angle is 0.88° (or a Bragg angle of 0.44°). With a period of 100 nm, $\theta = 0.088°$. These days, we deal with hierarchical structures, often having length scales in the micrometer-size range. With $d = 1000$ nm, $\theta = 0.0088°$ (or 32 s). At $\theta = 32$ s or 0.16 mrad, corresponding to making a scattering measurement 16 mm away from the incident beam with a sample located 100 m away from the detector. This would be a difficult task by any measure. Thus, the key point in any SAXS experimental setup is to try to reduce the background or stray X-rays at small scattering angles (so-called the minimization of parasitic scattering).

Over the years, there have been several designs on X-ray collimation systems. These are the four pinhole (or slit) system, the Kratky collimation system, and for very small scattering angles the use of Bonse−Hart channel-cut crystals. We shall refer to their designs for later discussions. It is suffice to mention that the descriptions and the original references have been presented in several excellent monographs.[3−7]

With synchrotron X-rays, the high power density and small beam divergence of the incident X-ray beam permit design of time-resolved SAXS/WAXD experiments[8] and the use of very small specimens. Furthermore, the tunability of X-ray wavelength over a range near the K or L edge of an element has made anomalous SAXS/WAXD a feasible approach for structure and morphology investigations of a specific element in the presence of other elements.[9] With more complex systems, SAXS/WAXD experiments are often coupled with other physical techniques, such as laser light scattering, Raman spectroscopy, thermal analysis, Fourier transform infrared spectroscopy, and different forms of rheological techniques. One may also perturb the system by suddenly changing the thermodynamic parameters, such as temperature jump, pressure jump, or rapid mixing of materials using the stop-flow approach or a mixing cell. The coupling of additional variables could help in the interpretation of SAXS/WAXD results of more complex polymer systems.

C. Light, X-rays, and Neutrons

The principles of scattering by light, X-rays, and neutrons are the same, being related to the interactions of radiation with matter. For X-rays and light,

Table 1. Advantages of Synchrotron X-rays (from a bending magnet source) for SAXS and WAXD

advantages	applications
1. high intensity small specimen better counting statistics	time-resolved experiments
2. small beam divergence small beam cross sections (vertical 0.14 ~mrad, horizontal 5−10 mrad)	time-resolved experiments
3. well-defined energy	
4. tunability of wavelength atom selectivity	anomalous SAXS and WAXD
5. pulsed source $\sim 10^7$/s, each ns wide	
6. polarization of beam	

the electromagnetic radiation differs in the wavelength, with visible light in the 350−700 nm range and X-rays varying from ca. 0.01 to ca. 0.2 nm. There is no intrinsic limitation over the wavelength in the electromagnetic spectrum from very short wavelength X-rays (in the γ-ray region) to the infrared region, except for the range between long-wavelength X-rays of about 3 nm and the vacuum ultraviolet region where the radiation is intensely absorbed by all materials and therefore rendering the scattering by such probing radiation difficult to deal with. For neutrons, the wavelength is on the order of 0.2−1.0 nm, but neutrons obey the de Broglie relation with $\lambda = h/p$, h and p being Planck's constant and the momentum, respectively. Due to the fact that the scattering by light, X-rays, and neutrons depends, respectively, on the differences in the refractive index (or dielectric constant), the electron density, and the scattering length (a nuclear property), the data treatment can be different because of the intrinsic property of each radiation and its specific interactions with matter are different. Nevertheless, we shall remember the similarity and the difference in dealing with three different but complementary types of radiation. Recently, we reviewed this subject elsewhere,[9] and the interested readers are encouraged to read this review.

II. X-ray Instrumentation

A. Conventional versus Synchrotron X-ray Sources

With conventional X-ray sources, the beam divergence and the limit of using essentially one wavelength (often in the form of a copper or molybdenum target) for each setting have practically made SAXS experiments a relatively difficult technique to undertake. These restrictions, however, have been removed with the advance of synchrotron X-rays, rejuvenating SAXS as a very useful technique for applications in biology, chemistry, physics, materials science, and engineering. Furthermore, it should not be overlooked that advances in the X-ray linear position-sensitive detectors and X-ray area detectors, together with multilayer monochromators that can also act as focusing mirrors, have made SAXS a viable technique even with conventional X-ray sources. Polymer chains seldom form single crystals. In the amorphous or semicrystalline state, the multilayer monochromator can provide adequate energy resolution on the order of 0.1−1% and can increase the power density of the incident X-ray beam by a factor of 10−100, when compared with conventional crystal monochromators that have energy resolutions often better than 0.01%, though mostly not essential for SAXS of polymers.

A summary on the advantages of synchrotron X-rays (from a bending magnet source) is listed in Table 1. It is suffice to state that the small beam divergence and the high brilliance of synchrotron X-rays permit experiments with small sample specimens as well as time-resolved and anomalous SAXS measurements, resulting in a much-expanded view on synchrotron SAXS applications. Aside from the informative and excellent review by Russell,[1] reviews on selected topics related to SAXS have appeared.[9−16] The advantages of using synchrotron X-rays from an insertion device, such as an undulator or a wiggler, perhaps are more than those from a bending magnet source. For example, the X-ray brilliance (a measure of the number of photons per second per solid angle per source area per unit bandwidth) from an undulator source can be several orders of magnitude higher than that from a bending magnet source. The characteristics of the X-rays from an undulator or a wiggler can be found in the *Handbook of Synchrotron Radiation* as listed in ref 1.

B. Synchrotron SAXS Beamlines

Koch[10] reviewed the state of the art for synchrotron SAXS in 1988. Bras and Ryan[8] subsequently listed the synchrotron SAXS beamlines up to 1996, including three in Daresbury, two at the Photon Factory, three at APS, one at SPring 8, one at SSRL, four at ESRF, four in Hamburg, two in Lure, one at NSLS, and one at ELECTRA, for a total of 20 synchrotron SAXS beamlines. Their Table 1[8] also listed the source of information for these beamlines. To our knowledge, NSLS has at least two more SAXS beamlines and China, Korea, and Taiwan have one each. Thus, the total number of synchrotron beamlines capable of SAXS experiments is increasing. Recently, DESY (Hamburg) is planning an X-ray-free electron laser (FEL) facility that can generate X-ray intensity even several orders of magnitude higher than the undulator beamlines. A dedicated SAXS station in this FEL facility, to our knowledge, is being planned.

The natural divergence of the X-ray beam generated from a synchrotron source (bending magnet, wiggler, or undulator) can be considered as the lowest natural limit for angular resolution of the instru-

ment. Thus, without touching the beam, one may expect the highest spatial resolution that can be obtained based on the incident beam divergence alone. This is, of course, not practical as most beamlines involve a long source-to-detector distance (in the range of tens of meters). As the detector dimension is limited, the beam size has to be reduced. The process of the beam reduction, inevitably, will produce parasitic scattering. In section II.B, we will briefly describe several means to minimize such undesired stray scattering. Riekel et al. recently demonstrated the SAXS capability from a microfocus beamline at ESRF (ID13).[17−20] The smallest achievable beam size is about 1 μm. This is a great accomplishment which can be attributed to the excellent arrangement of the collimation and focusing components. It is worth mentioning here that the smaller beam size is often balanced by a larger beam divergence in order to retain sufficient intensity.

Most synchrotron SAXS beamlines tend to use the slit collimation system for ease of operation in changing the beam dimensions because all the slit movements have to be operated by remote control. The more stringent requirement involves moving the slits inside the vacuum path because the number of windows should be reduced to a minimum in order to minimize the amount of parasitic scattering. This is a constant battle in instrumentation design for synchrotron SAXS experiments. It is noted that the high power density of the incident X-ray beam will be completely wasted if the parasitic background scattering were to increase proportionately. For the ease in alignment and its ability to change the incident beam dimensions, the slit collimation system and the corresponding complementary collimation systems are presented. The purpose of the presentation on the collimation systems is for the reader to have some idea on how a SAXS instrument is designed and constructed. It is by no means meant to be exhaustive, and only selected references are used.

C. Collimation Systems

1. Pinhole Collimator

The synchrotron radiation source in combination with a focusing mirror offers only directional collimation. In contrast, the pinhole (or slit) collimation system offers symmetric beam cross-section and has the ability to investigate anisotropic scattering patterns.[21] The pinhole (or slit) collimation system also makes the desmearing effect less serious. Over the years, the pinhole geometry has been discussed extensively.[4,22−38] It is important to note that many designs of the slit system use the geometry shown schematically in Figure 1 (reproduced from ref 4). The optical elements denote a double-crystal monochromator and a focusing mirror. A set of beam-defining slits is used to limit the incident beam cross-section and to take out unwanted background. The scatter slits, as shown in Figure 1, are used to follow the incident beam profile and to act as guard slits, especially for the set near the sample. It is important to note that although the cone produced by parasitic

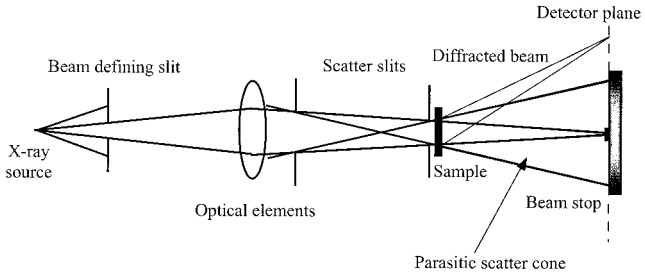

Figure 1. Schematic diagram of a slit collimation system for focused synchrotron X-rays. (Reprinted with permission from ref 4. Copyright 1982 Academic Press.)

scattering is governed by the two sets of scatter slits, fluctuations caused by the positions of the X-ray source, the beam defining slits, and the optical elements would increase the amount of parasitic scattering, especially for the slit set near the sample. Consequently, depending on the stability of all the components before the scatter slits, the beam stop has to be made larger and the expected parasitic scattering contribution should be higher than one would normally expect from theoretical computations alone.

The slit collimation system also suffers from having too many adjustable parameters. Each blade, in principle, should have a translational stage and three angular adjustments in order to locate the desired edge at the proper position. As shown in Figure 1, the two sets of scatter slits have four blades, requiring a total of 32 adjustments. Clearly, such an arrangement would make proper alignment a difficult practical task. Thus, many requirements of the slit alignment have to be designed into the system during construction. Nevertheless, it would remain a formidable task for a slit collimation system to reach the design limit in terms of parasitic scattering.

The quality of the blade can also influence the effectiveness of the collimation. The blade should be made of materials with heavy atomic number (good X-ray absorber), low fluorescent scattering background, and machinability, such as tantalum and tungsten (lead is too soft to be machined). In principle, any materials placed in the X-ray beam will always cause scattering (sometimes diffraction) and/or reflection, which then lead to unwanted parasitic background. The problem of scattering can be minimized by increasing the homogeneity of the blade material, and the problem of reflection can be eliminated by using a tilted smooth surface.

On the basis of the same principle as slit collimation, a pinhole collimation system immediately reduces the number of adjustable parameters required to align such a collimator. If one were to have the tapered pinholes (the smaller opening always faces the incident beam to minimize the reflection) aligned perpendicular to the propagation axis of the incident beam, only four translational stages to move the two pinholes in line with the incident X-ray beam are required. To avoid uncertainties due to fluctuations in the position of the X-ray source, the defining slits, and the optical elements, a third guard pinhole is added to the pinhole collimation system.[21] With three pinholes, the collimation system is self-sufficient and

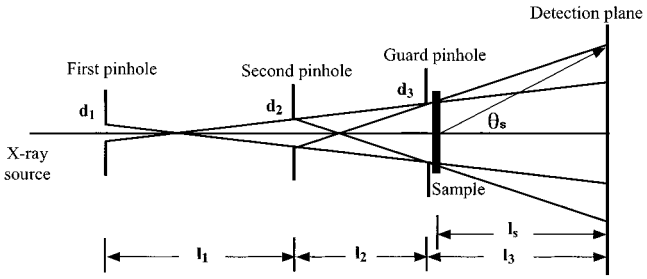

Figure 2. Schematic diagram of a pinhole collimation geometry. (Reprinted with permission from ref 21. Copyright 1994.)

should be relatively independent of the fluctuations discussed above.

Figure 2 shows a schematic diagram with three-pinhole collimation geometry.[21] The first and second pinholes define the incident beam. The third guard pinhole blocks the parasitic scattering due to the edge scattering from the *second* pinhole. It is noted that due to the intrinsic divergence of the synchrotron beam, the incident flux is mainly controlled by the size of the first pinhole. To achieve a high angular resolution and low parasitic scattering, the guard pinhole must be designed and placed in such a way that it is close to but does not touch the incident beam.

The smallest angle one could reach without a serious parasitic scattering problem, θ_s, can be described by the relation

$$\theta_s = \frac{d_2 + d_3}{2l_2} + \frac{d_3}{2l_3} + \frac{d_s}{2l_3} \qquad (1)$$

where d_s denotes a finite size for the detector element and d_3 [$=(d_1 + d_2)l_2/l_1 + d_2$] depends on l_1, l_2, d_1, and d_2. There is always a compromise between the incident intensity and the angular resolution. Here we refer the incident intensity as the total flux of X-rays reaching the sample. Clearly the total flux depends not only on the angular divergence of the incident beam, but also on its beam cross section. In the third-generation synchrotron X-ray sources, it is the brilliance that has an edge over this concern. The design of the pinhole collimation system depends also on the space limitation, especially in the length of the instrumentation setup. For example, for the X3A2 beamline at NSLS, we chose $l_1 = l_2 = 609$ mm (so that the total length was sufficiently short for easy transportation of the entire collimator between Stony Brook and NSLS by car) and $d_1 = d_2 = 0.3$ mm. Therefore, d_3 should be slightly larger than 0.9 mm. We used $l_s \approx l_3 = 1030$ mm and $d_3 = 1.0$ mm with the extra 0.1 mm as a compromise in alignment uncertainty and edge asymmetry. Theoretically, such a pinhole collimation geometry should yield a θ_s of 1.62 mrad for a CCD-based detector with $d_s = 0.135$ mm and a θ_s of 1.58 mrad for a Braun detector with $d_s = 0.046$ mm. It should be noted that the differences between Figures 1 and 2 are as follows. (1) Figure 1 has a focused X-ray beam, while Figure 2 does not. Thus, for a synchrotron X-ray beam with very small beam divergence, the choice of scatter slits (Figure 1) or of d_1 and d_2 depends on the incident beam

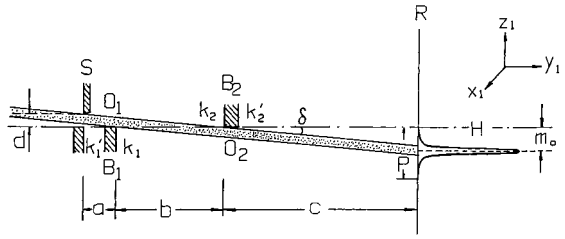

Figure 3. Section along the *y* direction of the synchrotron beam perpendicular to the *x*,*z* plane. Vertical z_1 scale is multifold stretched compared to the horizontal y_1 axis. Variable entrance slit S and blocks B_1 (middle block) and B_2 (bridge) are perpendicular to the x_1,z_1 plane. In the plane of registration R, the primary beam does not have a triangular (vertical) beam profile. A Gossip-shaped intensity beam profile is presented schematically to emphasize that the synchrotron radiation (as denoted by the dotted area) is highly collimated. M_0 is the distance from the maximum intensity to the plane H. The Gossip-shaped beam has fairly symmetrical long tails, mainly due to scattering by the edges k_1 and k_2. O_1 and O_2 represent the top surface of block B_1 and the bottom surface of block B_2, respectively. The small-angle X-ray diffractometer (SAXD) dimensions are $a = 16.7$ mm, $b = 402.0$ mm, c is variable from ~0.2 to 1.5 m. The subscript 1 denotes the coordinate system x_1,y_1,z_1 for the SAXD, where *x*,*y*,*z* denotes the coordinate system for the synchrotron primary beam. We want $x||x_1$, $z||z_1$, and the tilt y_1 with angle δ between *y* and y_1 using *x* as the rotation axis. (Reprinted with permission from ref 39. Copyright 1987.)

profile. (2) Figure 1 has two sets of scatter slits, while Figure 2 has a guard pinhole, in addition to the two defining pinholes. The guard pinhole is clearly redundant if the X-ray source position remains fixed. Unfortunately, in practice, fluctuations of the X-ray source position should be taken into account. Thus, the use of an additional guard pinhole is highly recommended.

2. Kratky Block Collimator[39]

Among the collimation systems proposed to achieve low parasitic scattering in SAXS, the concept of a block-collimation system, as first proposed by Kratky,[40,41] has stood the test of time because of its simplicity in construction and ease of operation. A more detailed description of the Kratky camera, including the compact camera, has been reported.[42,43] Another advantage of the Kratky block collimator, as shown in Figure 3, is that there is no guard slit required. In comparison with Figure 2, the Kratky block-collimation system can be made shorter than a comparable pinhole collimation system by a factor corresponding to that of l_2. It also differs from the slit collimation system of Figure 1 because the incident X-ray beam is defined by the Kratky collimator, where small fluctuations of the X-ray source provide very little contribution to the parasitic scattering. Furthermore, the Kratky block collimator is best with a slit geometry that coincides with the unequal divergence of the synchrotron X-ray beam. Consequently, a larger total flux from the use of a longer slit length can be accommodated. However, for the same reason, it is not usually used for experiments with anisotropic samples where the scattering from $x-z$ directions is different.

3. Bonse–Hart Channel-Cut Crystals Optics[44−46]

In a small-angle X-ray scattering experiment, the larger the inhomogeneity size in a system, the longer the X-ray wavelength or the smaller the scattering angle, i.e., the smaller the q value, is needed in order to determine the structures. A Kratky block-collimation system could usually reach a q value of about 0.04 nm^{-1}. This q value corresponds to an X-ray wavelength λ of 0.154 nm and a scattering angle of about 1 mrad. On the other hand, routine laser light scattering can cover a q range from 0.004 to 0.036 nm^{-1}. With a specially designed instrument, e.g., by using a prism cell,[47] the smallest accessible q value could be on the order of 0.0008 nm^{-1}. With synchrotron X-rays from an insertion device (such as a wiggler or an undulator), the intrinsic beam divergence is very small. Thus, by using long distances between the scatter slits (Figure 1) or the defining pinholes (Figure 2), it is expected that θ_s down to tens of μrad should be readily accessible. The use of Bonse−Hart X-ray optics is reserved only for special occasions since the scattered intensity at each scattering angle has to be measured separately. It can be used with conventional X-ray sources, and a high-flux/high-temperature setup has been reported.[48] No parallel methods for simultaneous measurements of the scattered intensity at many scattering angles have yet been devised.

In the 1940s, Fankuchen and Jellinek[49] and others[50−52] proposed to use one crystal to monochromatize the X-ray beam and another one as an analyzer for a SAXS instrument. However, the angular resolution was not sufficiently good if one were to reflect the X-rays only once in each of the crystals. In 1966, Bonse and Hart[53,54] increased the number of reflections in each of the crystals with a corresponding dramatic increase in the angular resolution.

There have been considerable interests in further development of the Bonse−Hart instrument,[55−68] particularly in synchrotron X-ray facilities, because of its potential applications to many current topics in materials research with length scales in the mesoscopic micrometer-size range. It should also be noted that many materials studies deal with high temperatures and involve temperature scanning, jumping, quenching, and annealing experiments. By using Super Invar as the basic building material for the posts, supports, and the microscrews, the thermal expansion effect could be minimized.[45] As the Bonse−Hart optics directly measure the small angles near the incident beam, the measurement device needs to be kept extremely stable over a range of temperatures.

Figure 4 shows a schematic diagram of the instrument setup[46] used in the X3A2 beamline at the NSLS. Two silicon crystals with channel cuts along the (111) reflection plane were used. The same crystals could accept an X-ray beam at different X-ray wavelengths, such as $\lambda = 0.06573$ or 0.154 nm. Each crystal had rocking, tilting, and translational adjustments. The microscrews were located 4.875 in. apart and had a resolution of 250 μm per revolution. The actuator (Klinger BM25-PP) had a resolution of 0.15

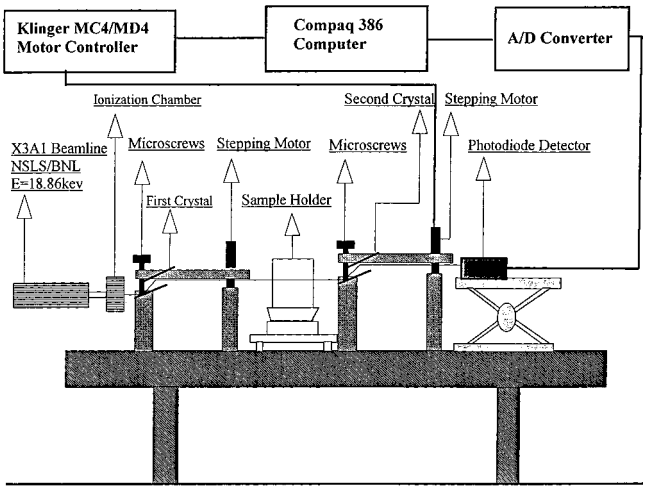

Figure 4. Schematic diagram of the high-energy Bonse−Hart instrument designed for synchrotron scattering experiments. (Reprinted with permission from ref 46. Copyright 1994.)

μm per step. With a distance of 3.75 in. from the pivot in the first crystal and 4.75 in. from the pivot in the second crystal, the angular resolutions were about 0.33 arc s for the first crystal and about 0.26 arc s for the second crystal. Due to the high penetration power of the shorter X-ray wavelength, higher order harmonic wavelengths from the synchrotron X-rays made attenuation of the incident X-ray more difficult. The distortion in the SAXS profile produced by higher harmonics should be considered.

4. USAXS

There are several dedicated ultra-small-angle X-ray scattering (USAXS) synchrotron facilities around the world, such as the X20 beamline (bending magnet) at NSLS, the 33-ID-D beamline (the undulator beamline at UNI−CAT) at APS, and the BW4 beamline in Hasylab, DESY. These facilities generally offer a very low angular resolution power and can easily characterize mesoscopic structures with dimensions up to about 1 μm. The typical optics of these facilities involve the combination of pinhole collimation, double- focusing mirrors, double-crystal monochromator, and/or channel-cut crystals to achieve the very low angular resolution. For example, the BW-4 USAXS beamline in the Hasylab uses pinhole collimation, double-focusing mirrors, and a double-crystal monochromator at a 38-pole wiggler line (see Figure 5). The sample to detector distance can be selected in the range from 4 to 16 m. At the short distance, the scattering angles from 1.24 to 50 mrad can be observed. At 16 m distance, scattering angles from 0.12 to 10 mrad can be achieved.

With the recent advance in the insertion device (ID), especially the undulator device, very low beam divergences can be obtained (e.g., the vertical divergence can be about 10 μrad, and the horizontal divergence can be about 25 μrad at a typical ID line in APS). Thus, in principle, any ID beamline in the third-generation synchrotron facility should have the resolution power to reach very low angles. However, as pointed out earlier, the beam needs to be reduced in size and monochromatized in wavelength, with the

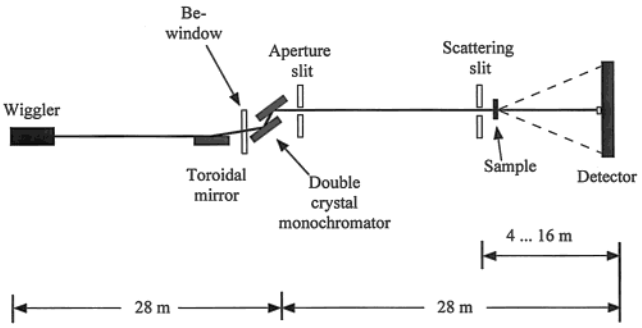

Figure 5. Schematic diagram of the USAXS beamline (BW4) in the Hasylab, DESY. (Diagram reproduced from the beamline description of BW4 at Hasylab, DESY.)

required optical components needed to be used in the downstream of the ID in order to specify the incident beam. A careless design of an individual optical component can significantly increase the parasitic scattering of the beam downward and destroy the low angular region of the beamline.

D. Detection Systems

With the high brilliance of synchrotron X-rays, the development of detector technology is still lagging behind. It is evident that close to 10 years after the review by Russell,[1] X-ray detectors for short-time time-resolved measurements have not yet met the many requirements demanded for fast point counters, linear position-sensitive detectors, and CCD area detectors.

Each detector has its own strengths and weaknesses. The selection depends on the particular application and the specifications of the detector as well as the X-ray wavelength. Generally, it is essential to consider the quantum efficiency, spatial resolution, temporal resolution, energy resolution, linearity, dynamic range, uniformity of response, count-rate limitations, and background noise of a detector at a specific X-ray wavelength in order to properly match the detector for a specific application. Russell[1] reviewed the gas-filled detectors, photodiode arrays, charged-coupled devices (CCDs), electro-optical devices, and channel electron multipliers. In this review, only a very brief discussion is presented, with emphasis on more recent advances.

1. Point Detectors

There are a variety of point detectors available for use in SAXS/WAXD experiments ranging from single-channel proportional counters, scintillation counters, to photodiode detectors. While the technology for proportional counters and scintillation counters has remained essentially unchanged, the more interesting development deals with the use of photodiode detectors[68,69] as an X-ray photon counter and, at high-count rates, as an analogue device to measure the photocurrent that is proportional to the X-ray intensity.[69]

For X-ray photon counting and correlation, the photodiode should be cooled to low temperatures (normally about −10 °C) in order to reduce thermal noise. The output signal could be amplified, discriminated, and counted by a scalar/timer or correlated by a digital correlator. At $\lambda = 0.0643$ nm, the dark count was negligible after discrimination.[68] A cooled photodiode with energy-dispersive capability together with photon counting in the ac mode by means of multichannel analysis and with current measurements in the dc mode is available commercially.[68] Such a cooled photodiode detector with a Be window and thermal isolation can reduce the dark current (count) by a factor of about 100, thus making weaker signal measurements feasible. The large dynamic range of the photodiode detector makes it suitable as a convenient point detector for X-rays. Nevertheless, for low count-rate experiments, the proportional and scintillation counters remain the appropriate detectors, especially when one wants to achieve a predetermined signal-to-noise ratio over a range of q where the intensity is a strong function of q. The recent development of a new kind of silicon drift detector demonstrates that very high count-rate performance (1 000 000 cps maximum input count rate, 400 000 cps output count rate) can be achieved by the point detector system.

2. Linear Position-Sensitive Detectors[70]

The use of linear position-sensitive detectors (LPSDs) increases the efficiency of SAXS/WAXD experiments drastically and makes time-resolved measurements feasible. Russell[1] reviewed the position-sensitive proportional counters. In particular, the Gabriel-type detectors[72−75] are very suitable for recording SAXS of extremely weak scatterers such as dilute polymer solutions. The general principle of this detector is simple. A proportional detector consists essentially of a cell with detecting gas (Ar/CO_2 or Xe/CO_2) and a thin (10 μm) central metal wire (Au-coated Cu wire). A high voltage is applied between the wire and the body of the detector. When an ionization event occurs in the gas, photoelectrons that are produced by the ionization are accelerated in the wire. In the vicinity of the wire, a Townsend avalanche occurs and provides a large amplification. A preamplifier picks up this electric signal, which is correlated with the energy of the incident event (intensity) and the position of the avalanche. Unfortunately, wire/gas detectors, which are quantum limited, have relatively low maximum count rates ($\leq 10^6$ X-ray photons per second), and further incremental improvements in wire/gas detectors are difficult to achieve. For many strong scatterers such as crystalline polymers, one often has to attenuate the incident synchrotron X-ray beam in order to protect the detector and thereby defeats one of the unique advantages of synchrotron X-rays.

Two types of photodiode array (PDA) detectors have been used with some success: (1) directly exposed X-ray PDAs[71−77] and (2) phosphor scintillators coupled to PDAs to convert X-ray photons to visible photons.[78] The first type has a higher gain than the second one[71] but has a narrower detectable X-ray energy range (2−20 keV) and suffers radiation damage resulting in a permanent rise in dark count noise and a decrease in sensitivity. Thus, its use has not been very popular. The second approach is quite feasible. For time-resolved studies, it is important to

select an appropriate phosphor with sufficiently short lifetimes, not only for the conversion of X-ray photons to visible photons, but also for the conversion again to visible photons inside the intensifier via fiber optics for acceptance by the photodiode array. The PDA-LPSDs have good spatial resolution, excellent linearity of response to the X-ray intensity, and stable pixel uniformity. All the instrument parameters can be calibrated, and the PDA-LPSDs are relatively low cost, when compared with CCD X-ray area detectors, and can be used for fairly fast (≤tens of ms per frame) time-resolved SAXS/WAXD experiments of symmetric systems or anisotropic systems that have been spatially averaged over all orientations. One drawback has been that the PDA-LPSDs have a limited spatial range, e.g., normally an effective length of only 25 mm for a photodiode array of about 1000 pixels is used.[69] Furthermore, its dynamic range is often limited.

3. Area Detectors

For weak signals, the Gabriel-type 2-dimensional multiwire proportional chamber (2D MWPC) area detectors generally have a low dark count rate that cannot be surpassed and can provide precise digital counting information on the X-ray intensity.[73−75] In a typical 2D MWPC area detector configuration, the anode consists of a central plane of metal wires, located between two planes of cathode wires. Each element of the cathode wires is connected to a single delay line. The signal pick up on this delay line thus is correlated with the energy and the position of the incident event along the cathode plane. Two anode planes are arranged perpendicular to each other. Such geometry can thus be used to resolve the position of the event in two dimensions. In the conventional design, all the wires (anode and cathodes) are prealigned in a straight-line fashion with a uniform spacing of about 0.5 mm apart. The entrance window is made of carbon composite which is used to withstand high gas pressures (∼6 atm). A much more advanced MWPC detector has recently been developed for a very high count rate and very fast read-out performance.[8]

The imaging plate,[79] either coupled directly with a scanner or operating separately from a scanner, offers the best compromise for routine operations. It has a large dynamic range, excellent spatial range and revolution, low background, and reasonable linearity. It is robust, and the operating cost is relatively low, especially for multiple users. However, it cannot be used easily for time-resolved experiments (its typical read-out time is 300 s, and the handling time is 150 s) and measurements of absolute intensity are difficult to achieve because the exposed imaging plate decays slowly and depends partly on the time period after exposure and before processing.

CCD X-ray area detectors have made incremental advances in recent years and are commercially available. X-rays could be detected directly by CCDs. However, the chip size is usually too small (≈25−50 mm on each side) for convenient applications. More importantly, the CCD would suffer radiation damage by direct exposure to X-rays, leading to an increase

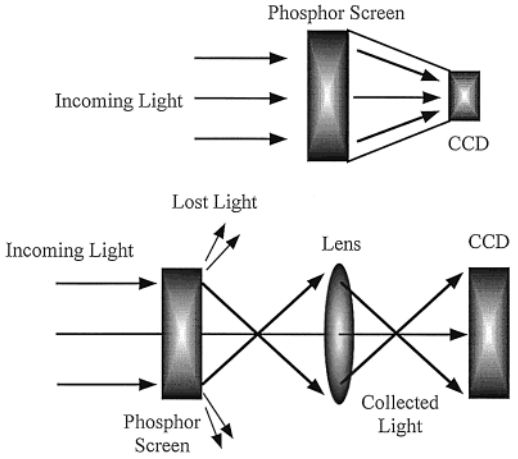

Figure 6. Fiber-optic-coupled CCDE detectors (top) have a significantly higher collection efficiency than comparable lens-coupled CCD detectors (bottom). The fiber bundle, with its larger light-capturing area, maintains the incident pattern of illumination and delivers it to the CCD. (Reprinted with permission from ref 91. Copyright 1988.)

in the dark count rate[80−82] and a limited dynamic range because each X-ray photon could produce hundreds of electron−hole pairs due to the high energy of the X-ray radiation.[83] Converting X-rays to visible light photons by means of an appropriate phosphor could avoid these problems but would introduce statistical noise.[84] After conversion, the image on the phosphor can be transferred to the CCD by using a lens system,[85] fiber-optic coupling,[86] an image intensifier and a lens system,[87−89] or an image intensifier and fiber-optic coupling.[90] Figure 6 shows a schematic comparison of the collection efficiency between a fiber-optic-coupled CCD detector and a lens-coupled CCD detector.[91] In a lens-coupled CCD detector, one can compensate for the light loss by using an image intensifier. However, this approach would increase the complexity of the instrument, decrease the dynamic range and the linearity due to limitations of the image intensifier, and result in a high background noise. Thus, commercial CCD X-ray area detectors now use the format of the configuration shown in the top of Figure 6. Large CCD chips (up to 4k pixels) or multiple CCD chips (often four chips with 1k pixels per chip), together with an appropriate fiber-optic taper, can provide a large enough spatial range and high enough spatial resolution for most purposes. However, in the time-resolved mode, a compromise has to be made in selecting the appropriate dynamic and spatial ranges as well as spatial resolution in order to achieve a reasonable number of frames per second.

Finally, it is noted that even with the popularity of CCD X-ray area detectors, further improvements on gas/wire counters should not be ignored. For example, a new type of centroid-finding method for position-sensitive detectors has allowed higher count rates and good spatial resolution.[92] A curved microstrip gas counter has been designed for synchrotron radiation time-resolved SAXS/WAXD experiments with count rates of up to 1 MHz per channel and a channel width of 0.4 mm.[93] Time-resolved SAXS/WAXD experiments allowing two-dimensional patterns to be recorded with exposure times as short as

40 ms have been achieved.[94] Thus, it is expected that even with the conventional approach, time-resolved measurements down to the millisecond range can be achieved.

III. Environment Controls for in-Situ or Time-Resolved Measurements

Recently, a comprehensive review on the subject of combining synchrotron SAXS with different experimental techniques has been made by Bras and Ryan.[8] In this section, we will briefly review the more recent development of some unique sample chambers for the combined techniques. We will place less emphasis on the instrumentation design aspects but more emphasis on the materials research (section V).

A. Temperature Chambers

Typical temperature chambers used for synchrotron SAXS measurements are in the transmission mode, employing some sorts of X-ray windows made of beryllium or Kapton films. These chambers can be modified directly from the hot stages for optical microscopy, which usually have good heating and cooling capability at moderate rates (1−100 °C/min). These chambers are suitable for routine polymer research. For time-resolved phase-transition study, such as isothermal crystallization, the moderate cooling rate may not be fast enough to allow the study of rapid structural changes. Several different cells have been designed for this purpose. For example, a dual-chamber temperature-jump unit was designed and constructed by Chu and co-workers.[95] The samples were initially equilibrated at one temperature (such as above the melting point, T_1) and were quickly jumped to a different temperature (T_2) for measurements using a pneumatic piston. The typical cooling rate during the jump was about 300 °C/min during the initial 95% of the temperature drop, which was similar to the fastest cooling rate used in DSC. The total time for the sample to reach the measurement temperature was 10−60 s, depending on the sample mass (several grams) and the thermal conditions. For a faster cooling rate experiment, one can consider the use of less sample mass, better thermal insulation, or even the use of stop flow.[96] For example, a rapid temperature-jump (T-J) device was designed for the kinetic SAXS measurements from solutions of biological macromolecular systems using a stop flow geometry.[96] The dead time of this apparatus was only a few hundred milliseconds. The structural change thus can be monitored in a time scale of less than a second. This type of measurement, however, is limited to small sample mass and the availability of detectors with fast time-resolution capability (in millisecond). For rapid heating experiments, one can consider the use of laser heating such as the apparatus designed by Hiragi et al.[97] The schematic diagram of the dual-chamber temperature-jump unit equipped with simultaneous SAXS/WAXD setup is illustrated in Figure 7.

On the basis of our experience in the SAXS beamlines (X3A2 and X27C) at NSLS, most kinetics studies of crystallization and phase transition in polymers have often been carried out with the dual-chamber temperature-jump device because the required resolution times are usually in seconds or even minutes. These resolution times can be easily accommodated by most detection systems. Examples for studies of phase transition in crystalline polymers, polymer blends, block copolymers, etc., will be discussed later. Recently, several commercial hot stages, which can also perform the function of thermal analysis such as differential scanning calorimetry (DSC) or differential thermal analysis (DTA),[98] have been used in time-resolved X-ray scattering experiments. Thus, in-situ thermal analysis and SAXS/WAXD measurements can be carried out simultaneously. These combined techniques have become quite routine in the synchrotron community these days.

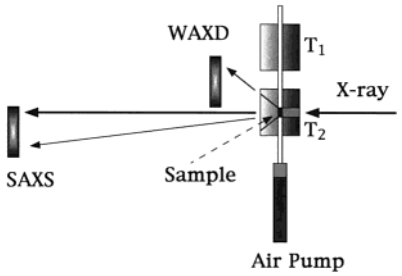

Figure 7. Schematic diagram of the dual-chamber temperature-jump unit equipped with simultaneous SAXS/WAXD setup constructed in our laboratory.

B. Pressure Cells

Extraordinarily high pressures have been known to strong-arm elements to yield exotic new materials. The best-known example is the high-pressure manufacture of synthetic diamond (from graphite), which is already a near billion-dollar industry. While there has been much interest dealing with the kinetics of phase transitions in polymers, it has been most difficult, if not impossible, to follow the morphological development from early times. This stems either from the inability to heat or cool a device rapidly enough or from the poor thermal conductivity of polymers. Phase transitions can also be brought about by rapid changes in pressure at a constant temperature. The major limitation up to this point has been the need to have exceptionally small volumes to produce a uniform pressure field. With very small scattering volumes, one can use thermally equilibrated high-pressure cells (e.g., diamond anvil cells) to generate sufficient pressure and to provide very rapid pressure changes. Thus, one has the potential of investigating the kinetics of relatively simple phase transitions such as the demixing of homopolymers, the microphase separation of block copolymers, and crystallization under high pressures.[99−103] In addition, more complex processes such as reaction-driven phase separation under pressure, as in the case of interpenetrating and semi-interpenetrating polymer networks, can also be studied.

In general, there are two types of pressure measurements that are of interest to the polymer community. One is the hydrostatic pressure experiment for the study of phase transformation in the solid

state (higher pressure); the other is the high-pressure study of polymers in liquid or solutions (lower pressure). The design and construction of the first type of high-pressure cell for SAXS experiments has been illustrated by Lorenzen et al.[100] This cell could operate up to 10 kbar and 300 °C using silicon oil as a pressure medium and diamond windows. Another apparatus, which has been used for pressure-jump experiments, was described by Steinhart et al.[101] In this apparatus, pressure from 1 atm up to 0.35 GPa was produced by a motor-driven, piston-type generator. This cell used two beryllium windows with a low background scattering that was suitable for SAXS measurements. Pressure-jump experiments with a resolution time of 5 ms were demonstrated. Pressl et al. designed a compact high-pressure cell with operating pressures to 3 kbar and temperatures between −20 and +80 °C.[102] The cell was designed to investigate the biological systems of interest, especially lipid−water dispersions. They have carried out a pressure-dependent SAXS study of phospholipid−water dispersion at constant temperature. Maeda et al. used a similar high-pressure cell to study the pressure-dependent polymorph of a liquid crystalline polyester.[103] They found that the formation of the crystal polymorph is substantially accelerated by the hydrostatic pressure and the heat treatment. Seto et al.[104] designed a high-pressure solution SAXS cell to study the pressure-induced phase transition in a ternary microemulsion consisting of dioctyl sulfosuccinate sodium salt (AOT), water, and *n*-decane. A pressure-jump experiment from the high-pressure lamellar phase to the low-pressure phase was carried out using this apparatus. A different design of high-pressure solution cell was also illustrated by Kato et al.[105] They used two synthetic diamond windows (maximum pressure 700 MPa), which allowed an accurate solvent background correction for quantitative analysis of the data. The pressure-induced phase transition in liquid crystal membranes by water[106] and the change of internal dynamics of DNA in water[107] were carried out by Gouner and co-workers. They used a high-pressure solution cell not only suitable for water but also for different solvents.

The use of supercritical solvents for polymer synthesis and processing has gained momentum for high-pressure studies of polymers. The properties of varying supercritical solvents including water, CO_2, and CF_3H have been recently characterized by Morita and co-workers using synchrotron SAXS.[108] They found that the behavior in the long-range inhomogeneity of water in the supercritical state was in discord with the ordinary behaviors for other compounds such as CO_2 and CF_3H. The use of CO_2 is of particular interest to the polymer community because of its environmental friendliness. Synchrotron SAXS is an ideal technique to study the phase behavior of polymers in supercritical CO_2. Several unique supercritical CO_2 SAXS experiments have been carried out recently. For example, the aggregation behavior of dilute poly(1,1-dihydroperfluorooctyl acrylate-*b*-vinyl acetate) diblock copolymer in supercritical CO_2 was carried out by Chu and co-workers.[109] In the isothermal process, large aggregates exhibiting domain-packing structures were formed in the pressure range from 190 to 226 bar. Block copolymer micelles were observed at 243 bar and 65 °C. The schematic diagram of the high-pressure cell for synchrotron SAXS study in the supercritical CO_2 environment designed by Chu et al. is shown in Figure 8.

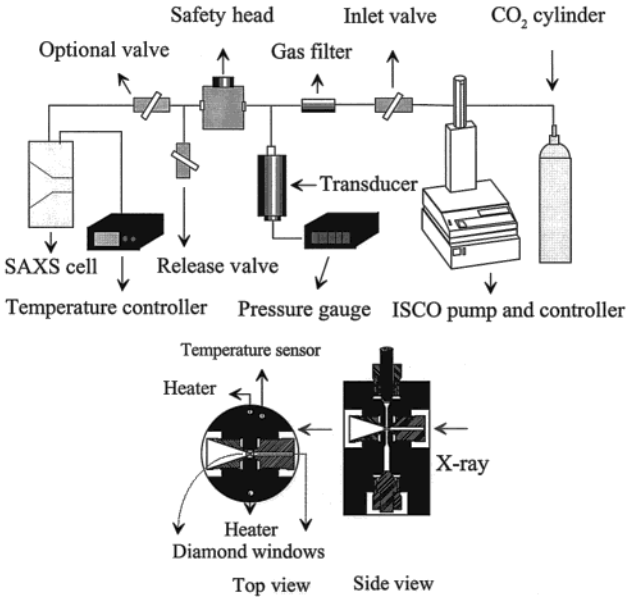

Figure 8. Schematics of the high-pressure supercritical CO_2 apparatus for SAXS experiment: (a) overall diagram of the apparatus and (b) the SAXS cell design. (Reprinted with permission from ref 109. Copyright 1999 American Chemical Society.)

C. Stretching Equipment

Dynamic studies of polymer films and fibers during tensile deformation have become very common in synchrotron experiments. These studies yield important information on the changes of structure and morphology during deformation, which can be related to the macroscopic properties of polymers. For example, during deformation, many important engineering resins exhibit the behavior of crazing. The features in craze fibril microstructures can be characterized by SAXS. Using synchrotron SAXS, the formation of crazes can be directly visualized in real time. Several glassy materials including polystyrene and polycarbonate have been investigated by Brown and Kramer.[110,111] Simultaneous measurements of the absorption of the primary beam by the samples allowed the total plastic strain to be calculated. In some semicrystalline systems, such as poly(ethylene terephthalate) (PET), the behavior of crazing during deformation was also observed. However, further deformation led to crystallization. In this study, the observed SAXS patterns during the transient state were more complex and required the use of WAXD to provide crystallization information. Recently, our laboratory has carried out a deformation study of poly(*p*-phenylene terephthalamide) (PPTA) fibers, also known as Kevlar fibers, which have high tensile strength, high Young's modulus, high thermal stability, and low creep, due to the fully extended macromolecular chains.[112,113] Unlike the usual crystalline

polymers, the chains in Kevlar are highly extended, which can form the so-called paracrystalline or mesomorphic structure with poor lateral order in the noncrystalline zone. The combination of SAXS and WAXD has proven to be very useful to study the changes of lattice structure, morphology, and macroscopic properties during deformation.

The deformation experiment involves the use of some kind of commercial or custom-built tensile stretching devices. The major requirement of the device is that it should provide symmetrical stretching, which guarantees that the focused X-rays can illuminate the same position on the sample during deformation. Otherwise, the sample detection position will be changed continuously, which can lead to uncertainties in conclusion.

In our laboratory we modified a tabletop nonsymmetrical stretching device to provide symmetrical deformation.[112] The modification can be briefly described as follows. The tensile stretching apparatus was a modified version of model 4410 from Instron Inc. and had a load capacity of 500 N. The maximal distance between the two grips was about 460 mm. Sample could be heated to a temperature up to 300 °C with a custom-designed sample chamber. The stretching speed could be adjusted from 0.2 to 1000 mm/min. The modified stretching unit adopted a custom-built vertical translational stage, which provided translational motion opposite to the programmed stretching with the same speed.

Recently, a fully integrated stretching system has been developed by Fuller and co-workers,[114] which allowed the study of polymer deformation via simultaneous SAXS/WAXD and stress−strain techniques. 2D SAXS/WAXD images were collected using two CCD-based area X-ray detectors, which provided video signal outputs. A video extensometer additionally provided sample strain and cross-section data during deformation. All three video signals were processed by a Synoptics i860 processor-based video framegrabber, which was capable of collecting data at a rate of 40 ms per frame. A strain gauge was used to reveal the mechanical yielding behavior of the sample. An electronic trigger mechanism was equipped to provide accurate synchronization of the X-ray data with sample dimensional changes and loading information. This integrated stretching system has been demonstrated to be a useful tool for the study of polymer deformation at rates relevant to practical processing.

D. Fiber Spinning Equipment

In polymer processing, the stake in understanding the fiber spinning technology is very high because the variations of the processing parameters can directly affect the properties of the final products. For fundamental studies of polymer physics, the spinning process also provides an important mean to look into the initial stage of crystallization during elongational flow. Very interesting results have recently been seen in the low-speed melt spinning of several polymers,[115−121] where SAXS signals persistently occurred before WAXD. This observation suggested that density fluctuations occurred prior to crystallization or might even be a precursor to crystallization.[116] In our opinion, this observation can also be attributed to an instrumentation artifact, which will be commented on later in section V.B.5. Below we will briefly describe two types of apparatus for fiber melt spinning and for fiber solution (gel) spinning.

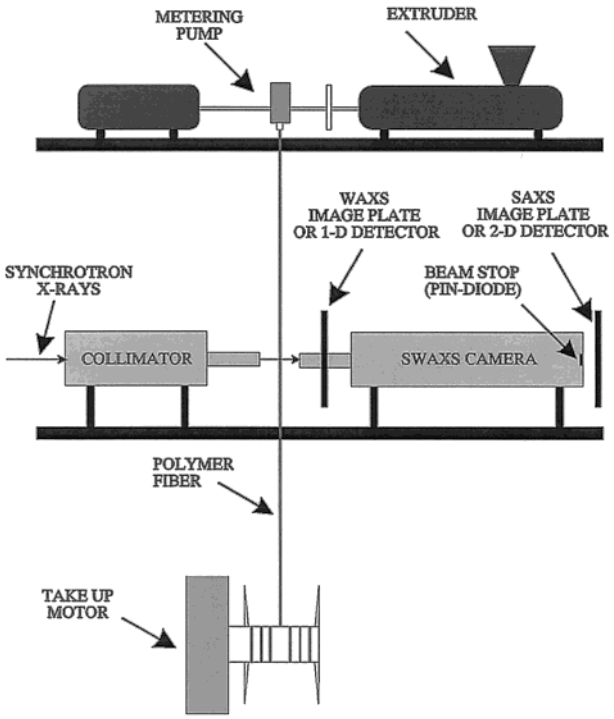

Figure 9. On-line simultaneous SAXS/WAXD melt spinning apparatus at the A1 beamline in Hasylab, DESY. The detection system contains two imaging plates. (Reprinted with permission from ref 115. Copyright 1993.)

The first fiber melt spinning device was built by Zachmann and co-workers in the A2 Polymer line at HASYLAB, DESY.[115] This melt spinning equipment consisted of a 20-mm single-screw extruder attached to a metering pump. The extruder and the metering pump were mounted on a horizontal platform that could be translated in the vertical direction with the use of a precise stepper-motor drive system (Figure 9). Distances ranging from 28 to 87.5 cm from the spinneret could be examined on the spinline using this apparatus. The main beam had a rectangular shape with the long axis normal to the fiber. The extruded fiber was taken up on a 19 cm diameter godet roll after passing through a ceramic guide used to minimize fiber movement and vibration. A very similar fiber spinning (film extrusion) apparatus was also constructed in the Daresbury Laboratory by Ryan and co-workers[116] to study the initial stages of polymer crystallization.

At Stony Brook, we also designed and constructed a portable melt spinning apparatus which consisted of a 3/4 in. Independent Laboratory single-screw extruder (C. W. Brabender Instruments Inc., NJ) and a custom-built vertical lifter with about 1.2 m of displacement (Applied Automation Research Corp., FL). The maximum extrusion temperature was about 325 °C. The extruder was mounted on a horizontal platform that could be translated in the vertical direction by computer control. The extruded fiber was

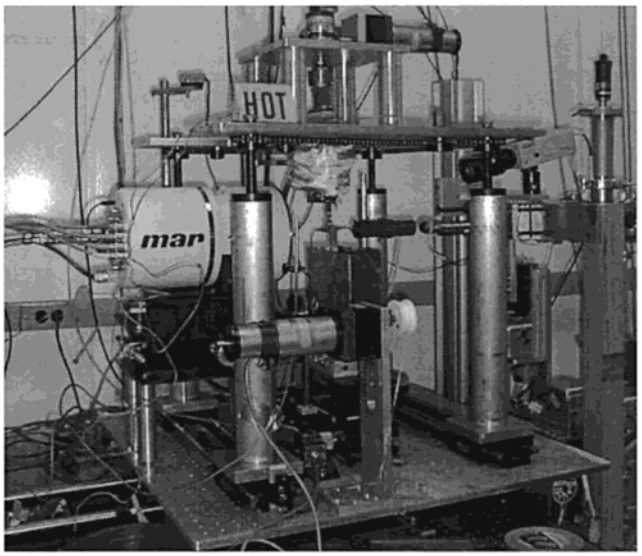

Figure 10. Photograph of the on-line WAXD solution spinning apparatus for the study of polybenzoxazole (PBO) at the X27C beam line of the NSLS, BNL.

taken up with a portable wind-up device after passing through a ceramic guide, which was used to minimize fiber movement and vibration for X-ray detection. Several spinneret dies were available to produce monofilament, multifilament, or film. The typical rate of the mass output from this extruder was 1−7 g/min. Once the fiber spinning commenced, the extruder could be translated remotely in the vertical direction, allowing measurements to be made along the spinline (20−65 cm from the spinneret, with a precision of 0.5 cm). The maximum take-up speed was about 2000 m/min. This spinning apparatus was made portable for transport to different synchrotron facilities.

A solution (or gel) spinning apparatus for synchrotron studies has been designed and built by scientists at Dow Chemical Co.[122−123] The photograph of this apparatus recently used for an in-situ fiber spinning study of polybenzoxazole (PBO) at the X27C beam line of the NSLS, BNL is shown in Figure 10. A capillary rheometer-like barrel was located on the top platform of this apparatus, which stored polymer solutions (gels) with a temperature capability of 300 °C. A motor-driven plunger was used to extrude the polymer solution. Several spinneret dies were available for making monofilament, multifilament, and film at high temperatures (to 250 °C). The top platform could be moved vertically over a distance of about 10 cm with 0.2 mm precision. The apparatus was mounted on a pair of precision optical rails perpendicular to the X-ray beam, permitting the alignment of the extruded filament or film for X-ray detection. A fine stepping motor, instead of the original linear motor, was used to achieve better precision control. The base of the apparatus was mounted on a high-precision translational stage for further alignment with the incident X-ray beam. A take-up wheel with an adjustable speed was used to change the draw ratio. A temperature-controlled water bath was installed for the coagulation process. The fiber after the spinneret was soaked into the water and wound back to the air before take-up. The water level (thus the total time of the fiber passing through the water bath) and the water temperature could be adjusted. With the fine stepping motor and the X-ray beam monitor system, the scattering measurement could be switched quickly from the point before coagulation to the point after coagulation.

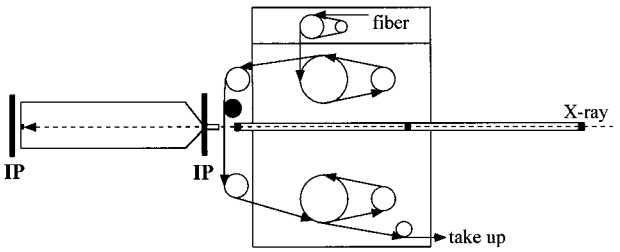

Figure 11. Schematic diagram of the continuous fiber draw unit (constructed in our laboratory at Stony Brook) constructed for simultaneous SAXS/WAXD measurements at the NSLS.

E. Fiber Drawing Apparatus

The stretching experiment described earlier can be used to probe the dynamic properties of fibers during deformation. However, in real industrial processes, the fibers are drawn or heated continuously. Thus, the stretching study can only be used to correlate with the industrial processes indirectly. For this purpose, a prototype fiber continuous drawing apparatus has been constructed in our laboratory to perform on-line SAXS/WAXD experiments of polymer fibers at the NSLS.[124−126] This draw unit (as shown in Figure 11) was originally designed by A. D. Kennedy of DuPont, modified by us, and constructed by Hills Inc., W. Melbourne, FL.

This draw apparatus was built in a compact format so that it can be accommodated in different synchrotron beam lines at the National Synchrotron Light Source (NSLS) or at the Advanced Photon Source. A brief description is provided as follows. Two high-torque servomotors that meet the requirement of drawing high-performance fibers were used to control the two feeding and collecting Godet rolls for the yarn (or filament). The speed of the two motors could be separately adjusted to a precision of 0.25 m/min, with a maximum speed of 750 m/min. The drawing speed could be continuously adjusted to achieve the desired draw ratio at different feeding speeds. There were two temperature-controlled heat pins along the fiber drawing path. The X-ray spectator point was at some distance down stream from the heat pins. The distance between the heat pins and the incident beam position was adjustable over a range of 3−150 mm. This adjustment permitted the observation of the crystallization process at a predetermined time period and temperature after the initial heating by the heat pins at a fixed draw ratio and feeding speed. This apparatus weighed about 200 lbs and could be moved horizontally (mutually perpendicular to the incident X-ray beam and the fiber draw direction) with a precision of 2.5 μm by a motor-controlled translational stage.

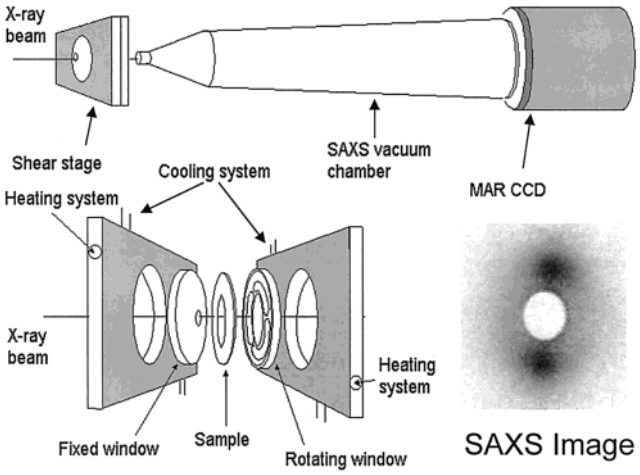

Figure 12. Schematics of the Linkam Shear stage, showing the placement of sample and the rotating and stationary plates. The synchrotron small-angle X-ray scattering (SAXS) setup with a MARCCD area detector is also shown.

F. Shear Apparatus

It has been demonstrated that the phenomena of flow-induced molecular orientation,[127] mixing/demixing,[128] and order−disorder transitions in block copolymers at large strains[129,130] can be investigated in real-time by synchrotron SAXS. The use of shear flow is often deployed because of its easy accessibility. The elongation flow, which is considered a stronger flow, has not been used extensively because of experimental difficulties. Generally speaking, there are two types of shear deformations that are of interest: (1) steady-state shear and (2) oscillatory shear. For these studies, several X-ray-modified rheometers have been demonstrated involving different types of shear geometry and different operational modes: parallel-plate shear apparatus, Couette flow shear apparatus, and modified rheometric solids analyzer (RSA-SL) rheometer.

The X-ray modification for the parallel-plate shear apparatus has been described by Burghardt and coworkers.[131] The schematic diagram of the shear stage with a similar X-ray modification made by us is shown in Figure 12, which can be described as follows. The Linkam Cambridge shear system (CSS) 450 was a high-temperature shearing stage often used to examine viscous liquid materials for in-situ optical microscopic studies. The modification for the X-ray detection involved the use of Kapton windows and the special construction of the rotating plates with small openings (see Figure 12). The sample was placed in a gap between two parallel X-ray windows. Shearing took place by rotating one of the disks using a precision stepper motor as the other disk remains fixed. The gap between the windows was adjustable, ranging from 10 to 2500 μm, using a second stepper motor. Each of the two quartz windows was in close thermal contact with a silver block heater that controlled the sample temperature. The sample temperature could be controlled from ambient conditions to 450 °C. To protect the motors and electronic components from heat damage, the shear cell was water-cooled.

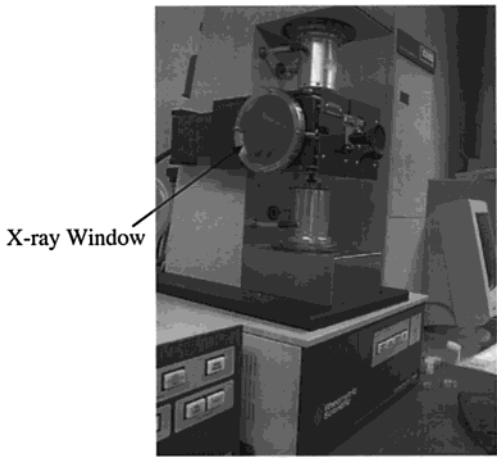

Figure 13. Photograph of a modified Rheometrics RSA-SL rheometer for synchrotron SAXS/WAXD measurements. This instrument was modified by our group at Stony Brook.

For the oscillatory shear experiment, a Rheometrics RSA-SL system has been modified in our laboratory (Figure 13). The modification included the incorporation of two vacuum paths (before and after the sample) and several X-ray windows (e.g., Kapton films) along the beam path. One section of the vacuum path was in a cone shape having a maximum scattering angle (θ) of about 30°. The maximum operating temperature for the environment chamber was about 500 °C (using hot air). This apparatus was suitable for the studies of stress-induced crystallization of (fully or lightly) cross-linked polymer melts, without the use of a sandwich shear cell. The experimental procedure for the solid-state elastomer did not need to use the sample holder, which was essentially the same as for typical dynamic mechanical analysis (DMA). Hamley et al. used a similar apparatus to study large-amplitude shearing on the orientation of cubic phases in gels of block copolymers formed in concentrated solutions[129] and on the bicontinuous cubic phase of a block copolymer melt.[130]

The synchrotron SAXS technique is an important tool to study polymer melts and solutions during flow. Many examples have been demonstrated by the neutron scattering method but only a few by X-ray scattering. There are significant advantages in using the SAXS technique rather than SANS. Very fast detection time with very small sample sizes (down to length scales of micrometers) can be achieved by synchrotron SAXS, which is suitable for time-resolved experiments. In contrast, neutron measurements usually require a collection time that is 100−1000 times longer.

IV. Combined Techniques

A. Simultaneous SAXS/WAXD

The simultaneous SAXS and WAXD techniques are perhaps one of the most frequently requested methods for studying the structure and morphology changes in real time during phase transformation. The principle of this combined method is quite simple. During the experiment, two position-sensitive detectors are placed in different locations, which should cover a

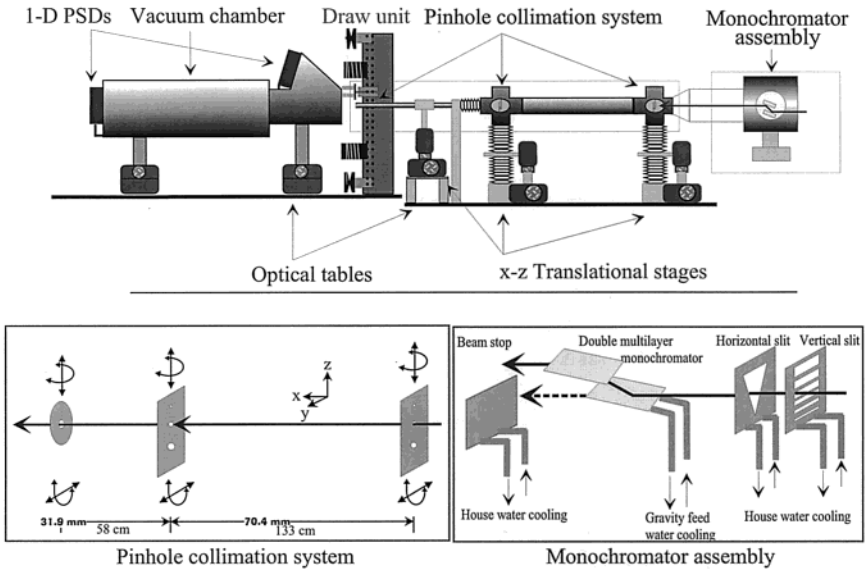

Figure 14. Schematics of simultaneous SAXS/WAXD setup for fiber drawing experiments at the X27C beamline in NSLS. The bottom diagrams illustrate the pinhole collimation system (left) and the double-multilayer monochromator (right).

wide angular range such as $\sim 100\ \mu\text{rad} < \theta < 0.5$ rad. This means that ca. four orders of magnitude in q ($=(4\pi/\lambda)\sin(\theta/2)$) can be obtained. The positioning of the two (or more) detectors depends on the structure, morphology, and orientation of the polymer system, the availability of detectors, and the available space for instrumentation. It is generally desired to have a minimal blank space between the SAXS and WAXD angular ranges and to operate the two detectors synchronously. Many polymer problems can be tackled by the use of simultaneous SAXS/WAXD techniques. These problems could include crystallization and melting, phase transformation of polymers (such as ethylene-based copolymers,[132−134] iPP,[135,136] PEEK,[137,138] PEN[139]), polymerization,[140] and the formation of colloids and gels,[141] just to name a few.

The simultaneous SAXS/WAXD techniques can arbitrarily be divided into two geometrical configurations. For isotropic systems, two one-dimensional (1D) position-sensitive detectors (PSDs) can be used. For anisotropic systems (such as dynamic stretching experiments), two area detectors are often needed, which sometimes impose challenges in the camera design. In 1992, Zachmann and co-workers first reported the use of simultaneous SAXS/WAXD to study the crystallization of polyethylene.[133] In 1993, Bras et al. described the instrumentation developed for performing simultaneous time-resolved SAXS/WAXD experiments using two gas-filled proportional detectors.[142] Recently, Bras and Ryan reviewed this subject.[8] They stated the importance of these techniques for understanding fundamental aspects of phase transformations as well as the applied fields of polymer processing. They also noted that the instrumentation limits in the detectors and the sample environmental chambers have hindered the experiments with shorter time resolution. For this purpose, Bras described the improved design of a dedicated station for real-time SAXS/WAXD experiments on a bending magnet beamline at the ESRF[143,144] and the development of a high-count-rate-curved PSD (1 MHz per channel) based on the microstrip gas counter (MSGC) technology for WAXD.[145] Laggner and co-workers also reported the design of a dedicated wiggler beamline for SAXS/WAXD measurements at ELETTRA.[146] This facility was designed specifically for time-resolved (resolution ca. 1 ms) structure studies on gels, liquid crystals, (bio)polymers, amorphous materials, muscles, and proteins in solutions.

For anisotropic systems, simultaneous 2D SAXS/WAXD measurements have been demonstrated by using two area detectors (MWPC or CCD) both with time-resolution capability.[147] However, this arrangement is not widely used because the WAXD image collected this way is often in a distorted form having only limited values for quantitative data analysis. If the time resolution is not the primary concern, such as for the steady-state experiments (fiber spinning or fiber drawing), two (or more) imaging plates (IP) can be used as X-ray area detectors. The WAXD IP contains a central opening which allows the passage of the SAXS signal. Because the typical time resolution of IP is several minutes, this system is only applicable to systems at equilibrium, under steady state, or at very slow kinetics conditions. One major challenge of using IP is that a quantitative comparison of different images is difficult to carry out since each image has a different background and a slightly different location of the scattering center. In addition, it is difficult to correct the incident beam fluctuations and the sample absorption. The schematic diagram of using two 1D PSDs to collect simultaneous SAXS/WAXD profiles during fiber drawing at the X27C beamline is illustrated in Figure 14. The bottom diagrams illustrate the pinhole collimation system and the double-multilayer monochromator.

B. Raman Spectroscopy

Raman scattering is a technique for studying vibrational spectra using coherent, intense, light beams generated by laser devices. Raman spectroscopy yields information on the vibrational modes of

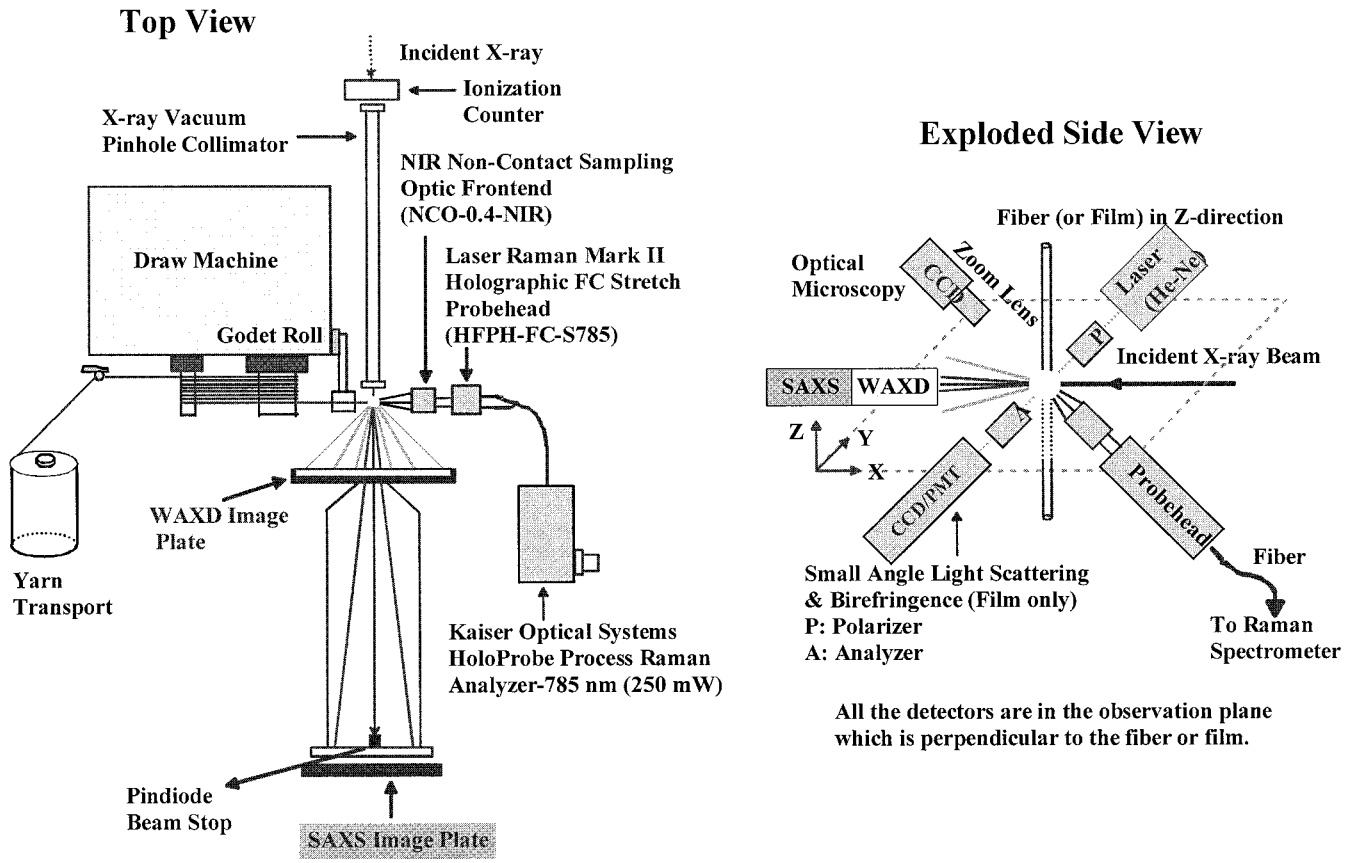

Figure 15. Schematic diagram of a combined Raman/SAXS/WAXD system to study the fiber drawing process. The apparatus, as shown in the exploded sideview, has been designed and is being constructed in our laboratory.

segments of the molecules and is concerned with small-length scales down to the molecular level, similar but not equivalent to WAXD. Raman scattering depends on the fourth moment of the orientation angle, in contrast to the second moment dependence found with birefringence and infrared dichroism. Purvis and Bower,[148] Shepard,[149] and Bower[150] carried out Raman polarization studies on several polymeric systems. They described the experimental arrangements in detail and also developed the theoretical background and illustrated the use of this technique to study polymer orientation.

In a typical study of crystalline polymers, the information obtained from Raman scattering can provide structures in the amorphous phase, which complements the structural information obtained from the crystals and the mesophases. For example, by examining the changes in the line width of carbonyl stretching of PET (fiber or film) as a function of temperature, the glass transition temperature can be estimated. In a polymerization process, some bonds are broken while others are formed. Then the decomposition of monomers or the formation of polymers can be monitored via Raman spectroscopy. The combination of Raman spectroscopy with X-ray scattering can provide complementary information on the structure of materials undergoing physical phase transitions or/and chemical reactions. The technique of Raman spectroscopy has been in existence for some time, and its applications to polymer physics have been well established. It has only been demonstrated recently that the combination of this technique with SAXS and WAXD is a powerful approach. The schematic diagram of a combined Raman/SAXS/WAXD system to study the fiber drawing process, designed by our laboratory, as shown in Figure 15, is being assembled. Ryan et al. also demonstrated the use of Raman spectroscopy in combination with synchrotron SAXS/WAXD to study the phase transitions in polymers.[151] They showed that the time resolution of Raman spectroscopy was on the order of a few seconds and comparable with the X-ray techniques.

One practical problem often encountered in the application of Raman spectroscopy is that many polymer systems (such as polyamides) emit intense flouresence-scattered light under the emission of a strong laser source. The fluorescence background can overwhelm the weak Raman signals. Consequently, a longer wavelength laser (e.g., 782 nm) is often used to minimize the flouresence background of the polymers.

C. Laser Light Scattering

The structure factor of complex systems in a large length scale can be obtained by using conventional light scattering (LS) and small-angle light scattering (SALS) techniques. Very often the structural information yielded by light scattering matches well with that from SAXS. Chu reviewed the subject of conformation and dynamics of colloidal aggregates in detergent and copolymer systems,[152] where the relationship between LS and SAXS was outlined. Chu concluded that the complex system could be exten-

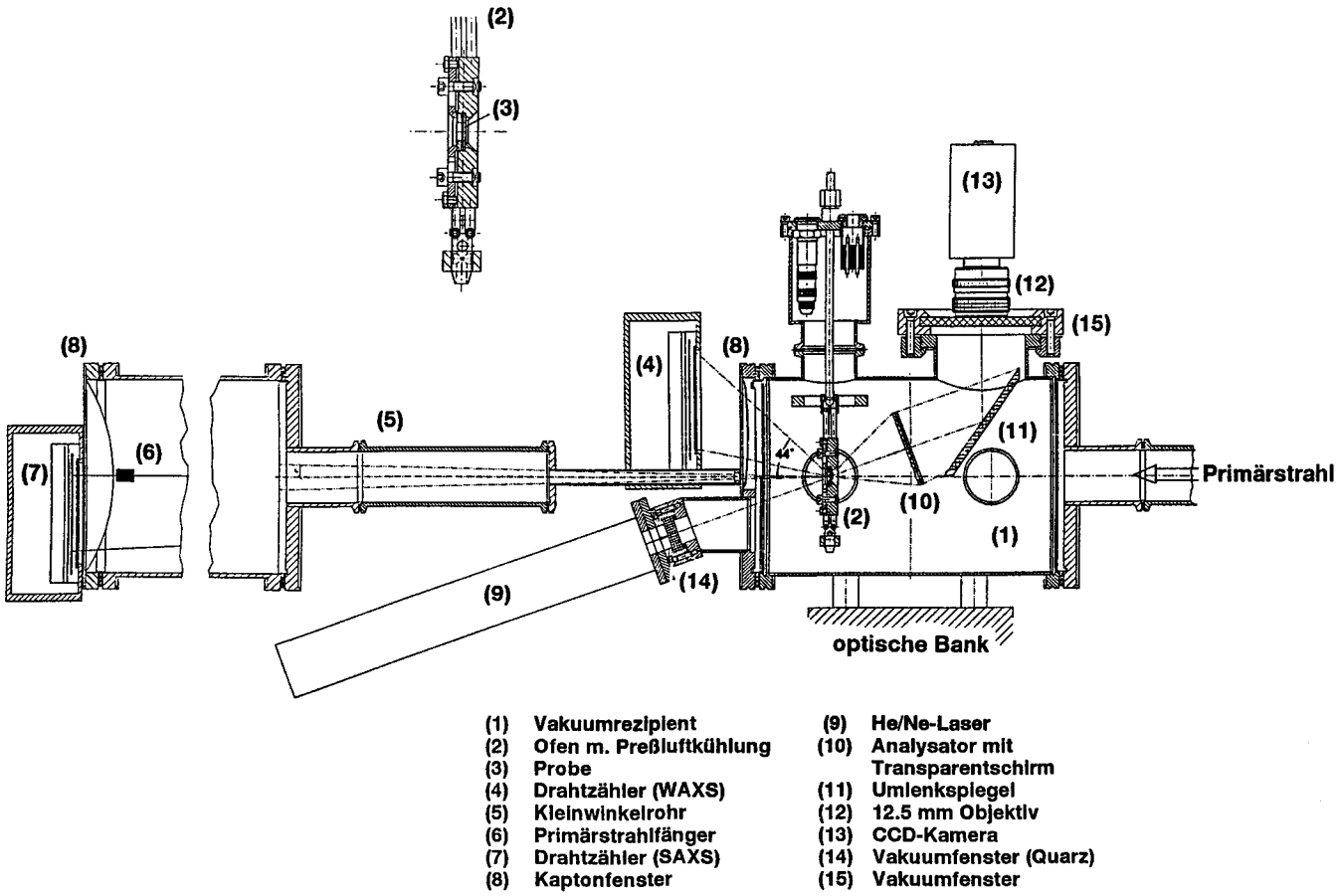

Figure 16. Schematic diagram of a combined laser light scattering/SAXS/WAXD system to study the polymer crystallization process. This apparatus was designed and constructed by Zachmann and co-workers at Hamburg. (Reprinted with permission from ref 156. Copyright 1993.)

sively investigated by combining laser light scattering and synchrotron SAXS with measurements of rheological properties of the supramolecules. The inter- and intramolecular interactions involving hydrophobic−hydrophilic interactions, solvent−nonsolvent considerations, and metal coordination could be revealed in detail by complementary scattering techniques to provide useful information on the size, size distribution, and conformation of the aggregates. Studies of microstructures of the colloidal aggregates at dilute concentrations became feasible only with the intense synchrotron X-rays. Li et al. demonstrated the study of the aggregation behavior of polydiacetylene in THF−PhMe mixed solvents using static light scattering (SLS), dynamic light scattering (DLS) and synchrotron SAXS.[153] The transition of single molecular coils to stretched-chain aggregates could be described approximately by the Avrami equation through SLS and SAXS experiments. On the basis of semiquantitative comparison of the angular distribution of scattered intensity with a variety of theoretical scattering form factors, the structure of the P4BCMU aggregates was best described by ribbonlike unsymmetrical elliptic cylinders.[154]

Recently, Chu and co-workers designed and constructed a unique high-pressure fiber-optic light-scattering spectrometer that was capable of investigating the molecular dissociation and association behavior as well as the polymerization process in supercritical fluids.[155] Multiple fiber-optic probes and graded index microlenses were used to transmit the incident laser beam and to receive the scattered light from the high-pressure cell. With the miniaturization and flexibility provided by optical fibers, this high-pressure light-scattering cell was modified and could be transported to a synchrotron facility for synchrotron SAXS measurements. The modification involved the use of a different set of diamond windows for X-ray transmissions. This spectrometer was used successfully for the in-situ study of the molecular association behavior of a 1,1-dihydroperfluorooctylacrylate and vinyl acetate diblock copolymer in supercritical carbon dioxide under pressures up to 552 bar. The schematic diagram of the apparatus is illustrated in Figure 7.

Zachmann and co-workers designed and constructed an apparatus that was capable of measuring SAXS, WAXD, and SALS signals simultaneously.[156] They used this apparatus to study the crystallization of polymers. A schematic diagram of this apparatus is illustrated in Figure 16. By comparing the changes in the integrated intensity from SAXS and WAXD as well as the scattering data from SALS, they revealed the mechanism in structural evolution during secondary crystallization, which involved the mechanisms of crystal thickening, formation of new crystals within the lamellar stacks, and formation of new lamellar stacks.

D. Fourier Transform IR Spectroscopy

Absorption in the infrared wavelength range occurs by interactions between the incident radiation field and the dipoles in the medium. These dipoles may be either permanent, as in the case of the fluorine−carbon atom dipoles in polyvinylidene fluoride, or induced as a consequence of unsymmetrical stretching or bending of carbon−carbon bonds, as in the case of polyethylene. Infrared dichroism (D) arises from the anisotropy of the absorption, which is defined as the ratio of absorbances for the polarization directions parallel and perpendicular in a plane containing the incident beam. The infrared dichroism is related to the orientation function of the dichroic groups in the polymer chains.

There are many polymer problems in which the combination of Fourier transform infrared (FTIR) and SAXS can make significant contributions toward the development of more in-depth understanding. Elwell et al. reviewed the system of segmented polyurethane copolymers.[157] They concluded that the structure development during reactive processing of water-blown, flexible copoly(urethane-urea) foams could be well characterized by the combination of time-resolved FTIR spectroscopy, synchrotron SAXS, and rheology. FTIR spectroscopy monitored the microphase separation transition (MST) of isocyanate functional groups and followed the kinetics associated with nucleation and growth. Synchrotron SAXS probed the kinetics of the reaction-induced phase-separation process, the mechanism, the length scales, and the resultant morphology. Dynamic rheometry monitored the rheological properties associated with the evolving morphology. Lee et al. also demonstrated that the information of segment and domain orientations in poly(butylene succinate) (PBS) and polytetramethylene glycol (PTMG) segmental block copolymers during deformation could be obtained by synchrotron SAXS and IR dichroic methods.[158] Recently, Panick et al. demonstrated that the combination of pressure-jumped FTIR and synchrotron SAXS yielded important information about the pressure-induced unfolding and refolding of wild-type staphylococcal nuclease.[159,160] FTIR spectroscopy monitored the changes in the tertiary and secondary structures of the protein upon pressurization, while SAXS gave information about the chain collapse of the molecules in solution. The effect of pressure on the kinetics resulted in a larger positive activation volume for folding than for unfolding, and this effect led to a significant slowing down of the folding rate with increasing pressure. These studies indicated that the changes in the secondary structure in folding/unfolding reactions of Snase were probably dependent upon the same rate-limiting step as the changes in the tertiary structure. Similar high-pressure FTIR and SAXS studies were carried out to investigate the denaturation and aggregation of β-lactoglobulin and its genetic variants, as well as the structural development of dipalmitoylphosphatidylcholine bilayer membranes under pressure.[161]

The combined techniques of IR and synchrotron SAXS are relatively more difficult to carry out than the combined techniques of Raman and SAXS. To optimize the IR signals, thin and optically clear samples have to be used. The thin sample often compromises the X-ray signals. In contrast, the concern over the sample thickness is not as severe for Raman study. Ryan et al. used the combined techniques of synchrotron SAXS and FTIR to study the structure development and reaction kinetics during the polymerization process of segmented block copolyurethanes.[162,163] This study confirmed that the main driving force for structure development in polyurethanes was due to phase separation rather than hydrogen bonding.

V. Applications

A. Materials-Based Studies

1. Block Copolymers

The SAXS technique offers some unique research opportunities to study block copolymer systems either in the solid state or in solution. The intricate structures and the complex morphologies of block copolymers usually show a dimension in the range of 1−100 nm that is ideal to be studied by SAXS. Several comprehensive reviews of this subject are available (for examples, see refs 164 and165).

A block copolymer can exhibit multiple SAXS peaks due to its periodic microdomain structure having a long-range order. Information on the microdomain morphology can be obtained from the relative positions of these peaks. They can exhibit specific spatial relationships depending on the shape of the microdomain structure. For example, the ratio of the q values at the scattering maxima should be 1, 2, 3, 4,... for lamellae; 1, $\sqrt{3}$, $\sqrt{4}$, $\sqrt{7}$, $\sqrt{9}$,... for cylinders in a hexagonal array; 1, $\sqrt{2}$, $\sqrt{3}$, $\sqrt{4}$, $\sqrt{5}$,... for spheres in a body-centered cubic array, etc. A sample diagram is shown in Figure 17, which illustrates the temperature-dependent SAXS profiles of a polystyrene-*b*-polyisoprene (PS-*block*-PI) block copolymer obtained by the Hashimoto group.[166]

The synchrotron SAXS method adds another dimension to the study of block copolymers, i.e., the rapid kinetics of the phase transition can be followed in real time. For example, Floudas et al. studied several order-to-order transitions (OOT) in poly(isoprene-*b*-ethyleneoxide) diblock copolymer involving crystalline lamellar phase (Lc), hexagonal mesophase (Hex), and bicontinuous cubic phase (Gyroid).[167,168] They concluded that the transitions followed typical nucleation and growth behavior. Kim et al. combined the rheological characterization with SAXS to investigate the OOT between the Hex and body-centered cubic (BCC) phases in polystyrene PS-*block*-PI and PS-*block*-PI-*block*-PS systems.[169−171] They found that the transition between HEX and BCC was thermally reversible.[171] Hamley et al. studied the Lc to gyroid transition in poly(oxyethylene)−poly(oxybutylene) (EB) diblock copolymer and also reported that the transitions were thermally reversible.[129,130] The dynamics as well as the kinetics of the transition from the lamellar microphase to the isotropic melt in butadiene-styrene diblock copolymers were also studied by Ruland and co-

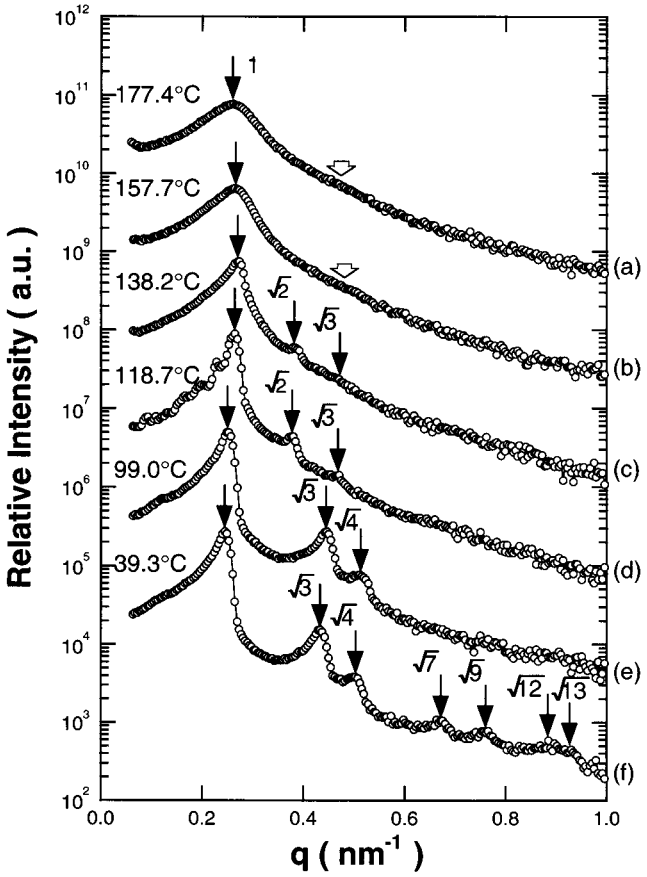

Figure 17. Temperature-dependent SAXS profiles of a polystyrene-*block*-polyisoprene (PS−PI) block copolymer. The top two profiles (177.4 °C, 157.7 °C) represent the bcc-sphere phase; the other profiles represent the hexagonal cylinder phase. (Reprinted with permission from ref 166. Copyright 2000 American Chemical Society.)

workers.[172−175] They found that the transition appeared in the form of pronounced singularities in the height and width of the main scattering maximum as a function of temperature, which could be modeled theoretically.

External fields such as tensile deformation have been used to manipulate the morphologies of block copolymers in solids. Thomas and co-workers studied the large strain deformation behavior of isoprene (PI)-rich SIS triblock copolymers with ordered double-gyroid (DG) morphology.[176] These oriented and biaxially textured samples were made by roll casting and annealing. They found that the different connectivities in PS led to dramatic and significantly different deformation modes. The microphase separation of block copolymers under high pressure has been investigated.[99−103] For example, Steinhoff et al. used synchrotron SAXS to investigate the disorder-to-order transition in polystyrene/polyisoprene and polystyrene/polymethyphenyl siloxane block copolymers.[177]

The crystallization process in the confined spacing of the ordered block copolymer has been studied by several research groups recently. Zhu et al. demonstrated that when the PEO blocks crystallized in a one-dimensionally confined lamellar space of poly(ethylene oxide)-*block*-polystyrene (PEO-*b*-PS) diblock copolymer, the crystal orientation (the *c*-axis of the PEO crystals) within the nanoscale-confined space can be controlled precisely by the crystallization temperature.[178,179] Ryan et al. studied the crystallization behavior of the poly(ethylene) (PE) block on PE−poly(ethyl ethylene) (hydrogenated 1,4-polybutadiene/1,2-polybutadiene) and PE−poly(ethylene-propylene) (hydrogenated 1,4-polybutadiene/1,4-polyisoprene) diblock copolymers.[180] Time-resolved simultaneous SAXS, WAXD, and DSC experiments were performed on the quenched samples from melts with lamellar and hexagonal-packed cylinder structures. They found that the original microphase-separated morphologies were completely destroyed due to PE chain folding upon crystallization. The WAXD data revealed that PE crystallized into its usual orthorhombic form in all samples.

In some block copolymers, when one block has a heterogeneous length distribution, the ordered phase can become inaccessible. However, the system may still exhibit microphase separation with one component being segregated from the rest of the segments as in segmental polyurethane (PU). The synchrotron SAXS technique has been used quite extensively to follow the kinetics of microphase separation and crystallization/melting of the constituent components in these block copolymers. For example, Krakovsky et al. used synchrotron SAXS to study the microphase separation kinetics of a PU network based on the poly(butadiene)diol (PBD) chain extender.[181,182] Li et al. studied the kinetics and thermodynamics of microphase separation in PU by SAXS.[183,184] Floudas et al. studied the kinetics of crystallization in model triarm star block copolymers containing two crystallizable blocks: PEO and poly(ϵ-caprolactone) (PCL) and an amorphous PS block.[185] Nojima et al. investigated the melting behavior of poly(ϵ-caprolactone)-*block*-polybutadiene (PCL-*b*-PB) copolymers, crystallized at various temperatures.[186−188] The strong SAXS intensity peak due to a sharp diffraction changed into a diffuse peak upon heating, indicating that a morphological transition from the crystal lamellar morphology of PCL to the microdomain structure or the homogeneous melt has occurred. Chu et al. investigated the crystallization and microphase separation of compatible mixtures of tetrahydrofuran−methacrylate diblock copolymers (PTHF-*b*-PMMA) with a THF homopolymer (PTHF).[189] Chu and co-workers also studied the process of slow spinodal decomposition in a poly(styrene-*b*-*tert*-butylstyrene) cast thin film.[190]

The supramolecular structures of block copolymers in solutions can also be studied by the synchrotron SAXS technique.[191] Hilfiker et al. studied the structure of isoprene−styrene block copolymer in aniline solutions.[192] They found that the solutions formed aggregates. Earlier investigations could not detect whether the aggregates were micelle-like or vesicle-like. Only with the high intensity of synchrotron radiation, it was possible to obtain good quality SAXS data, which confirmed that the aggregates were vesicle-like when the PS block was sufficiently short. Synchrotron SAXS experiments were also carried out in solutions of polyoxy(ethylene−propylene−ethylene) EPE triblock copolymer in xylene−water mix-

tures and of PEP triblocks in water.[185] The copolymers were found to form aggregates in selective solvents. With SAXS, the internal structure of self-assembled supramolecular systems (micelles and vesicles) was determined. In addition, synchrotron SAXS was also used to examine the chain length ratio, chain sequence, and total chain length in diblocks and triblocks poly(styrene/*tert*-butylstyrene) as well as the effects of charge (SPS)/polarity and solvent quality on the microstructures of polymer colloids.[190,193]

Recently, the large-scale grain size of the lamellar structures in styrene−butadiene block copolymers has been characterized by ultra small-angle X-ray scattering (USAXS) measurements.[194] All of the block copolymer specimens displayed a scattering peak in the USAXS regime, and the grain size was estimated using the spherical form factor. The calculated Porod's law constant and the value of the scattering invariant were consistent with the scattering mechanism proposed. The USAXS grain-size estimate was further verified by TEM. Grain size in a given polymer was found to be a function of annealing temperature and time.

2. Ionomers

The unique class of ion-containing polymers (ionomers) consists of clusters or domains that are generated by ionic interactions of the charged segments in the polymer chains. These clusters usually have a dimension in the range of 1−4 nm that can be characterized by the SAXS technique. A comprehensive review of the SAXS studies of bulk ionomers has recently been made by Chu.[195] The high brilliance of synchrotron SAXS was found to be particularly useful to resolve the details of the ionic structure. For example, Chu et al. demonstrated that precise synchrotron SAXS curves of Na and Zn salts of sulfonated polystyrene could be obtained by using a modified Kratky block collimation system.[196,197] The results supported the formation of ion-rich phases by showing a corresponding glass transition temperature. The ionic domain structures at elevated temperatures could be analyzed by using Porod's law and the Fourier transformation technique.

Using the synchrotron SAXS technique, the crystallization, melting, and dissolution behavior of zinc stearate (ZnSt) in ZnSt-filled sulfonated poly(ethylene-*co*-propylene-*co*-ethylidene norbornene) (SEPDM) ionomers was studied in real time by Jackson et al.[198] Temperature-dependent SAXS patterns showed that upon melting some or all of the ZnSt rapidly dissolved into the matrix, where ionic aggregates in the neat ionomer persisted up to 300 °C, which was way above the melting point of PE. Inomata et al. used synchrotron SAXS to study the behavior of isothermal crystallization of an associated polymer blend, consisting of one-end-aminated polystyrene (APS) and one-end-sulfonated poly(ethylene glycol) (SPEG).[199] Different sample preparation schemes were found to have a profound impact on the phase transition and the kinetics properties of the blend. The difference in the formation of microphases and macrophases in the molten state was responsible for the difference in the crystallization rate of the samples, e.g., the crystallization rate of homopolymer was greater than that of solvent-cast sample, which was greater than that of freeze-dry sample because the freeze-dry sample had the smallest SPEG domains available for crystallization.

The ionic behavior of certain ionomers can only appear in the presence of solvent such as water. These ionomers can be used as proton-exchange membranes. One example is the system of sulfonated styrene−ethylene/butylenestyrene triblock copolymer and sulfonated hydrogenated, random copolymer of styrene and butadiene, which has been studied by high-resolution SANS and synchrotron SAXS.[200] Rabeony et al. investigated the structure development in these membranes upon swelling in water.[200] The dry triblock copolymer exhibited a lamellar structure with a long spacing of 37 nm but with no evidence of sulfonic acid aggregation. Upon hydration, the long spacing increased to 63 nm while retaining the lamellar morphology. The dry random copolymer exhibited an "ionomer peak" at about 5 nm, which increased to 9 nm upon hydration. The ionic behavior of Nafion membranes in water was also studied by synchrotron SAXS by Wu et al.[201] They demonstrated that the Debye−Bueche correlation function approach could be applied to the analysis of the SAXS data. This method was less biased than the fitting of the SAXS profile with a more restrictive assumed morphological model. The sizes of the ion/water aggregates and the most probable interaggregate distance were found to increase with increasing side chain length. A liquidlike model could describe the spatial arrangement of the ion/water aggregates.

3. Liquid Crystalline Polymers

The changes of mesomorphic structure of liquid crystalline polymers in solutions (lyotropic) and in melts (thermotropic) can also be characterized by synchrotron SAXS. For example, Perez-Mendez et al. used the simultaneous synchrotron SAXS/WAXD technique to study the behavior of cholesteric polyesters in aqueous solution and their interactions with the lipid membrane.[202] The chiral behavior with liposomes of racemic lipids and enantiomeric lipids was considered for drug delivery applications. He et al. studied the structure of a self-assembled hydrogen-bonded main chain liquid crystalline polymer by melt mixing two complementary components, A and B, which in their individual states did not exhibit liquid crystallinity.[203] The combined synchrotron SAXS/WAXD/DSC experiments revealed that the polymeric salt had an AABB chain structure and formed a smectic layer with a length of the A−B repeating unit. Buchner et al. investigated the molecular ordering, phase transitions, and chain mobility in liquid crystalline poly(ethylene naphthalene-2,6-dicarboxylate) and its copolyesters with *p*-hydroxybenzoic acid using the combined method of WAXD and DSC.[204] Campoy et al. used synchrotron SAXS to study the polymorphic transformations that occurred with increasing temperatures and the corresponding structural changes in blends of nylon 6 and a liquid crystal copolyester Vectra.[205]

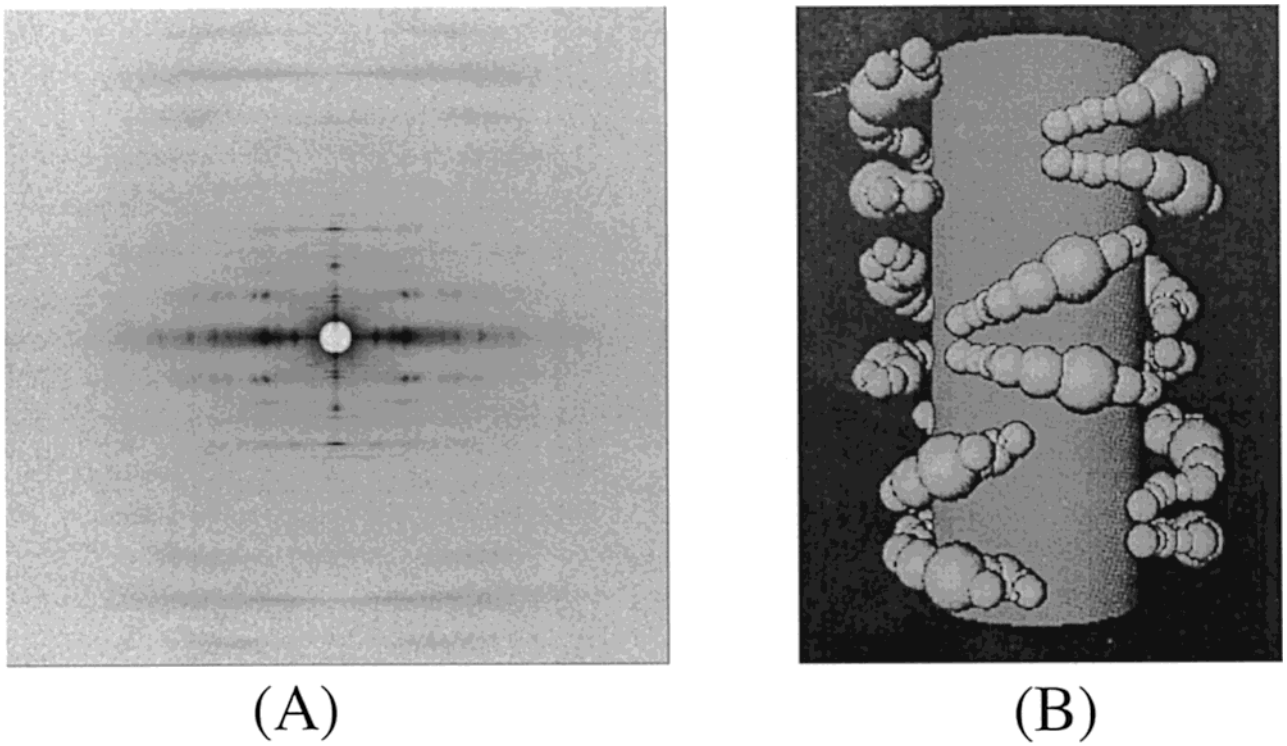

Figure 18. 2D SAXS image from a muscle bundle, under ATP-depleted conditions. The layer lines mainly arise from the actin filament with myosin bound to it (the first layer line is at 365 Å spacing). The corresponding supramolecular structure is illustrated at right. (Reprinted with permission from refs 210 and 211. Copyright 1995.)

In-situ fiber spinning X-ray scattering experiments from the lyotropic dope of rigid polybenzoxazole (PBO) were carried out by Dow scientists.[122,123] The general scheme for drawing PBO fibers started with a dry-jet wet-spinning process from a 13−15% polymer solution in polyphosphoric acid (PPA). The fiber structure was then developed by coagulation in H_2O. The drawing process before coagulation was studied in detail by in-situ synchrotron WAXD. From this work, the effects of line tension, spin draw ratio (SDR), and temperature on the orientation parameter and the microdomain size were determined. Typically, orientation parameters of about 0.95 were obtained for the uncoagulated monofilament with SDR values of about 20. Coagulation brought about the rapid formation of a crystal solvate with a monoclinic unit cell structure. At the same time, a microfibrillar microstructure was fixed in the filament by SAXS.[206]

4. Biopolymers

Most biopolymers exhibit some forms of mesoscopic properties in aqueous solutions. As the electron density contrast under the in vitro environment is weak and the mesoscopic structure can be complex, these systems are ideal to be studied by synchrotron SAXS with well-defined high-intensity beams. Bordas and Koch demonstrated the use of X-ray scattering and diffraction techniques to study monodiperse macromolecules in solutions, dispersed solids, and partially ordered systems.[207] In this section, several recent synchrotron SAXS studies of biopolymers are reviewed.

For complex structures, Salditt et al. used synchrotron SAXS to study the mutilayered, self-assembled structures of mixtures of DNA and cationic liposomes.[208] In these mixtures, DNA was confined between charged lipid bilayers and formed a two-dimensional (2D) smectic ordering. Bouwstra et al. studied structural changes of the lipids in human and hairless mouse stratum corneum after heating the stratum corneum to various temperatures using synchrotron SAXS.[209] Yu and co-workers used synchrotron SAXS to address the question as to how muscle generates force and produces physical displacements at the expense of using the energy released by ATP hydrolysis. Skeletal muscle fibers mainly consisted of two types of protein filaments, the myosin-containing filaments and the actin-containing filaments.[210,211] Force was generated by interactions between myosin and actin. Conformational changes were found within the actin−myosin complex, and significant movement of the filaments was seen during shortening. A typical SAXS pattern of the myosin-containing filaments and the molecular modeling schematics are illustrated in Figure 18.

In the case of a less complex structure, diffuse SAXS profiles can be detected. Jenkins et al. studied the effects of hydrolysis on the structure of three types of starch and their subsequent gelation behavior.[212] By fully fitting the SAXS curves from different regions within the starch granule, they verified the preferential destruction of the amorphous phase during the hydrolysis process. The structures of starch, in fact, are quite complex. Donald et al. used the microfocus SAXS technique to scan across the starch granule and reported the intricate lamellar structures within the granule.[213] Sano et al. reported the size and shape of A-protein of tobacco mosaic virus coat protein (TMVP) and cucumber green

mottle mosaic virus coat protein (CGMMVP) by synchrotron SAXS.[214] They concluded that in the A-protein structure, the globular core structure was a subunit which could be modeled as a thin isosceles triangular prism composed of four globular cores joined by rather flexible segments. These cores were probably related to four helical regions in a subunit and could rearrange their relative positions according to external conditions. Barteri et al. used SAXS to study the influence of glycerol on the structure and stability of ferric horse heart myoglobin.[215] They found that both tertiary and secondary (α-helix) conformations of the protein were influenced by glycerol. Congiu Castellano et al. studied the conformational changes of lyophilized samples of apo-, mono-, and diferric-human transferrin by the fractal analysis of the SAXS data.[216] Miles et al. used synchrotron SAXS to study 11S soya globulin. Submaxima at higher angles were recorded which have not been seen previously.[217] Such detailed information in the scattering curve is important for structural modeling of this protein. Bonnete et al. used agarose gels in combination with synchrotron SAXS to follow hen egg white (HEW) lysozyme nucleation and growth.[218] The advantage of using gels rather than solutions was that the nucleation centers could be trapped in the gel network, allowing the time-resolved experiment by SAXS.

To clarify the mechanisms of folding and unfolding in proteins, several studies of thermal denaturation of proteins have been carried out at low protein concentrations as thermal denaturation accompanied a great tendency of aggregation. By using synchrotron SAXS, Shigeki et al. found that the presence of repulsive interparticle interaction between proteins could maintain solute particles separation to prevent further aggregation in thermal denaturation processes of hen egg-white lysozyme (HEWL).[219] As pointed out earlier, the pressure-induced folding/unfolding of wild-type staphylococcal nuclease (Snase WT) was studied by Panick et al.[159,160] They found that the pressure-induced denatured state at >3 kbar retained some degree of β-like secondary structure, and the molecules could not be described as a fully extended random coil.

B. Phenomenon-Based Studies

1. Polymer Solutions and Gels

SAXS is one of the best available techniques to measure the compactness and shape of macromolecules, especially when the size is small, such as proteins (for examples, Kataoka et al.,[220−222] Flanagan et al.,[223,224] Nishi et al.,[225] and Lattman[226]). The molecular parameters revealed by solution SAXS include the radius of gyration (R_g), the maximum dimension, the shape, and the globularity. Furthermore, high-q SAXS profiles will provide information on the polymer inner structure, which can be correlated, for example, in the case of proteins, with interactions between secondary structural elements. The SAXS results thus complement the results obtained by other techniques, such as NMR. As a result, SAXS has been combined with magnetic birefringence to study the orientational behavior of microtubules assembled in strong magnetic fields (Bras et al.[227]) and with other techniques to study the polymer association process (Uversky and Fink[228] and Chu et al.[109]).

SAXS of polymers in solution invariably leads to the protein-folding problem as one of the most challenging research topics of current interest. Earlier results have emphasized the structural characterization of the native and equilibrium molten globule. SAXS studies of the equilibrium molten globule states of cytochrome *c*, apomyoglobin, and α-lactalbumin as well as of partially folded fragments of nuclease have been reported (Dolgikh et al.,[229] Flanagan et al.,[223,224] Kataoka et al.,[220−222] and Gast et al.[230]). Recent SAXS studies of the equilibrium unfolding of hen lysozyme at low pH have provided evidence for the formation of a subpopulation of partially folded molecules (Chen et al.[231]). With synchrotron X-rays, both stopped-flow (Kihara[232]) and temperature-jump (Hiragi et al.[97]) systems have been developed for kinetic solution SAXS studies. The kinetic studies indicate a major problem of molecular association or aggregation during the protein-folding process (Eliezer et al.[233,234]). More intense X-ray sources are required as the data collection time becomes too short for fast kinetic studies (Kataoka and Goto[235]). Eliezer et al. were able to obtain the radius of gyration of sperm whale apomyoglobin 100 ms after initiation of folding by rapid dilution of a solution containing 5.6 M urea.[233,234] In essence, only integrated SAXS intensity was applied successfully for a direct monitoring of fast intramolecular globularization during protein folding (Semisotnov et al.[236]). Equilibrium unfolding of hen egg lysozyme as a function of urea concentration at pH 2.9 has been studied by solution SAXS as well as by far and near UV CD at 222 and 298 nm, respectively (Chen et al.[237]). By using a combination of time-resolved SAXS and time-resolved tryptophan fluorescence, together with the rate of formation of native molecules using interrupted refolding experiments, the structural characteristics of a nonspecifically collapsed state of lysozyme at low pH have been reported.

The analysis of radial autocorrelation functions in terms of long-range and short-range correlations has been used to examine the details of SAXS profiles. The type of information that can be extracted on the overall structure, as well as the internal structure of polymers, makes SAXS a useful probe. In recent years, while Kratky plots of SAXS data are useful to study association-induced folding of globular proteins (Uversky et al.[238]), attempts have been made to calculate SAXS profiles using a variety of approaches. These approaches include rigid body motion in crystalline lysozyme as probed by molecular dynamics simulation for X-ray diffuse scattering (Hery et al.[239]) as well as modification of the atomic structure factor of subunits of thiamine diphosphate from the original crystallographic model. More importantly, SAXS has recently been analyzed with a new method to retrieve convergent model structures that fit the experimentally determined scattering profiles (Chacon et al.[240]). Instead of attempting to complete the Debye formula

Table 2.

method		obtainable parameters
Guinier plot	ln $I(q)$ vs q^2	radius of gyration, molecular weight (or aggregation)
Kratky plot	$q^2 I(q)$ vs q	to get peak intensity and persistence length
$P(r)$	$(1/2^2) \int I(q)(\sin qr/qr)dq$	d_{max} (molecular size/shape)
$I(q)$ at high q values		internal structure

for all the possible mass distributions, low-resolution structures of proteins in solution are retrieved with an algorithm that efficiently searches the configurational space and evolves best-fit bead models based on X-ray crystal structures in the presence of noise. Approaches that try to take into account the time-evolution of tertiary and secondary structures with known native and denatured states of proteins can clearly improve the SAXS technique as a powerful tool to investigate the kinetics of protein folding as well as the interactions with other macromolecular assemblies. While these approaches are often not applicable to polymer solutions in general, it is noted here that for synthetic polymers with more complex molecular architecture, one can then take a similar route of analysis.

The characteristic length scales determined from SAXS deal with not only the overall size and shape of the polymer molecule, but also its internal secondary structure, if any. The length scales of secondary and tertiary structures of the protein, as expressed in terms of the hydrodynamic radius (R_h) from dynamic light scattering (DLS), the radius of gyration (R_g), and the intraparticle scattering factor *P(q)* from SAXS and the secondary structure, if any (e.g., from CD), imply the use of appropriate experimental setups in the different techniques which satisfy the required temporal and angular ranges (e.g., delay time increment and range in DLS and appropriate q range in SAXS). For synchrotron SAXS with modern X-ray optics and detection systems, the excess scattered intensity, I, can be obtained over a large range of q. It is essential to reduce the parasitic scattering and background so that $I(q)$ at large q values can have an acceptable signal-to-noise ratio.

The excess scattered intensity from a macromolecule can be expressed in terms of a difference in the electron density, $\Delta\rho(= \rho_1 - \rho_o)$, between that of the macromolecule (ρ_1) and of the solvent (ρ_o) as well as the volume (v) of the macromolecule

$$I(q) = (\Delta\rho v)^2 F^2(q) \tag{2}$$

where $F(q)$ is the normalized form factor ($F(0) = 1$) with

$$F(q) = \int \rho_1(r) e^{-iqr}\, dV \tag{3}$$

and V being the scattering volume of the macromolecule. It is noted that solution SAXS only measures the electron density distribution averaged in time over all orientations.

Kataoka and Goto showed an instructive table (Table 2) outlining the analytical methods of solution SAXS in terms of obtainable parameters and corresponding properties.[235] It is, of course, understood that the data analysis includes corrections for parasitic scattering, background, attenuation, incident intensity variation, and desmearing[4] before one proceeds with any determination of the structural parameters. In particular, the distance distribution function $P(r)$ involves a conventional Fourier transformation with the main problems being the termination effect due to finite q ranges of the experiment and the remaining background scattering at large q values. One must be careful with the Fourier ripples.

Synchrotron SAXS has also been used to investigate solutions of native DNA at different ionic strengths and temperatures. For large DNA fragments, the mass per unit length, the radius of gyration of the cross-section of DNA, and the apparent second virial coefficient (A_2) could be obtained from the Zimm plot in the rodlike approximation (Barone et al.[241]). The positive and almost constant A_2 value suggested dominating repulsive interactions even at resolutions of 5−8 nm. The rodlike−wormlike transition temperature was found to increase with increasing ionic strength.

The ability to mix liquids in microseconds has expanded the accessible time scales and ushered in a new era for kinetic studies (Beechem[242]). Regenfuss et al. pioneered the development of a continuous-flow *microsecond* mixing device.[243] Microsecond mixing studies of protein folding have appeared only recently (Takahashi et al.,[244,245] Chan et al.[246]) utilizing a T-mixer version of the original Regenfuss et al. design.[243] On the basis of an adaptation of this design, Shasty et al. reported a detailed description of the assembly and operation of a modern microsecond mixing, continuous-flow instrument in which the reaction kinetics were followed by measuring fluorescence versus distance downstream from the mixer.[247] With a mixing time of about 15 μs after its initiation and a dead-time of the measurement of 45 $\pm$ 5 μs, the work revealed that the kinetic data become accessible down to about 50 μs. Kinetic studies over a time scale ranging from $\sim$50 μs to tens of seconds should enhance our understanding of the mechanism of protein folding, as well as a wide variety of other important biological reactions. It was noted that shorter time scale measurements (e.g., laser-based T-jump approach in the nanosecond range) were also needed to help bridge the gap between the reaction rate theory (picoseconds to nanoseconds) and the biological structure/function (ΔA per picosecond to microsecond to millisecond to second).

In the Shasty et al. capillary mixing apparatus,[247] the quartz flow cell had a 250 μm diameter channel that might be translated into a more demanding need on the quantity of protein required to undertake a thorough kinetic study on the protein-folding problem. Furthermore, this arrangement, while excellent for optical measurements, could not be adapted easily for SAXS experiments. The mixer designed by the

Eaton group[246] was more robust and had been adapted for SAXS measurements, although the mixer construction was quite demanding. Recently, Knight et al.[248] developed a rapid-mixing microchannel continuous-flow cell that has been adapted successfully by Sol Gruner at Cornell University for synchrotron SAXS experiments (Pollack et al.[249]). The Austin design (Knight et al.[248]) can be modified to perform kinetic studies using either X-rays or lasers with identical geometrical pathways. In addition, it has the potential to reach even shorter reaction times and uses a smaller volume, which can be further reduced in combination with micro X-ray beams available at the third-generation synchrotron light sources, such as the Advanced Photon Source.

2. Colloidal Suspensions, Micellar Solutions, and Microemulsions

Small colloidal particles in suspensions as well as microemulsions and micelles often have sizes very suitable for measurements by means of SAXS. Characteristics of aerosol-OT reversed micellar formation (Hirai et al.[193,250]) as well as the structures of microcapsules (Dobashi et al.[251]) and of block copolymers (Hilfiker et al.[192] and Wu el al[252,253]) have been investigated by means of SAXS, especially in combination with laser light scattering. SAXS has also been used to study thermotropic phase transitions (Hirai et al.[254]) and the sol−gel process (Gaponov et al.[255]).

SAXS studies of dilute suspensions of photonic colloidal crystals were reported by Vos et al.[256,257] and Megens et al.[258,259] They found that scattering from dilute suspensions was related to the particle form factor. The radius, size distribution, and information about the internal structure of the particles could be determined from the analysis. With the experimentally determined particle form factor, structure factors were extracted from the diffraction patterns of the colloidal crystals. The crystal structure, lattice parameters, and average orientations were then determined. Thus, a combination of SAXS/WAXD can be used effectively to study the morphology and crystal structures of colloids. More examples included a similar SAXS study by Diat et al.,[260] crystallization study by Nojima et al.,[261] in-situ crystallization study by de Moor et al.,[262] and phase separation kinetics study by Li et al.[263]

A morphological characterization of bicontinuous phase-separated polymer blends and one-phase microemulsions has been reported by Jinnai et al.[264] The morphological similarity of the two systems permitted one to use the same approach to carry out the analysis. Berk developed a theory to analyze the scattering data from bicontinuous microemulsions and subsequently to generate the three-dimensional morphology.[265] Chen et al. proposed a peaked spectral function with a power law decay at large wavenumbers.[266] By applying this approach (called a modified Berk or MB theory) with a three-parameter spectral function and the Cahn[267] clipping scheme to calculate the Debye correlation function (Debye el al[268]) for the scattered intensity, the random wave model could then be used to generate the 3D morphologies. The analysis was complex, and the experimental demand for precision and the q range was relatively high, often requiring intensity measurements covering 4−5 orders of magnitude. A representation of the 3D morphology for a polymer blend and a bicontinuous microemulsion is shown in Figure 19.

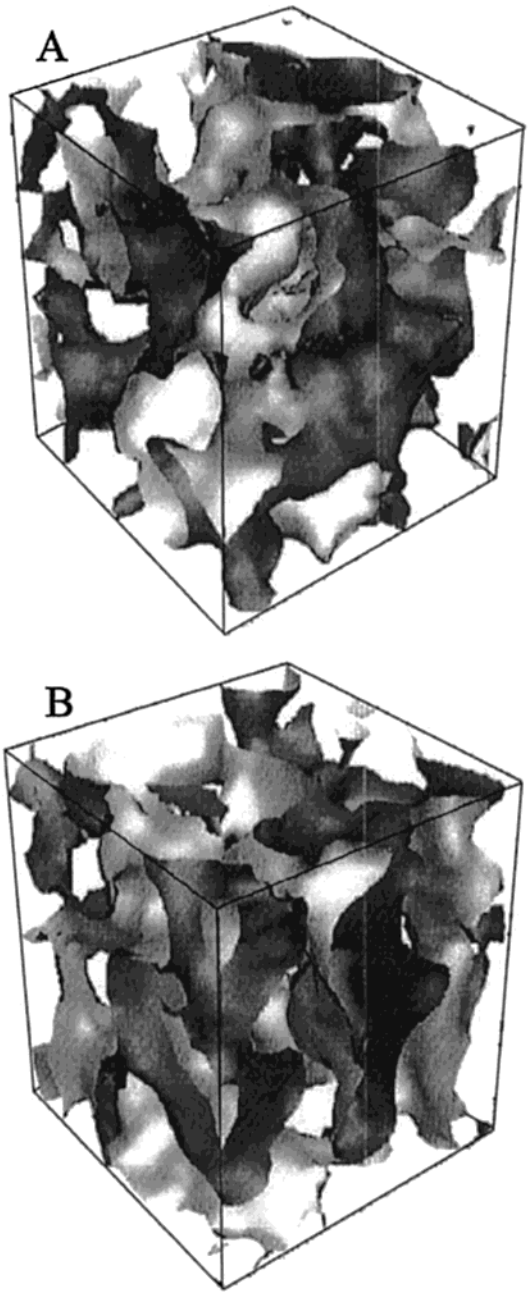

Figure 19. (A) 3D morphology of the phase-separated polymer blend (box size, 22.4^3 μm^3). (B) 3D morphology of the one-phase bicontinuous microemulsion at the hydrophile−lipophile balanced temperature (box size, 800^3 $Å^3$). Both are generated from the MB theory with three fitting parameters obtained from the best fit to the corresponding scattering profiles. (Reprinted with permission from ref 264. Copyright 1997 American chemical Society.)

3. Polymer Gels

SAXS and laser light scattering are powerful and complementary tools to investigate the structure and dynamics of polymer networks in solutions (gels). The structural changes in polymer gels can be induced by pH (Hirai et al.[269]), temperature (Izumi et al.,[270]

Liao et al.[271]), ionic strength, and other physical parameters.[272] Some example studies are listed as follows.

The level of pH has a profound effect to change structures in polymer gels. Hirai et al. studied the pH-induced structural change in poly(vinyl alcohol) (PVA) hydrogels cross-linked with poly(acrylic acid) (PAA) by means of synchrotron SAXS.[269] The physically cross-linked gel formed by blending of PVA and PAA in an aqueous solution was compared with the chemically cross-linked gel by esterification of PVA with PAA in the hydrogel state. The chemical cross-linking was found to convert the physical cross-links into a folded structure. SAXS results suggested that the folded structure exhibited a fractal rough interface, which could change into the structure of percolation clusters at a high pH level. The gels immersed in pH 8 showed a remarkable structural change accompanying the swelling. The conformational change of the PAA chains, induced by the pH change, was used to explain the presence of a structural change in an interpenetrating polymer network.

Temperature also plays an important role on the structure in gels. The spinodal decomposition behavior in a covalently cross-linked *n*-isopropylacrylamide gel was studied by Liao et al. using SAXS.[271] Following a temperature jump into the two-phase region, the scattered intensity was found to increase with time and eventually to become saturated.[271] The early-stage data could be described by the linear Cahn−Hilliard−Cook (CHC) theory.[267] At later times, a pinning of the structure was also observed. The behavior of a two-stage melting process in dilute gels of poly(γ-benzyl L-glutamate) was studied by Izumi et al. using synchrotron SAXS.[270] DSC heating trace exhibited two endotherms, indicating the melting of two types of aggregates. SAXS measurements showed that the two-stage melting of the aggregates was due first to the melting of bundles of three rods and then to that of bundles of two rods. Above the two-stage melting temperature, the gels transformed into isotropic solutions with no aggregation of polymer chains.

The presence of inorganic particulate often induced gellike structures in polymer solution, which can be studied by synchrotron SAXS but not light scattering as the solution is opaque. For example, de Lange et al. used synchrotron SAXS to study the sol−gel behavior in polymeric SiO_2 with SiO_2/TiO_2, SiO_2/ZrO_2, and SiO_2/Al_2O_3 binary sols.[272] This system was designed for ceramic membrane applications. The aggregation of silica sols was found to obey the tip-to-tip cluster−cluster aggregation model in the initial stages.

Gel can form self-assembled structures. For example, the sol−gel transition of gellan gum aqueous solution in the absence of added salts was studied by Izumi et al.[273] using synchrotron SAXS. Results indicated that the cloudy gels exhibited three scattering peaks, which were in the simple ratio of 1:2:3, suggesting that the junction zones in these gels were formed by a lamellar structure. These peaks shifted to a lower scattering vector as the content of the added ions was increased, indicating the formation of larger lamellae. The flow-induced orientational and morphological changes in structured gels were studied by Vigild et al.[274] They investigated face-centered cubic (fcc) and body-centered cubic (bcc) phases in gels of poly(oxyethylene)−poly(oxybutylene) diblock copolymers and for the bicontinuous cubic 'gyroid' structure in a poly(ethylene-*alt*-propylene)−poly(dimethylsiloxane) diblock copolymer melt. The orientations of the micellar bcc phases in the gels and the gyroid structure (belonging to the bcc space group) following large-amplitude shearing were essentially the same, i.e., directionally oriented crystals are produced in both cases, in which (111) directions were oriented along the shear direction. A typical SAXS profile of PMMA gel with C_{12}TA complex is shown in Figure 20 (Zhou et al.[275]). The scattered peaks are indexed by a cubic structure of *Pm*3*n* space group. The dotted line represents the calculated scattering curve based on the connected unit cell model shown in the inset.

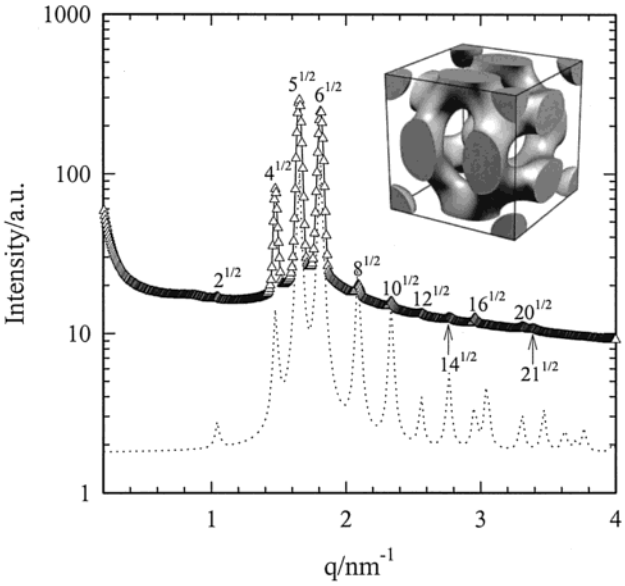

Figure 20. SAXS profile of PMMA gel with C_{12}TA complex. The scattered peaks are indexed by a cubic structure of *Pm*3*n* space group. The dotted line represents the calculated scattering curve based on the connected unit cell model shown in the inset. (Reprinted with permission from ref 275. Copyright 2000 American Chemical Society.)

4. Polymer Blends

Commodity polymers can be made useful by mixing them under appropriate conditions. The key aspect is the structure−property relationship of the materials, which can form microphase domains in a phase separation process. The understanding of this process can lead to improved properties.

One common SAXS study is based on the binary blends, in which one or both components can crystallize. The kinetics of crystallization can be followed under isothermal conditions in real time by simultaneous SAXS, WAXD, and small-angle light scattering (SALS). Stein and co-workers carried out a study involving blends of linear high-density polyethylene (HDPE) and branched linear low-density polyethylene (LLDPE).[95,276] In this study, variables

such as degree of crystallinity, crystal perfection, lamellar thicknesses, and their distribution, spherulite size, and spherulite optical anisotropy have been followed. It was found that the crystallization process exhibited non-Avrami behavior, and the resultant morphology was controlled by the competition between crystallization and diffusion of the crystallizing chains. A further investigation can involve studies of crystallization where phase separation will occur in the amorphous phase. This can take place when molecular weights of the components and/or the degree of branching in LLDPE are sufficiently high. Nojima et al. used synchrotron SAXS to study the crystallization of poly(ϵ-caprolactone) and poly(ϵ-caprolactone)/poly(vinyl chloride) blends as well as poly(ϵ-caprolactone) and polystyrene oligomer blends.[277,278] In their systems, the SAXS curves indicated a possible coexistence of the crystal region and the amorphous region throughout the morphological formation in the blend. Cheung et al. studied the evolution of crystalline structures in poly(ϵ-caprolactone)/polycarbonate blends.[279] An insertion mechanism was proposed in which the PCL was crystallized in the amorphous intralamellar phase. Eersels et al. investigated the effect of transreaction processes on the morphology of semicrystalline aliphatic/aromatic polyamide (PA) blends.[280] They concluded that polyamide copolymers consisted of both crystallizable PA 46 and noncrystallizable PA 6I sequences after the transreaction. Hsiao et al. studied the crystallization behavior of poly(ether ether ketone)/poly(ether imide) blends,[281] and they reported that PEEK crystallized in densely crystalline lamellar stacks through all stages of primary crystallization, noting that the noncrystalline PEI was almost entirely excluded from the stacks at all times during spherulitic growth. Wang et al. used simultaneous SAXS/WAXD techniques to study the microstructures of PEEK/PEKK blends at both structural and lamellar levels.[282] Liu et al. studied the crystallization of miscible blends of semicrystalline poly(vinylidene fluoride) (PVF2) and semicrystalline poly(1,4-butylene adipate) (PBA).[283,284] They concluded that that PBA could crystallize as a thick lamella in the PVF2 interlamellar region and that there was a mixed amorphous phase on either side of the PBA lamella, i.e., between the PBA and PVF2 crystal lamellae. Yeh et al. studied the effects of miscible polymer diluents on the development of lamellar morphology in poly(oxymethylene) (POM) blends.[285] They reported that lamellar thickening with time in the long-time secondary crystallization region was observed in neat POM and the blend with 10% low-T_g diluent, while this process was inhibited with the high-T_g diluent due to the higher T_g values of the interlamellar species.

In addition to the crystallization study, several different types of SAXS experiments have also been carried out for polymer blends. Vandermarliere et al. studied the morphological changes during melting of polycaprolactone and poly(styrene-*co*-acrylonitrile) blends.[286] Wilkson et al. studied the melting, reaction, and recrystallization behavior in a reactive PC−PBT blend.[287] They reported that increasing transesterification resulted in a progressive reduction in the melting and crystallization temperatures and degree of crystallinity with the development of a mixed-phase glass. Inomata et al. used synchrotron SAXS to study an associated polymer blend consisting of one-end-aminated polystyrene (APS) and one-end-sulfonated poly(ethylene glycol) (SPEG).[199]

For blends containing no crystallizable components, synchrotron SAXS is also useful to characterize the structure and to correlate with the properties. Okamoto et al. studied plastic deformation (crazing and shear yielding) of high-impact polystyrene/poly(2,6-dimethyl-1,4-phenylene ether) blends.[288] Chu et al. used synchrotron SAXS to study the local concentration fluctuations in a poly(2-chlorostyrene) and polystyrene blend, which was induced by temperature jumps. They concluded that the blends in the immediate neighborhood of the critical mixing point could be used to locate the critical mixing point precisely.[289−291] Rabeony et al. used a combination of SAXS, calorimetry, and cloud point measurements to determine the phase diagram of the poly(cyclohexyl acrylate) and poly(2-bromostyrene) blends.[292]

5. Polymer Crystallization

The combined synchrotron SAXS and WAXD technique is an ideal tool to study the structural and morphological changes during crystallization and melting in polymers. The published articles in this area are abundant: (poly(aryl ether ketones),[293−304] polyimides,[305,306] aromatic polyesters,[307−316] ethylene-based copolymers,[317−324] biodegradable aliphatic polyesters,[325,326] poly(ethylene oxides) and copolymers,[327−332] and polyamides[333−335]). In this section, we will emphasize some new findings in the field of polymer crystallization from the use of synchrotron SAXS. These findings are as follows.

During isothermal crystallization study, the evolution of a distinct scattering maximum is usually observed. For semicrystalline polymers, these SAXS profiles can be analyzed via a combination of the correlation function $\gamma(r)$ and the interface distribution function $g(r)$.[336−339] Using a finite lamellar stacks model, morphological variables such as long period (L), lamellar thickness (l_c), amorphous layer thickness (l_a), and the scattering invariant Q can be calculated. For the analysis of time-resolved SAXS profiles, Hsiao and Verma[340] devised a practical approach to extract morphological variables. The principle of the calculation is based on alternative expressions of the Porod law. The approach enables a continuous estimate of the Porod constant and corrections for liquid scattering and finite interface between the two phases, from the time-resolved data. Figure 21 shows typical morphological results derived from the SAXS profiles for PE during isothermal crystallization. It is found that during primary crystallization, both average long period (L) and lamellar thickness (l_c) exhibit a significant decrease. During secondary crystallization, these values show a smaller decrease over a longer period of time, which is approximately linear with log time.

The decrease in the long period with time during crystallization appears to be a universal behavior in

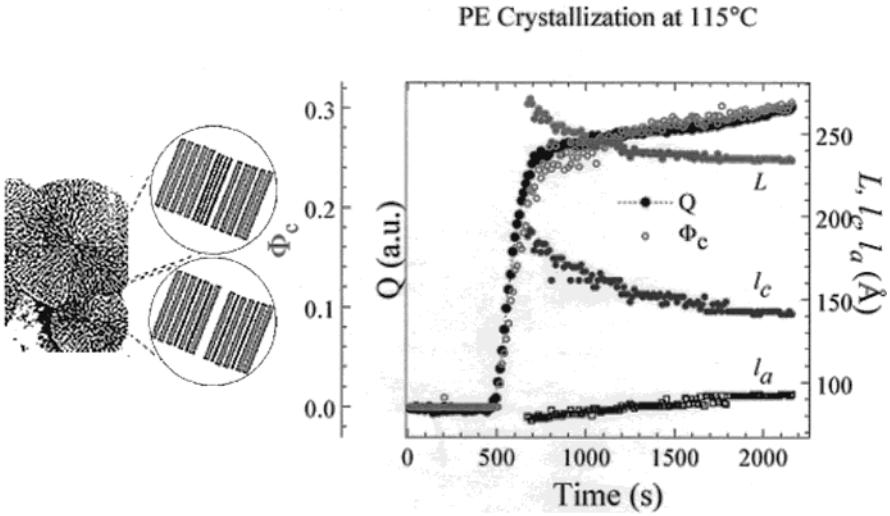

Figure 21. Changes of long period (L), crystal lamellar thickness (l_c), amorphous layer thickness (l_a), invariant (Q), and crystallinity (Φ_c) during isothermal crystallization of PE (at 115 °C). The left diagram illustrates the possible lamellar insertion mechanism during secondary crystallization.

semicrystalline polymers. This decrease was first documented by Zachmann and co-workers in PET[341] and later by Keller in PS[342] and has been reproduced recently by several other authors in a variety of other systems (PEEK,[293,297−299,303] PET,[307−311] PBT,[315] ethylene-based copolymers,[317−324] and PLA, PGA, and PGA-*co*-PLA[325]). The observed decrease in long period with crystallization time for semicrystalline semi-stiff polymers is in stark contrast to the reported increase in long spacing for flexible polymers (see, for example, the work of Fischer and Schmidt [343] in polyethylene). The dual-lamellar stack model can best describe the changes in the long period during isothermal crystallization. In this model, primary lamellar stacks are formed first comprising thicker crystalline lamellae whereas secondary lamellar stacks are formed later. The decrease in the average long spacing is due to the formation of secondary lamellar stacks between the existing stacks or the insertion of thinner lamellae within the existing stacks. It was found that both secondary and primary lamellar stacks could undergo a great deal of crystal perfection and rearrangement with time. In semi-stiff chain polymers such as PBT,[315] PET,[307−310] PGL,[325] and nylon,[333] no lamellar thickening process could be observed during the isothermal annealing process. Very often these stiff-chain polymers exhibited a multiple-melting behavior during heating in DSC, which was due to the consequence of sequential melting of thinner secondary lamellae, thicker primary lamellae, and recrystallized crystallites with good lateral crystal perfection. These behaviors have been verified by the SAXS/WAXD measurements during heating of the polymers. The PEO system exhibited both isothermal thickening and isothermal thinning processes due to the thermodynamic driving force of integral folding from nonintegral folded chain crystals.[327−332] The effects of chain branching and polymer blending could significantly retard the thickening process.[317−321]

For the determination of correct lamellar thickness, we would like to caution one aspect of the correlation function method. Briefly, the SAXS data can be "unambiguously" analyzed to obtain an average long period (sum of the lamellar and amorphous layer thicknesses) and two estimates for the crystal and amorphous thicknesses. The long period (L) can be calculated from the first maximum in the correlation function. However, for the estimate of lamellar thickness, the correlation function has to be compared with the calculation of a model electron density profile. The ideal two-phase model is often used for this purpose, and most authors favor the method outlined by Strobl and Schneider.[338] Although the analysis reveals two thicknesses of the constituent phases, it cannot distinguish which one represents the crystal lamellar thickness. Since it is not possible to mathematically identify the correct value of the lamellar thickness from the SAXS data alone, information from other techniques is required for this purpose.

An interesting observation has been reported during isothermal crystallization of some quenched glassy polymers such as PET[342−347] and poly(ether ketone ketone) (PEKK)[348] samples. It was found that the SAXS peak appeared *before* the WAXD crystalline peaks. It was thought that the SAXS peak was brought about by density fluctuations on the order of 80−200 Å while the WAXD crystalline peaks were brought about by the three-dimensional crystalline order. Thus, the appearance of the SAXS peak before the WAXD peaks suggested that density fluctuations might serve as a precursor to initial crystallization. Using simultaneous SAXS/WAXD methods, Ryan and co-workers observed this behavior during melt crystallization of iPP[349−351] while Hsiao and co-workers also saw this behavior during melt crystallization of PBT.[315] Imai et al.[344−347] and Olmsted et al.[351] suggested that density fluctuations in the induction period might follow the mechanism of spinodal decomposition. The thermodynamic driving force for the spinodal decomposition could be due to the coupling between the chain conformations, which induced a liquid−liquid binodal within the equilibrium liquid−crystal solid coexistence region. However, a recent study by Hsiao and co-workers[352,353] indicated that the observation of SAXS signals before

WAXD could be explained simply by the detection limits of the different techniques. They reported that WAXD detected only a minimum level of crystallinity at about 1%, SAXS detected about 0.1%, and light scattering (LS) detected about 0.01%. In addition, the initial stages of the crystallization kinetics data from WAXD, SAXS, and LS during isothermal melt crystallization of iPP all could be described by a simple Avrami equation, which was inconsistent with the spinodal decomposition behavior but more in line with the nucleation and growth processes. Thus, the detailed nature on the initial stages of polymer crystallization still awaits further more definitive experiments.

6. Chemical Reactions (Polymerization)

During the process of polymerization (in solutions or in melts) or curing, the electron density of the forming polymer is likely to be larger than the reacting medium. As a result, the scattering contrast is often increased and the process can be monitored by time-resolved synchrotron SAXS. Several examples are listed as follows.

Ryan and co-workers[354−358] studied the in-situ polymerization and microphase separation processes of polyurethanes using a reaction injection molding (RIM) apparatus coupled with synchrotron SAXS. They reported that the microphase separation transition (MST) occurred at a critical conversion of isocyanate functional groups and hydrogen bonding followed the kinetics associated with the process of nucleation and growth. Microphase separation generated a nonequilibrium, co-continuous morphology with a size scale of about 100 Å. Winans et al.[359] used synchrotron SAXS to carry out reactivity studies on coals, asphaltenes, and polymers. The objective of this study was to examine changes in the structures of coals, asphaltenes, and polymers during thermal reaction. Lyakhov et al.[360] used the synchrotron SAXS methods to study the structure of the reaction zone for topochemical transformations and the kinetics of phase formation in solid−solid and sol−gel processes in situ. Ogasawara et al.[361] studied the acid-catalyzed condensation reaction of perfluorooctyltrimethoxysilane (PFOS) and *n*-octyltrimethoxysilane (OTMS) in ethanol with time-resolved SAXS. Diffuse SAXS profiles from PFOS and OTMS have been interpreted as from mass fractals with fractal dimension (Df) = 2 (PFOS) and Df = 1.7 (OTMS). They suggested that those small clusters, such as monomers, dimers, and trimers, were formed in the initial step, while larger clusters were formed in the second step.

7. Polymer Nanocomposites

Nanocomposites are a broad family of materials consisting of two or more component phases, at least one of which has dimensions between 1 and 100 nm. Over the past several years, nanocomposite materials prepared by dispersing nanometer-scale inorganic particles or molecular clusters in a soft condensed matter matrix (such as polymeric or biological templates) have emerged as useful alternatives to conventional materials and macroscopic composites. The nanocomposites can exhibit markedly improved properties when compared with the neat matrix materials or conventional composites, and they may supplant more traditional materials for many applications where high strength-to-weight ratios are required under extreme conditions. The state of the nanoparticle dispersion can be characterized by synchrotron SAXS in a straightforward fashion.

Vaia et al.[362] used synchrotron SAXS to study the mesoscopic structure of polymer-layered silicate nanocomposites. They reported the presence of ultra-long-range (20−60 nm) mesoscopic order in polyamide six-layered silicate nanocomposites at ultralow loadings (0.8%). These superstructures agreed with theoretical excluded volume calculations and predictions based on modified Onsager free energy functional in combination with the Flory−Huggins free energy of mixing. Barber et al. studied the dispersion of nanoscopic clay particles in thermoplastic polymers such as polystyrene/sulfonated polystyrene, PET/sulfonated PET, and polypropylene/carboxylated polypropylene with SAXS, TEM, and DSC.[363] Ionomeric compatibilizers were used to facilitate a homogeneous dispersion of the clay nanoparticles in the polymer matrix. Chaker et al.[364] studied the structure of silica−polypropylene glycol (PPG) nanocomposites with weak physical bonds between the organic (PPG) and inorganic (silica) phase, prepared by the sol−gel process, with synchrotron SAXS. The shape of the measured SAXS profiles agreed with that expected for scattered intensity produced by fractal aggregates sized between 30 and 90 Å. The correlation length of the fractal aggregates was found to decrease and the fractal dimension was found to increase with increasing silica content. Becker et al. used SAXS and TEM to investigate the mesoscopic structure of thermoplastic nanocomposites containing functionalized silica nanoparticles.[365] The materials were based on a thermoplastic matrix of a copolymer of methyl methacrylate and 2-hydroxyethyl methacrylate with spherical 10-nm silica particles as fillers. Depending on the surface modification of the particles, it was possible to control the aggregation of the filler particles. Beck-Tan et al. studied the dendrimer-based nanocomposites by synchrotron SAXS and SANS.[366] Nanocomposites containing a dendritic polymer matrix such as PAMAM [methyl propenoate-1,2-ethanediamine copolymer] and copper sulfide inorganic nanoparticles were prepared. They reported that no perturbation of the dendritic species occurred on complexation, and secondary supermolecular aggregation was seen in nanocomposite solutions (by SAXS).

8. Polymers in Flow

In typical flexible or semi-flexible chain polymers, the stability of the oriented chains during flow depends on the relaxation behaviors of the polymer chains in the melt. The longer chain molecules take a longer time for relaxation from deformation than the shorter ones and thus have a better chance to remain oriented. The orientation of the chain segments can induce crystallization. Hsiao and coworkers[132] used synchrotron SAXS to follow the behavior of orientation-induced crystallization in iPP

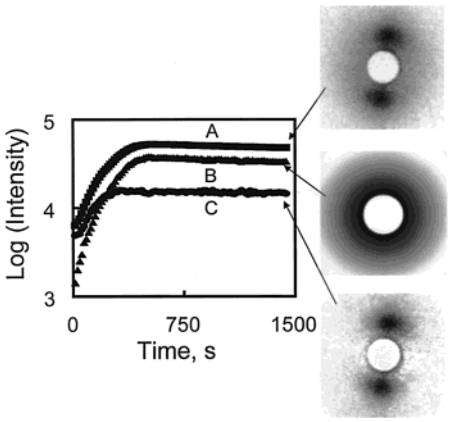

Figure 22. Time evolution SAXS intensity changes during flow-induced crystallization of iPP by step shear (shear rate = 102 s^{-1}, strain = 1428%, temperature = 140 °C): (A) total scattered intensity, (B) scattered intensity from the unoriented crystals, and (C) scattered intensity from the oriented crystals after the step shear. The images correspond to SAXS patterns after t = 300 s.

subcooled melt at 140 °C after step-shear. Two unexpected findings were made: (1) no evidence of the 'shish' morphology and (2) a significant increase in crystallization rate of unoriented crystals. The mass fraction of unoriented crystals during flow relaxation was determined by the following procedures. The total scattered intensity from SAXS was deconvoluted into two contributions from the oriented crystals and unoriented crystals, respectively. The scattered intensity arising from the unoriented crystals (isotropic) was azimuthal independent (a function of the scattering vector q only), while the intensity arising from the oriented crystals was azimuthal dependent (functions of q and ϕ (azimuthal angle)). Typical time evolution profiles of the total scattered intensity (curve A), the intensity from unoriented crystals (curve B), and the intensity from oriented crystals (curve C) after step-shear (shear rate = 102 s^{-1}, strain = 1400%, temperature = 140 °C) are shown in Figure 22.

In Figure 22, it is seen that the total scattered intensity rises rapidly after the application of shear pulse. The initial oriented intensity has a large fraction immediately after shear; the rate of the rise is the fastes, but the magnitude of the rise is the lowest. The unoriented intensity has a low initial value, which arises from the amorphous melt. This intensity rise, representing the evolution of randomly distributed crystals, is found to also increase rapidly with a rate that is only slightly slower than the oriented crystal growth but is still much faster than the growth in the quiescent state. This is rather unexpected as we anticipated that the development of unoriented crystals should mirror the process in the quiescent melt.

On the basis of these observations, Hsiao et al. argued that orientation affects the crystallization both thermodynamically and hydrodynamically.[367] The thermodynamic effect involves entropy reduction of oriented chains and favors the formation of primary nuclei. The hydrodynamic effect generates the landscape of orientation in chains, which leads to growth of a different morphology. They showed that only the polymer molecules above a "critical orientation molecular weight" (M^*) could become oriented at a given shear rate (γ^{Y}). The M^* values at different shear rates were determined from the area fractions of the molecular weight distribution of the polymer. The observed M^* and shear rate has a relationship, $M^* \propto \gamma^{\dot{Y}-\alpha}$, with α being an exponent (0.15 for iPP). They further reported that the variation of molecular weight has little influence on the value of M^*.[368]

The molecular orientation of rigid chain polymers during flow can be directly measured by synchrotron SAXS techniques. Burghardt and co-workers[369−372] used SAXS to characterize the molecular orientation in thermotropic liquid crystalline polymers in both simple and complex (channel) flows. Extensional gradients in a slit-contraction flow significantly increased molecular orientation. In sharp slit-expansion flow, a bimodal molecular orientation state was seen where one population was aligned in the downstream direction and the other was perpendicular to the expected local streamlines. Orientation changes dramatically in contraction and expansion regions, which cannot be explained by changes in superficial velocity alone. In lyotropic solutions, Burghardt et al.[131,373] used X-ray scattering to monitor molecular orientation and investigated the coexistence of hexagonal and nematic phases in highly concentrated PBG/cresol solutions under shear flow. Beyond a threshold concentration, the diffuse nematic lobe in X-ray scattering patterns was found to be accompanied by sharp reflections indicating lateral packing of molecules in a hexagonal arrangement. Relaxation experiments at high shear rates indicated that the final state of the solution was highly sensitive to the presence of the hexagonal phase during shear. They also reported that X-ray and optical data were consistent in showing decreasing orientation in hydroxypropyl) cellulose (HPC) solutions during relaxation, but discrepancies were found in relaxation of PBG solutions.

9. Polymers under Deformation

The deformation mechanism of synthetic polymers and biological fibers (such as spider silks, worm silks, and muscles) has become a major research interest in the polymer community in recent years. To study the structural changes in the mesoscopic and nanoscopic scales during deformation, synchrotron SAXS is definitely one of the most powerful characterization techniques. Several example studies are listed as follows.

Hsiao and co-workers[112,113,124−126,374] carried out online structural and morphological studies on Kevlar 49, iPP, and nylon fibers during a continuous drawing process using simultaneous 2D SAXS and WAXD techniques. A novel image analysis method was used to extract quantitative fractions of the crystal, amorphous, and mesomorphic phases from two-dimensional (2D) WAXD patterns. Results showed that about 20 wt % in the Kevlar 49 fiber had a mesophase morphology. SAXS patterns indicated that the superstructure of the Kevlar 49 fiber was fibrillar in nature. WAXD results of iPP fibers showed that the α-form crystals were quite defective in the initial

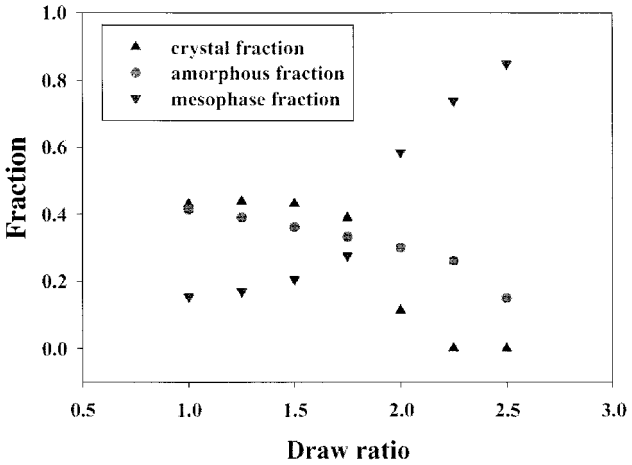

Figure 23. Fractions of crystal, mesormorphic, and amorphous phases of partially crystallized iPP fibers as a function of draw ratio during continuous drawing at room temperature.

state and converted to the mesomorphic modification by drawing at room temperatures. They argued that the constituents of the mesophase in the drawn iPP fibers are oriented bundles of chains with random helical hands which have only partial packing ordering, similar to the mesophase in Kevlar fibers. Hsiao et al.[124] also investigated the structure and morphology development during the heat-draw process of nylon 66 fibers by synchrotron X-ray techniques. They confirmed that the triclinic cell structure persisted above the Brill transition temperature (about 443 K). With increasing temperature, the unit-cell dimension *a* (dominated by hydrogen bonding) remained almost unchanged while *b* increased and *c* decreased (both show a step-change at 403 K, prior to the Brill transition). The constant value of *a* agreed with the argument that the hydrogen bonding is relatively immobile at high temperatures prior to melting. Mass fractions of crystal, mesormorphic, and amorphous phases during continuous drawing of partially crystallized iPP fibers as a function of draw ratio at room temperature is shown in Figure 23

Lee et al.[375] investigated the microphase morphology during the deformation of the segmented block copolymers with synchrotron SAXS and FTIR methods. Depending on the initial orientation of the hard domains, the deformation behavior was found to be very different. While the hard domains oriented along the deformation direction could undergo the extension of the domain separation, the perpendicular ones showed the shear compression. Further drawing was found to cause the breakup of the hard domains, followed by the formation of fibril structure oriented along the deformation direction. Stribeck[376−378] developed a method for the quantitative analysis of 2D SAXS patterns during deformation of segmented copolymers. This method has been applied to a series of images recorded during stretching of a segmented two-phase elastomer. In the study of poly(ether ester) thermoplastic elastomer, the soft domain needles were found to show strain-induced hardening.[376] Results indicated that two microfibrillar components (an intact and a damaged one) were present, which could be identified in the SAXS patterns from samples deformed at medium elongation ratios as well as in the patterns recorded during relaxation from medium elongation.[377] Although the scattering patterns differed considerably, the hard domain distributions extracted from the analysis were identical in both cases. The difference between elongated and relaxed states was in the distribution of the soft domain dimensions. There were also indications for a nonuniform elasticity of the soft domains. Furthermore, only a few microfibrils were simultaneously carrying the load during deformation. They were destroyed one by one, until the fiber broke as a whole.

Synchrotron SAXS has also been used to study the crazing behavior during deformation of glassy polymers. Salomons et al.[379] used SAXS to study deformation mechanisms in liquid rubber-toughened polystyrene. They reported that that crazing was the predominant mechanism of plastic strain in this toughened polystyrene system. Mills et al.[380] investigated the mechanism during fatigue deformation of polystyrene using time-resolved SAXS techniques. At the maximum of the load cycle, the SAXS pattern showed a well-defined streak normal to the craze fibrils. During the unloading part of the cycle, the streak decreased in intensity and was spread into a diffuse profile. The loss of intensity was attributed to the decrease in the volume fraction of the craze. The diffuse spreading of the profile was due to the disorientation of the craze fibrils as they buckled by compression of the surrounding polymer matrix.

10. Polymer Fiber Spinning

The studies of structure and morphology development during fiber melt spinning using in-situ simultaneous synchrotron SAXS and WAXD techniques have recently been carried out in several laboratories. The process of fiber melt spinning is essentially a nonisothermal crystallization process during extensional flow. This process not only is of practical importance; it also represents a case of orientation-induced crystallization in strong flow where the underlying physics is still not understood.

Cakmak et al.[115] carried out on-line SAXS and WAXD studies on melt-spinning of poly(vinylidene fluoride) tape at a variety of take-up speeds. As the take-up speed increased, the crystallization onset position moved away from the die and the *d* spacing observed at the onset increased. The shape of the discrete scattering pattern started as a meridional streak and changed into to a lope. Kolb et al.[121] recently studied the high-speed spinning process of poly(ethylene terephthalate) by the on-line wide-angle X-ray scattering method. For take-up speeds of 3600 m/min and higher, the crystal reflections were found to appear at a distance of 40 cm from the spinneret after the necking region. The crystallization speed increased proportionally to the take-up speed. Below 3500 m/min, no crystallization and no necking could be detected up to a distance of 90 cm from the spinneret. They also investigated a lower speed spinning of poly(propylene).[120] The WAXD data suggested that highly oriented crystals grew out of an apparently unoriented amorphous matrix near the spinneret. Once crystallized, the orientation of the

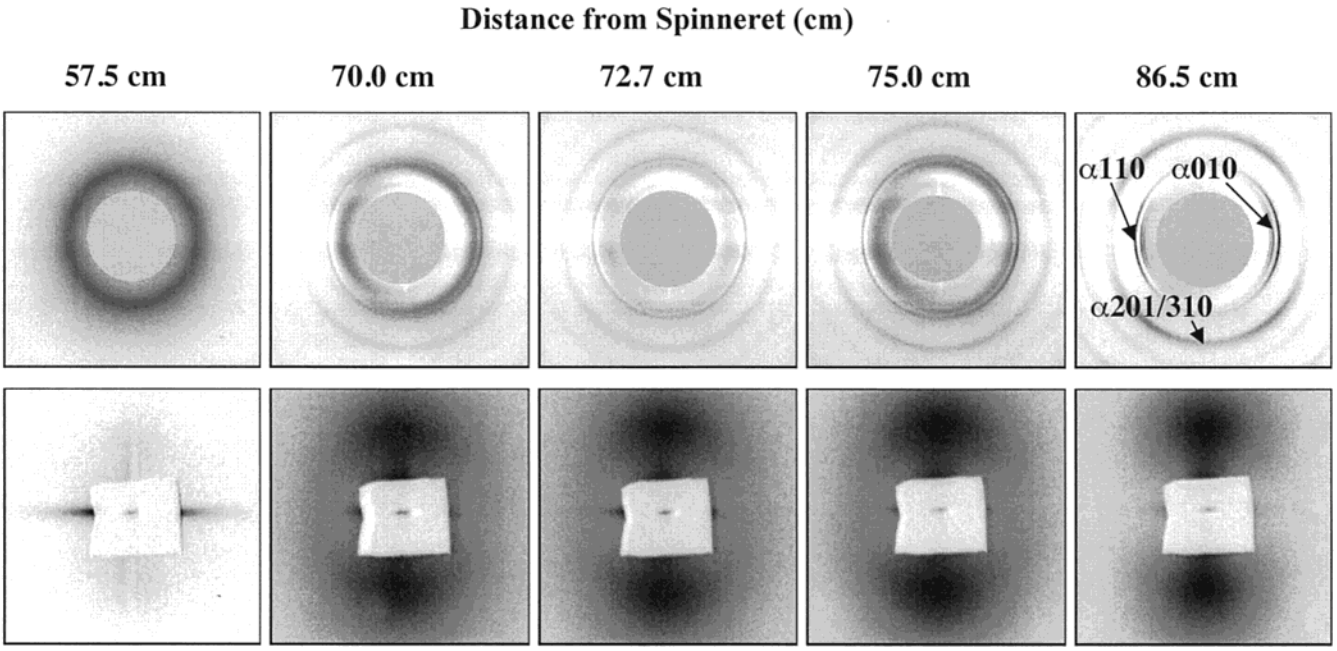

Figure 24. Two-dimensional SAXS and WAXS images for a variety of spinneret distances at a take-up speed of 10.6 mpm for poly(vinylidene fluoride) (PVDF). (Reprinted with permission fromref 118. Copyright 1999 American Chemical Society.)

crystallites was found to stay constant along the spin line. Both WAXD and SAXS signals were found to occur at the same distance from the spinneret within the resolution of the apparatus. A comparison of WAXD and SAXS showed that the crystallization and the formation of the superstructure followed the same kinetics (no sign of spinodal decomposition).

Samon et al.[117] used the same apparatus to study the melt spinning of nylon 6 fiber. For low-speed (50 mpm) situations, the nylon chains were found to crystallize into independent hydrogen-bonded sheets that started to interact with each other as their concentration increased. For higher speed situations, the nylon chains crystallized directly into the interacting hydrogen-bonded sheet structure. Upon conditioning at room temperature for 24 h, this interacting hydrogen-bonded sheet structure transformed into the well-known three-dimensional α and γ phases of nylon 6, probably existing in a shish kebab structure. The crystallization orientation function was constant along the spinline for a constant take-up speed and increased as take-up speed was increased. They also carried out melt spinning and subsequent annealing of polybutene-1 fiber.[119] For all take-up speeds examined, the phase II crystals mainly were formed, with only a small population of the phase I crystals existing. As the take-up speed was increased, the crystallinity also increased, indicating that strain-induced crystallization prevailed. The transformation from phase II to phase I was found to be functions of time and processing take-up speed. The dependence appeared to be connected to local stress enhancement via chains connecting crystallites. Perhaps the most interesting results were obtained from the melt spinning of PE and PVDF fibers.[118] Simultaneously collected two-dimensional SAXS and WAXS images for a variety of spinneret distances at a take-up speed of 10.6 mpm for poly(vinylidene fluoride) (PVDF) during fiber spinning are shown in Figure 24. It is seen that the equatorial streak occurs prior to the meridional streak (or lobe) in the SAXS patterns. This clearly favors the shish kebab mechanism proposed by Keller et al.[343] This result does not favor the spinodal decomposition mechanism as a precursor to crystallization. Hsiao and co-workers suggested a model of structural development during fiber spinning, which involved the formation of defective shish crystals followed by the formation of kebab crystals. The defective shish kebab structure eventually transformed into a well-defined lamellar structure. This model was consistent with the qualitative appearance of the two-dimensional SAXS and WAXS patterns as well as the quantitative analysis of the SAXS/WAXS data using position-sensitive wire area detectors.

VI. Concluding Remarks

The scattering techniques using light, neutrons, and X-rays are extremely useful to study the structure, size, and shape of large molecules such as polymers in solids, liquids, and solutions with dimensions from micrometers to Angstroms. The principles for the scattering techniques (including diffraction, a subfield of scattering), which involve the interaction of radiation with matter, are the same. The data collected by these methods (scattering and diffraction) are in reciprocal space and need to be analyzed with varying mathematical operations to construct the information in real space. Very often the solution of the transformation from reciprocal space to real space is not unique and some modeling approach has to be carried out to extract the structural information. In the past two decades, the availability of synchrotron X-rays has revolutionized the research opportunities by scattering in the fields of biology, chemistry, physics, materials science, and engineering. Many dynamic experiments on transient proper-

ties that were not possible before can now be carried out in real time (resolution in seconds to milliseconds) and/or in situ.

There is no doubt that the field of nanoscience and nanotechnology (including organic/inorganic nanocomposites, biological systems, nanoparticles) has become a major research thrust in biology, chemistry, physics, materials science, and engineering whereby small-angle scattering techniques (X-rays, neutrons, and light) are proven powerful tools to characterize the structure, morphology, and dynamics of these materials. With the advances on more intense light sources (e.g., synchrotron X-rays and neutrons) and better detectors (e.g., larger CCD area detectors), the data collection rate in time-resolved scattering experiments can be overwhelming (>100 GB/day). Unlike macromolecular (protein) crystallography, the software development for scattering analysis and visualization has fallen behind the experimental capability. Most scattering software is ad hoc in nature, lacking transportability and generality. We envision that a major consortium effort to tackle the software needs for processing very large scattering data sets will take place. In addition, the development of specialized synchrotron SAXS techniques by combining them with spectroscopic and/or other techniques, the microfocus SAXS method, the anomalous SAXS method, and the photon correlation method will be advanced in order to tackle complex but important and interesting problems in soft condensed matter.

VII. Acknowledgments

The authors gratefully acknowledge support of the work on the X-ray scattering of polymers and related topics by agencies of the Federal Government, including the Department of Energy (DEFG0286ER45237.016 and DEFG0299ER45760), the National Science Foundation (Polymers Program, DMR9984102), the U.S. Army Research Office (DAAD190010319), and the National Human Genome Research Institute (6R0 1HG0138606).

VIII. References

(1) Russell, T. P. In *Handbook on Synchrotron Radiation*; Brown, G. S., Moncton, D. E., Eds.; North-Holland: Amsterdam, 1991; Vol. 3, pp 379. For a brief qualitative discussion, see also: Smith, N. *Phys. Today* **2001**, *54* (1), 29.
(2) For example, see: Krishnamurti, P. *Indian J. Phys.* **1930**, *5*, 473.
(3) Guinier, A.; Fournet, G. *Small-Angle Scattering of X-rays* (translated by C. B. Walker); John Wiley & Sons: New York, 1955.
(4) *Small Angle X-ray Scattering*; Kraty, O., Glatter, O., Eds.; Academic: London, 1982.
(5) *Small Angle X-ray Scattering*; Brumberger, H., Ed.; Gordon & Breach: New York, 1976.
(6) *Scattering Techniques Applied to Supramolecular and Nonequilibrium Systems*; Chen, S.-H., Chu, B., Nossal, R., Eds.; NATO ASI Series B73; Plenum Press: New York, 1981.
(7) Katime, I. A.; Quintana, J. R. In *Comprehensive Polymer Science: The Synthesis, Characterization, Reactions & Applications of Polymers*; Booth, C., Price, C., Eds.; Pergamon Press: Oxford, England, 1989; Vol. 1, Chapter 5.
(8) Bras, W.; Ryan, A. J. *Adv. Colloid Interface Sci.* **1998**, *75*, 1.
(9) Hsiao, B. S.; Chu, B. Scattering: Light, Neutrons and X-rays. *Encyclopedia of Chemical Physics and Physical Chemistry*; Institute of Physics Publishing: London, 2000.
(10) Koch, M. H. J. *Makromol. Chem., Macromol. Symp.* **1988**, *15*, 79.
(11) Pedersen, Jan S. *NATO ASI Ser., Ser. C* **1995**, *451*, 57.
(12) Yamamoto, M.; Fujisawa, T.; Nakasako, M.; Tanaka, T.; Uruga, T.; Kimura, H.; Yamaoka, H.; Inoue, Y.; Iwasaki, H.; et al. *Rev. Sci. Instrum.* **1995**, *66* (2), 1833.
(13) Chu, B. *NATO ASI Ser., Ser. E* **1996**, *327* (Solvents and Self-Organization of Polymers), 409.
(14) Chu, B. *NATO ASI Ser., Ser. E* **1996**, *327* (Solvents and Self-Organization of Polymers), 383.
(15) Rabeony, M.; Shao, H.; Liang, K. S. *Annu. Technol. Conf.−Soc. Plast. Eng.* **1998**, *56* (2), 2070.
(16) Rabeony, M.; Shao, H.; Liang, K. S.; Siakali-Kioulafa, E.; Hadjichristidis, N. *J. Reinf. Plast. Compos.* **1999**, *18* (7), 642.
(17) Martin, C.; Mohendrasingam, A.; Fuller, W.; Harvie, J. L.; Blundell, D. J.; Whitehead, J.; Oldman, R. J.; Riekel, C.; Engstroem, P. *J. Synchrotron Radiat.* **1997**, *4* (4), 223.
(18) Riekel, C.; Engstroem, P.; Martin, C. *J. Macromol. Sci.-Phys.* **1998**, *B37*, 587.
(19) Martin, C.; Eeckhaut, G.; Mohendrasingam, A.; Blundell, D. J.; Fuller, W.; Oldman, R. J.; Bingham, S. J.; Dieing, T.; Riekel, C. *J. Synchrotron Radiat.* **2000**, *7* (4), 245.
(20) Riekel, C.; Burghammer, M.; Muller, M. *J. Appl. Crystallogr.* **2000**, *33* (3), 421.
(21) Chu, B.; Harney, P.; Li, Y.; Linliu, K.; Yeh, F.; Hsiao, B. S. *Rev. Sci. Instrum.* **1994**, *65* (3), 597.
(22) Leigh, J. B.; Rosebaum, G. *J. Appl. Crystallogr.* **1974**, *7*, 117.
(23) Hendrix, J.; Koch, M. H. J.; Bordas, J. *J. Appl. Crystallogr.* **1979**, *12*, 467.
(24) Hasegrove, J. C.; Faruqi, A. R.; Huxley, H. E.; Arndt, J. *J. Phys.* **1977**, *E10*, 1035.
(25) Stephenson, G. B. Ph.D. Thesis, Stanford University, 1982.
(26) Stephenson, G. B. *Nucl. Instrum. Methods Phys. Res., Sect. A* **1988**, *266*, 447.
(27) Amemiya, Y.; Wakabayashi, K.; Hamanaka, T.; Wakabayashi, T.; Matsushita, T.; Hashizume, H. *Nucl. Instrum. Methods* **1983**, *208*, 471.
(28) Tchoubar, D.; Rousseaux, F.; Pons, C.; Lemonnier, M. *Nucl. Instrum. Methods* **1978**, *152*, 301.
(29) Dubuisson, J. M.; Dauvergne, J. M.; Depautex, C.; Vachette, P.; Williams, C. E. *Nucl. Instrum. Methods Phys. Res., Sect. A* **1986**, *246*, 636.
(30) Wakatsuki, S.; Hodgson, K. O.; Eliezer, D.; Rice, M.; Hubbard, S.; Gillis, N.; Doniach, S.; Spann, U. *Rev. Sci. Instrum.* **1992**, *63*, 1736.
(31) Zachmann, H. G.; Wutz, C. *Polym. Prepr. (Am. Chem. Soc., Div. Polym. Chem.)* **1992**, *33*, 261.
(32) Cogan, K. A.; Gast, A. P.; Capel, M. *Macromolecules* **1991**, *24*, 6512.
(33) Stuhrmann, H. B. *Adv. Polym. Sci.* **1985**, *67*, 123.
(34) Bordas, J.; Koch, M. H. J.; Clout, P. H.; Dorrington, E.; Boulin, C.; Gabriel, A. *J. Phys.* **1980**, *E13*, 938.
(35) Koch, M. H. J.; Bordas, J. *Nucl. Instrum. Methods* **1983**, *208*, 461.
(36) Bras, S.; Craievich, A.; Sanchez, J. M.; Williams, C.; Zanotto, E. D. *Nucl. Instrum. Methods* **1983**, *208*, 489.
(37) Caffrey, M.; Bilderback, D. H. *Nucl. Instrum. Methods* **1983**, *208*, 495.
(38) Bras, W.; Derbyshire, G. E.; Ryan, A. J.; Mant, G. R.; Felton, A.; Lewis, R. A., Hall. C. J.; Greaves, G. N. *Nucl. Instrum. Methods Phys. Res., Sect. A* **1993**, *326*, 587.
(39) Chu, B.; Wu, D.-Q.; Wu, C. *Rev. Sci. Instrum.* **1987**, *58* (7), 1158.
(40) Kratky, O. *Z. Elektrochem.* **1954**, *58*, 49.
(41) Kratky, O. *Z. Elektrochem.* **1958**, *62*, 66.
(42) Kratky, O.; Skala, Z. *Z. Elektrochem.* **1958**, *62*, 73.
(43) Kratky, O.; Stabinger, H. *Colloid Polym. Sci.* **1984**, *262*, 345.
(44) Chu, B.; Li, Y.-J.; Gao, T. *Rev. Sci. Instrum.* **1992**, *63* (9), 4128.
(45) Chu, B.; Li, Y.-J.; Harney, P. J.; Yeh, F.-J. *Rev. Sci. Instrum.* **1993**, *64* (6), 1510.
(46) Chu, B.; Yeh, F.-J.; Li, Y.-J.; Harney, P. J.; Rousseau, J.; Darovsky, A.; Siddons, D. P. *Rev. Sci. Instrum.* **1994**, *65* (10), 3233.
(47) Chu, B.; Xu, R.-L.; Maeda, T.; Dhadwal, H. S. *Rev. Sci. Instrum.* **1988**, *59*, 716.
(48) Koga, T.; Hart, M.; Hashimoto, T. J. *Appl. Crystallogr.* **1996**, *29*, 318.
(49) Fankuchen, I.; Jellinek, M. H. *Phys. Rev.* **1945**, *67*, 201.
(50) DuMond, J. W. *Phys. Rev.* **1947**, *72*, 83.
(51) Beeman, W. W.; Kaesberg, P. *Phys. Rev.* **1947**, *72*, 512.
(52) Warren, B. E. *J. Appl. Phys.* **1949**, *20*, 96.
(53) Bonse, U.; Hart, M. *Z. Phys.* **1966**, *189*, 151.
(54) Bonse, U.; Hart, M. In *Small-Angle X-ray Scattering*; Brumberger, H., Ed.; Gordon and Breach: New York, 1966; p 121.
(55) Gravatt, C. C.; Brady, G. W. *J. Appl. Crystallogr.* **1969**, *2*, 289.
(56) Koffman, D. M. *Adv. X-Ray Anal.* **1968**, *11*, 332.
(57) Schwahn, D.; Miksovsky, A.; Rauch, H.; Seidl, E.; Zugarek, G. *Nucl. Instrum. Methods Phys. Res. A* **1985**, *239*, 229.
(58) Nave, C.; Diakun, G. P.; Bordas, J. *Nucl. Instrum. Methods Phys. Res., Sect. A* **1986**, *246*, 609.
(59) Bonse, U.; Pahl, R.; Nussardt, R. HASYLAB Annual Report, 1987; p 383.

(60) Siddons, D. P.; Riekel, C.; Hastings, J. B. *J. Appl. Crystallogr.* **1990**, *23*, 401.
(61) Lambard, J.; Zemb, Th. *J. Appl. Crystallogr.* **1991**, *24*, 555.
(62) Matsuoka, H.; Kakigami, K.; Ise, N.; Kobayashi, Y.; Machitani, Y.; Kikuchi, T.; Kato, T. *Proc. Natl. Acad. Sci. U.S.A.* **1991**, *88*, 6618.
(63) Long, G. G.; Jemian, P. R.; Weertman, J. R.; Black, D. R.; Burdette, H. E.; Spal, R. *J. Appl. Crystallogr.* **1991**, *24*, 30.
(64) North, A. N.; Dore, J. C.; Mackie, A. R.; Howe, A. M.; Harries, J. *Nucl. Instrum. Methods Phys. Res., Sect. B* **1990**, *47*, 283.
(65) Matsuoka, H.; Kakigami, K.; Ise, N. *Rigaku J.* **1991**, *8*, 21.
(66) Lesieur, P.; Zemb, T. In *Structure and Dynamics of Strongly Interacting Colloids and Supramolecular Aggregates in Solution*; Chen, S.-H., et al., Eds.; Kluwer Academic Publishers: The Netherlands, 1992; pp 713−729.
(67) Lambard, J.; Lesieur, P.; Zemb, T. *J. Phys. I Fr.* **1992**, *2*, 1191.
(68) Chu, B.; Ying, Q.-C.; Yeh, F.-J.; Patkowski, A.; Steffen, W.; Fischer, E. W. *Langmuir* **1995**, *11*, 1419.
(69) Chu, B.; Wu, D. Q.; Howard, R. L. *Rev. Sci. Instrum.* **1989**, *60*, 3224.
(70) Gabriel, A. *Rev. Sci. Instrum.* **1977**, *48*, 1303.
(71) Borso, C. S.; Danyluk, S. S. *Rev. Sci. Instrum.* **1980**, *51*, 1669.
(72) Stephenson, G. B. Ph.D. Thesis, Stanford University, SSRL Report 82/05, 1982.
(73) Gabriel, A.; Koch, M. H. J. *Nucl. Instrum. Methods* **1994**, *A346*, 286.
(74) Cipriani, F.; Gabriel, A.; Koch, M. H. J. *Nucl. Instrum. Methods* **1992**, *A313*, 554.
(75) Gabriel, A.; Dauvergne, F.; Nolting, H. F.; Koch, M. H. J. *Nucl. Instrum. Methods* **1994**, *A349*, 461.
(76) Allinson, N. M.; Baker, G.; Greaves, G. N.; Nicoll, J. K. *Nucl. Instrum. Methods Phys. Res., Sect. A* **1988**, *266*, 592.
(77) Jucha, A.; Bonin, D.; Dartyge, E.; Flank, A. M.; Fontaine, A.; Raoux, D. *Nucl. Instrum. Methods* **1984**, *226*, 40.
(78) Gamble, R. C.; Baldeschwieler, J. D. *Rev. Sci. Instrum.* **1979**, *50*, 1416.
(79) See for example, Amemiya, Y.; Miyahara, J. *Nature* **1988**, *336*, 89.
(80) Allinson, N. M. *Nucl. Instrum. Methods* **1982**, *201*, 53.
(81) Stern, R. A.; Liewer, K.; Janesick, J. R. *Rev. Sci. Instrum.* **1983**, *54*, 198.
(82) Turner, L. K.; Mantus, D. S.; Ling, Y. C.; Bernius, M. T.; Morrison, G. H. *Rev. Sci. Instrum.* **1989**, *60*, 996.
(83) Fuchs, H. F.; Wu, D. Q.; Chu, B. *Rev. Sci. Instrum.* **1990**, *61*, 712.
(84) Gruner, S. M.; Milch, J. R. *Trans. Am. Crystallogr. Assoc.* **1982**, *18*, 149.
(85) Rodricks, B.; Clarke, R.; Smither, R.; Fontaine, A. *Rev. Sci. Instrum.* **1989**, *60*, 2586.
(86) Callcott, T. A.; Tsang, K.-L.; Zhang, C. H.; Ederer, D. L.; Arakawa, E. T. *Nucl. Instrum. Methods Phys. Res., Sect. A* **1988**, *266*, 578.
(87) Naday, I.; Strauss, M. G.; Sherman, I. S.; Kraimer, M. R.; Westbrook, E. M. *Opt. Eng.* **1987**, *26*, 788.
(88) Strauss, M. G.; Naday, I.; Sherman, I. S.; Kraimer, M. R.; Westbrook, E. M.; Zaluzec, N. J. *Nucl. Instrum. Methods Phys. Res., Sect. A* **1988**, *266*, 563.
(89) Templer, R. H.; Gruner, S. M.; Eikenberry, E. F. Photo-Electronic Image Devices. In *Advances in Electronic and Electron Physics*, Morgan, B. L., Ed.; Academic: London, 1988; Vol. 74.
(90) Eikenberry, E. F.; Gruner, S. M.; Lowrance, J. L. *IEEE Trans. Nucl. Sci.* **1986**, *33*, 542.
(91) Grant, J. *Laser Focus World* **1988**, *24*, 211−213.
(92) Chemloul, M.; Comparat, V. *Nucl. Instrum. Methods Phys. Res., Sect. A* **1995**, *367* (1−3), 290.
(93) Zhukov, V.; Udo, F.; Marchena, O.; Hartjes, F. G.; van den Berg, F. D.; Bras, W.; Vlieg, E. *Nucl. Instrum. Methods Phys. Res., Sect. A* **1997**, *392* (1−3), 83.
(94) Fuller, W.; Mahendrasingam, A.; Hughes, D. J.; Martin, C.; Heeley, E. L.; Oatway, W. B. *Polym. Prepr. (Am. Chem. Soc., Div. Polym. Chem.)* **1997**, *38* (2), 71−72.
(95) Song, H. H.; Wu, D. Q.; Chu, B.; Satkowski, M.; Ree, M.; Stein, R. S.; Phillips, J. C. *Macromolecules* **1990**, *23* (8), 2380.
(96) Inoue, H.; Hiragi, Y. *Shimadzu Hyoron* **1991**, *48* (3), 265.
(97) Hiragi, Y.; Nakatani, H.; Kajiwara, K.; Inoue, H.; Sano, Y.; Kataoka, M. *Rev. Sci. Instrum.* **1988**, *59* (1), 64.
(98) Koberstein, J. T.; Russell, T. P. *Polym. Mater. Sci. Eng.* **1984**, *51*, 141.
(99) Hajduk, D.; Gruner, S. M.; Erramilli, S.; Register, R. A.; Fetters, L. J. *Macromolecules* **1996**, *295*, 1473.
(100) Lorenzen, M.; Riekel, C.; Eichler, A.; Haeussermann, D. *J. Phys. IV* **1993**, *3* (C8), 487.
(101) Steinhart, M.; Kriechbaum, M.; Pressl, K.; Amenitsch, H.; Laggner, P.; Bernstorff, S. *Rev. Sci. Instrum.* **1999**, *70* (2), 1540.
(102) Pressl, K.; Kriechbaum, M.; Steinhart, M.; Laggner, P. *Rev. Sci. Instrum.* **1997**, *68* (12), 4588.
(103) Maeda, Y.; Toriumi, H. *Makromol. Chem.* **1993**, *194* (11), 3123.
(104) Seto, H.; Okuhara, D.; Nagao, M.; Komura, S.; Takeda, T. *Jpn. J. Appl. Phys., Part 1* **1999**, *38* (2A), 951.
(105) Kato, M.; Fujisawa, T. *J. Synchrotron Radiat.* **1998**, *5* (5), 1282.
(106) So, P. T. C.; Gruner, S. M.; Erramilli, S. *Phys. Rev. Lett.* **1993**, *70* (22), 3455.
(107) Hong, M. K.; Narayan, O.; Goldstein, R. E.; Shyamsunder, E.; Austin, R. H.; Fisher, D. S.; Hogan, M. *Phys. Rev. Lett.* **1992**, *68* (9), 1430.
(108) Morita, T.; Kusano, K.; Ochiai, H.; Saitow, K.; Nishikawa, K. *J. Chem. Phys.* **2000**, *112* (9), 4203.
(109) Liu, L.; Cheng, Z.; Inomata, K.; Zhou, S.; Chu, B. *Macromolecules* **1999**, *32* (18), 5836.
(110) Brown, H. R.; Kramer, E. J. *J. Macromol. Sci. Phys.* **1981**, *B19* (3), 487.
(111) Brown H. R.; Kramer, E. J. *J. Polym. Sci. Polym. Phys.* **1987**, *25*, 1765.
(112) Ran, S. F.; Fang, D. F.; Zong, X.; Hsiao, B. S.; Chu, B.; Cunniff, P. M. *Polymer* **2001**, *42*, 1601.
(113) Ran, S.; Zong, X.; Fang, D.; Hsiao, B. S.; Chu, B.; Cunniff, P M.; Phillips, R. A. *J. Mater. Sci.*, in press.
(114) Hughes, D. J.; Mahendrasingam, A.; Martin, C.; Oatway, W. B.; Heeley, E. L.; Bingham, S. J.; Fuller, W. *Rev. Sci. Instrum.* **1999**, *70* (10), 4051.
(115) Cakmak, M.; Teitge, A.; Zachmann, H. G.; White, J. L. *J. Polym. Phys. Polym. Phys.* **1993**, *31*, 371.
(116) Terrill, N.J.; Fairclough, P. A.; Towns-Andrews, E.; Komanschek, B. U.; Young, R. J.; Ryan, A. J. *Polymer* **1998**, *39*, 2381.
(117) Samon, J. M.; Schultz, J. M.; Wu, J.; Hsiao, B. S.; Yeh F.; Kolb, R. *J. Polym. Sci., Part B: Polym. Phys.* **1999**, *37*, 1277.
(118) Samon, J. M.; Schultz, J. M.; Hsiao, B. S.; Seifert, S.; Stribeck, N.; Gurke, I.; Collins, G.; Saw, C. *Macromolecules* **1999**, *32* (24), 8121.
(119) Samon, J. M.; Schultz, J. M.; Hsiao, B. S.; Wu, J.; Khot, S. *J. Polym. Sci., Part B: Polym. Phys.* **2000**, *38* (14), 1872.
(120) Kolb, R.; Seifert, S.; Stribeck, N.; Zachmann, H. G. *Polymer* **2000**, *41* (8), 2931.
(121) Kolb, R.; Seifert, S.; Stribeck, N.; Zachmann, H. G. *Polymer* **1999**, *41* (4), 1497.
(122) Radler, M. J.; Landes, B. G.; Nolan, S. J.; Broomall, C. F.; Chritz, T. C.; Rudolf, P. R.; Mills, M. E.; Bubeck, R. A. *J. Polym. Sci., Part B: Polym. Phys.* **1994**, *32*, 2573.
(123) Nolan, S. J.; Broomall, C. F.; Bubeck, R. A.; Radler, M. J.; Landes, B. G. *Rev. Sci. Instrum.* **1995**, *66*, 2652.
(124) Hsiao, B. S.; Kennedy, A. D.; Leach, R. A.; Chu, B.; Harney, P. *J. Appl. Crystallogr.* **1997**, *30* (6), 1084.
(125) Ran, S.; Zong, X.; Fang, D.; Hsiao B. S.; Chu, B. *J. Appl. Crystallogr.* **2000**, *33* (4), 1031.
(126) Ran, S.; Cruz, S.; Zong, X.; Fang, D.; Chu, B.; Hsiao, B. S.; Ross, R.; Chang H.; Londono, D. *Adv. X-ray Anal.* **2000**, 43.
(127) Romo-Uribe, A.; Windle, A. H. *Proc. R. Soc. London, Ser. A* **1999**, *455* (1983), 1175.
(128) Higgins, J. S.; Gerard, H. *Macromol. Symp.* **2000**, *149*, 165.
(129) Hamley, I. W.; Fairclough, J. P. A.; Ryan, A. J.; Mai, S.-M.; Booth, C. *Phys. Chem. Chem. Phys.* **1999**, *1* (9), 2097.
(130) Hamley, I. W.; Pople, J. A.; Gleeson, A. J.; Komanschek, B. U.; Towns-Andrews, E. *J. Appl. Crystallogr.* **1998**, *31* (6), 881.
(131) Hongladarom, K.; Ugaz, V.; Cinader, D.; Burghardt, W. R.; Quintana, J. P.; Hsiao, B. S.; Dadmum, M. D.; Hamilton W.; Butler, P. D. *Macromolecules* **1996**, *29* (16), 5346.
(132) Somani, R. H.; Hsiao, B. S.; Nogales, A.; Srinivas, S.; Tsou, A. H.; Sics, I.; Balta-Calleja, F. J.; Ezquerra, T. A. *Macromolecules*, in press.
(133) Bark, M.; Zachmann, H. G.; Alamo, R.; Mandelkern, L. *Makromol. Chem.* **1992**, *193* (9), 2363.
(134) Mathot, V. B. F.; Scherrenberg, R. L.; Pijpers, M. F. J.; Bras, W. *J. Therm. Anal.* **1996**, *46* (3−4), 681.
(135) Zachmann, H. G.; Wutz, C. *NATO ASI Ser. C* **1993**, *405* (Crystallization of Polymers), 403−14.
(136) Martorana, A.; Piccarolo, S.; Sapoundjieva, D. *Macromol. Chem. Phys.* **1999**, *200* (3), 531.
(137) Wang, W.; Schultz, J. M.; Hsiao, B. S. *J. Macromol. Sci., Phys.* **1998**, *B37* (5), 667.
(138) Krueger, K. N.; Zachmann, H. G. *Macromolecules* **1993**, *26* (19), 5202.
(139) Bark, M.; Zachmann, H. G. *Acta Polym.* **1993**, *44* (6), 259.
(140) Herzberg, O.; Gehrke, R.; Epple, M. *Polymer* **1998**, *40* (2), 507.
(141) Dokter, W. H.; Beelen, T. P. M.; van Garderen, H. F.; van Santen, R. A.; Bras, W.; Derbyshire, G. E.; Mant, G. R. *J. Appl. Crystallogr.* **1994**, *27* (6), 901.
(142) Bras, W.; Derbyshire, G. E.; Ryan, A. J.; Mant, G. R.; Felton, A.; Lewis, R. A.; Hall, C. J.; Greaves, G. N. *Nucl. Instrum. Methods Phys. Res., Sect. A* **1993**, *A326* (3), 587.
(143) Bras, W. *J. Macromol. Sci., Phys.* **1998**, *B37* (4), 557.
(144) Bras, W.; Ryan, A. J. *J. Appl. Crystallogr.* **1997**, *30* (5), 816.
(145) Zhukov, V.; Udo, F.; Marchena, O.; Hartjes, F. G.; van den Berg, F. D.; Bras, W.; Vlieg, E. *Nucl. Instrum. Methods Phys. Res., Sect. A* **1997**, *392* (1−3), 83.
(146) Amenitsch, H.; Bernstorff, S.; Kriechbaum, M.; Lombardo, D.; Mio, H.; Pabst, G.; Rappolt, M.; Laggner, P. *Nuovo Cimento Soc. Ital. Fis., D* **1998**, *20D* (12bis), 2181.

(147) Bras, W.; Mant, G. R.; Derbyshire, G. E.; O'Kane, W. J.; Helsby, W. I.; Hall, C. J.; Ryan, A. J. *J. Synchrotron Radiat.* **1995**, *2*, 87.
(148) Purvis, J.; Bower, D. I. *Polymer* **1974**, *15*, 645.
(149) Shepard, I. W. *Rep. Prog. Phys.* **1975**, *38*, 565.
(150) Bower, D. I. *J. Polym. Sci., Polym. Phys. Ed.* **1972**, *10*, 2135.
(151) Bryant, G. K.; Gleeson, H. F.; Ryan, A. J.; Fairclough, J. P. A.; Bogg, D.; Goossens, J. G. P.; Bras, W. *Rev. Sci. Instrum.* **1998**, *69* (5), 2114.
(152) Chu, B. *Polymer* **1992**, *33* (19), 4009.
(153) Li, Y.; Chu, B. *Macromolecules* **1991**, *24* (14), 4115.
(154) Chu, B.; Xu, R.; Li, Y.; Wu, D. Q. *Macromolecules* **1989**, *22* (9), 3819.
(155) Zhou, S.; Chu, B.; Dhadwal, H. S. *Rev. Sci. Instrum.* **1998**, *69* (5), 1955.
(156) Zachmann, H. G.; Wutz, C. *NATO ASI Ser. C* **1993**, *405* (Crystallization of Polymers), 403.
(157) Elwell, M. J.; Ryan, A. J.; Grunbauer, H. J. M.; Van Lieshout, H. C. *ACS Symp. Ser.* **1997**, *669* (Polymeric Foams), 143.
(158) Lee, H. S.; Park, H. D.; Cho, C. K. *J. Appl. Polym. Sci.* **2000**, *77* (3), 699.
(159) Panick, G.; Malessa, R.; Winter, R. *Biochemistry* **1999**, *38* (20), 6512.
(160) Panick, G.; Malessa, R.; Winter, R.; Gert, R.; Frye, K. J.; Royer, C. A. *J. Mol. Biol.* **1998**, *275* (2), 389.
(161) Czeslik, C.; Reis, O.; Winter, R.; Rapp, G. *Chem. Phys. Lipids* **1998**, *91* (2), 135.
(162) Bogg, D.; Derbyshire, G. E.; Bras, W.; Cooke, J.; Elwell, M. J. A.; Naylor, S.; Ryan, A. J. *Nucl. Instrum. Methods Phys. Res., Sect. B* **1995**, *97* (1−4), 536.
(163) Bras, W.; Derbyshire, G. E.; Bogg, D.; Cooke, J.; Elwell, M. J.; Komanschek, B. U.; Naylor, S.; Ryan, A. J. *Science* **1995**, *267* (5200), 996.
(164) Sakurai, S. *Curr. Trends Polym. Sci.* **1996**, *1*, 119.
(165) Bates, F. S.; Fredrickson, G. H. *Phys. Today* **1999**, *52* (2), 32.
(166) Kimishishima, K.; Koga, T.; Kanazawa, Y.; Hashimoto, T. *ACS Symp. Ser.* **2000**, *739* (Scattering from Polymers), 514.
(167) Floudas, G.; Ulrich, R.; Wiesner, U.; Chu, B. *Europhys. Lett.* **2000**, *50* (2), 182.
(168) Floudas, G.; Ulrich, R.; Wiesner, U.; Chu, B. *Polym. Prepr. (Am. Chem. Soc., Div. Polym. Chem.)* **1999**, 593.
(169) Lee, H. H.; Kim, J. K. *ACS Symp. Ser.* **2000**, *739* (Scattering from Polymers), 470.
(170) Kim, J. K.; Lee, H. H.; Lee, K. B. *Polym. Mater. Sci. Eng.* **1998**, *79*, 330.
(171) Kim, J. K.; Lee, H. H.; Ree, M.; Lee, K.-B.; Park, Y. *Macromol. Chem. Phys.* **1998**, *199* (4), 641.
(172) Burger, C.; Wolff, T.; Ruland, W. *Polym. Prepr. (Am. Chem. Soc., Div. Polym. Chem.)* **1994**, *35* (1), 563.
(173) Burger, C.; Wolff, T.; Ruland, W. *Polym. Prepr. (Am. Chem. Soc., Div. Polym. Chem.)* **1994**, *35* (1), 593.
(174) Wolff, T.; Burger, C.; Ruland, W. *Macromolecules* **1993**, *26* (7), 1707.
(175) Wolff, T.; Burger, C.; Ruland, W. *Macromolecules* **1994**, *27* (12), 3301.
(176) Dair, B. J.; Thomas, E. L.; Avgeropoulos, A.; Hadjichristidis, N.; Capel, M. *Polym. Mater. Sci. Eng.* **1998**, 76.
(177) Steinhoff, B.; Ruellmann, M.; Wenzel, M. *Macromolecules* **1998**, *31*, 36.
(178) Zhu, L.; Chen, Y.; Zhang, A.; Calhourn, B. H.; Chun, M.; Quirk, R. P.; Cheng, S. Z. D.; Hsiao B. S.; Yeh, F. J.; Hashimoto, T. *Phys. Rev. B* **1999**, *60* (14), 10022.
(179) Zhu, L.; Cheng, S. Z. D.; Calhoun, B. H.; Ge, Q.; Quirk, R. P.; Thomas, E. T.; Hsiao, B. S.; Yeh, F. J.; Lotz, B. *J. Am. Chem. Soc.* **2000**, *122* (25), 5957.
(180) Ryan, A. J.; Hamley, I. W.; Bras, W.; Bates, F. S. *Macromolecules* **1995**, *28* (11), 3860.
(181) Krakovsky, I.; Urakawa, H.; Kajiwara, K. *Polymer* **1997**, *38* (14), 3645.
(182) Krakovsky, I.; Bubenikova, Z.; Urakawa, H.; Kajiwara, K. *Polymer* **1997**, *38* (14), 3637.
(183) Li, Y.; Gao, T.; Chu, B. *Macromolecules* **1992**, *25* (6), 1737.
(184) Li, Y.; Gao, T.; Liu, J.; Linliu, K.; Desper, C. R.; Chu, B. *Macromolecules* **1992**, *25* (26), 7365.
(185) Floudas, G.; Reiter, G.; Lambert, O.; Dumas, P.; Yeh, F.-J.; Chu, B. *ACS Symp. Ser.* **2000**, *739* (Scattering from Polymers), 448.
(186) Nojima, S.; Kikuchi, N.; Rohadi, A.; Tanimoto, S.; Sasaki, S. *Macromolecules* **1999**, *32* (11), 3727.
(187) Nojima, S.; Kanda, Y.; Sasaki, S. *Polym. J.* **1998**, *30* (8), 628.
(188) Nojima, S.; Kato, K.; Yamamoto, S.; Ashida, T. *Macromolecules* **1992**, *25* (8), 2237.
(189) Chu, B.; Li, Y. *Prog. Colloid Polym. Sci.* **1993**, *91*, 51.
(190) Liu, L.; Yeh, F.; Chu, B. *Macromolecules* **1996**, *29* (16), 5336.
(191) Takenaka, M.; Linliu, K.; Ying, Q.; Chu, B.; Peiffer, D. *Macromolecules* **1995**, *28* (8), 2700.
(192) Hilfiker, R.; Wu, D. Q.; Chu, B. *J. Colloid Interface Sci.* **1990**, *135* (2), 573.
(193) Hirai, M.; Kawai-Hirai, R.; Takizawa, T.; Yabuki, S.; Nakamura, K.; Hirai, T.; Kobayashi, K.; Amemiya, Y.; Oya, M. *J. Phys. Chem.* **1995**, *99*, 6652.
(194) Myers, R. T.; Karbach, A.; Bellare, A.; Cohen, R. E. *ACS Symp. Ser.* **2000**, *739* (Scattering from Polymers), 436.
(195) Chu, B. Small-angle X-ray scattering (SAXS) studies of bulk Ionomers. (Editor(s): Schlick, Shulamith.) *Ionomers* **1996**, 35.
(196) Chu, B.; Wu, D. Qing; MacKnight, W. J.; Wu, Chi; Phillips, J. C.; LeGrand, A.; Lantman, C. W.; Lundberg, R. D. *Macromolecules* **1988**, *21* (2), 523.
(197) Wang, J.; Li, Y.; Peiffer, D. G.; Chu, B. *Macromolecules* **1993**, *26* (10), 2633.
(198) Jackson, D. A.; Koberstein, J. T.; Weiss, R. A. *J. Polym. Sci., Part B: Polym. Phys.* **1999**, *37* (21), 3141.
(199) Inomata, K.; Liu, L.; Nose, T.; Chu, B. *Macromolecules* **1999**, *32* (5), 1554.
(200) Rabeony, M.; Wnek, G. E.; Serpico, J. M. *Polym. Mater. Sci. Eng.* **1999**, 372.
(201) Wu, D. Q.; Liang, B.; Hsiao, B. S.; Li, Y.; Chu, B. *Polym. Prepr. (Am. Chem. Soc., Div. Polym. Chem.)* **1992**, *33* (1), 350.
(202) Perez-Mendez, M.; Fayos, J.; Mateo, C. R. *Adv. Biochirality* **1999**, 325.
(203) He, C.; Donald, A. M.; Griffin, A. C.; Waigh, T.; Windle, A. H. *J. Polym. Sci., Part B: Polym. Phys.* **1998**, *36* (10), 1617.
(204) Buchner, S.; Chen, D.; Gehrke, R.; Zachmann, H. G. *Mol. Cryst. Liq. Cryst.* **1988**, *155* (Pt. B), 357.
(205) Campoy, I.; Gomez, M. A.; Marco, C. *Polymer* **1999**, *41* (6), 2295.
(206) Cohen, Y. *Mater. Res. Soc. Symp.* **1989**, *134*, 195.
(207) Bordas, J.; Koch, M. H. J. Daresbury Lab. Rep. DL/SCI/R, 1979, (DL/SCI/R13, Appl. Synchrotron Radiat. Study Large Mol. Chem. Biol. Interest), 12.
(208) Salditt, T.; Koltover, I.; Radler, J. O.; Safinya, C. R. *Phys. Rev. E: Stat. Phys., Plasmas, Fluids, Relat. Interdiscip. Top.* **1998**, *58* (1), 889.
(209) Bouwstra, J.; Gooris, G. S.; Bras, W. *Paperback APV* **1993**, *31*(Dermal and Transdermal Drug Delivery), 67.
(210) Malinchik S.; Yu, L. C. *Biophys. J.* **1995**, *68*, 2023.
(211) Kraft, T.; Chalovich, J. M.; Yu, L. C.; Brenner, B. *Biophys. J.* **1995**, *68*, 2404.
(212) Jenkins, P. J.; Donald, A. M. *Starch/Staerke* **1997**, *49* (7/8), 262.
(213) Waigh, I. A.; Donald, A. M.; Heidelbach, F.; Riekel, C.; Gidley, M. J. *Biopolymers* **1999**, *49*, 91.
(214) Sano, Y.; Inoue, H.; Kajiwara, K.; Hiragi, Y.; Isoda, S. *J. Protein Chem.* **1997**, *16* (2), 151.
(215) Barteri, M.; Gaudiano, M. C.; Santucci, R. *Biochim. Biophys. Acta* **1996**, *1295* (1), 51.
(216) Congiu Castellano, A.; Barteri, M.; Bianconi, A.; Borghi, E.; Cassiano, L.; Castagnola, M.; Della Longa, S.; La Monaca, A. *Biophys. J.* **1993**, *64* (2, Pt. 1), 520.
(217) Miles, M. J.; Morris, V J.; Carroll, V.; Wright, D. J.; Bacon, J. R.; Nave, C. *Int. J. Biol. Macromol.* **1984**, *6* (5), 291.
(218) Bonnete, F.; Vidal, O.; Robert, M. C.; Tardieu, A. *J. Cryst. Growth* **1996**, *168* (1−4, Crystallization of Biological Macromolecules), 185.
(219) Shigeki; Hirai, M. *Biophys. J.* **1999**, *76* (4), 2192.
(220) Kataoka, M.; Hagihara, Y.; Mihara, K.; Goto, Y. *J. Mol. Biol.* **1993**, *229*, 591.
(221) Kataoka, M.; Flanagan, J. M.; Tokunaga, F.; Engelman, D. M. In *Synchrotron Radiation in the Biosciences*; Chance, B., Deisenhofer, J., Ebashi, S., Goodhead, D. T., Helliwell, J. R., Huxley, H. E., Iizuka, T., Kirz, J., Mitsui, T., Rubenstein, E., Sakabe, N., Sasaki, T., Schmahl, G., Stuhrmann, H. B., Wuthrich, K., Zaccai, G., Eds.; Clarendon Press: Oxford, 1994; pp 187−194.
(222) Kataoka, M.; Nishii, I.; Fujisawa, T.; Ueki, T.; Tokunaga, F.; Goto, Y. *J. Mol. Biol.* **1995**, *249*, 215.
(223) Flanagan, J. M.; Kataoka, M.; Shortle, D.; Engleman, D. M. *Proc. Natl. Acad. Sci. U.S.A.* **1992**, *89*, 748.
(224) Flanagan, J. M.; Kataoka, M.; Fujisawa, T.; Engleman, D. M. *Biochemistry* **1993**, *32*, 10359.
(225) Nishi, I.; Kataoka, M.; Tokunaga, F.; Goto. Y. *Biochemistry* **1994**, *33*, 4903.
(226) Lattman, E. E.; Fiebig, K. M.; Dill, K. A. *Biochemistry* **1994**, *33*, 6158.
(227) Bras, W.; Diakun, G. P.; Diaz, J. F.; Maret, G.; Kramer, H.; Bordas, J.; Medrano, F. J. *Biophys. J.* **1998**, *74*, 1509.
(228) Uversky, V. N.; Fink, A. L. *Biochemistry* **1998**, *63*, 456.
(229) Dolgikh, D. A.; Gilmanshin, R. I.; Brazhnikov, E. V.; Bychkova, V. E.; Semisotnov, G. V.; Venyaminov, S. Y.; Ptitsyn, O. B. *FEBS Lett.* **1981**, *136*, 311.
(230) Gast, K.; Damaschun, H.; Misselwitz, R.; Muller-Fronhme, M.; Zirwer, D.; Damaschun, G. *Eur. Biophys. J.* **1994**, *23*, 297.
(231) Chen, L.; Hodgson, K. O.; Doniach, S. *J. Mol. Biol.* **1996**, *261*, 658.
(232) Kihara, H. *J. Synchrotron Radiat.* **1994**, *1*, 74.
(233) Eliezer, D.; Frank, P.; Gillis, N.; Newton, W. E.; Doniach, S.; Hodgson, K. O. *J. Biol. Chem.* **1993**, *268*, 20953.
(234) Eliezer, D.; Jennings, P. A.; Wright, P. E.; Doniach, S.; Hodgson, K. O.; Tsuruta, H. *Science* **1995**, *270*, 487.

(235) Kataoka, M.; Goto, Y. *Folding Des. (Rev.)* **1996**, *1*, R107.
(236) Semisotnov, G. V.; Kihara, H.; Kotova, N. V.; Kimura, K.; Amemiya, Y.; Wakabayashi, K.; Serdyuk, I. N.; Timchenko, A. A.; Chiba, K.; Nikaido, K.; Ikura, T.; Kuwajima, K. *J. Mol. Biol.* **1996**, *262*, 559.
(237) Chen, L.; Wildegger, G.; Kiefhaber, T.; Hodgson, K. O.; Doniach, S. *J. Mol. Biol.* **1998**, *276*, 225.
(238) Uversky, V. N.; Karnoup, A. S.; Segel, D. J.; Seshadri, S.; Doniach, S.; Fink, A. L. *J. Mol. Biol.* **1998**, *278*, 879.
(239) Hery, S.; Genest, D.; Smith, J. C. *J. Mol. Biol.* **1998**, *279*, 303.
(240) Chacon, P.; Moran, F.; Diaz, J. F.; Pantos, E.; Andreu, J. M. *Biophys. J.* **1998**, *74*, 2760.
(241) Barone, G.; Sayers, Z.; Svergun, D.; Koch, M. H. J. *J. Synchrotron Radiat.* **1999**, *6* (5), 1031.
(242) Beechem, J. M. *Biophys. J.* **1999**, *74*, 2141.
(243) Regenfuss, P.; Clegg, R. M.; Fulwyler, M. J.; Barrantes, F. J.; Jovin, T. M. *Rev. Sci. Instrum.* **1985**, *56*, 283.
(244) Takahashi, S.; Ching, Y. C.; Wang, J.; Rousseau, D. L. *J. Biol. Chem.* **1995**, *270*, 8405.
(245) Takahashi, S.; Yeh, S.-R.; Das, T. K.; Chan, C.-K.; Gottfried, D. S.; Rousseau, D. L. *Nat. Struct. Biol.* **1997**, *4*, 44.
(246) Chan, C.-K.; Hu, Y.; Takahashi, S.; Rousseau, D. L.; Eaton, W. A.; Hofrichter, J. *Proc. Natl. Acad. Sci. U.S.A.* **1997**, *94*, 1779.
(247) Shasty, M.; Ramachandra, C.; Luck, S. D.; Roder, H. *Biophys. J.* **1998**, *74*, 2714.
(248) Knight, J. B.; Vishwanath, A.; Brady, J. P.; Austin, R. H. *Phys. Rev. Lett.* **1998**, *80*, 3863.
(249) Pollack, L.; Tate, M. W.; Darnton, N. C.; Knight, J. B.; Gruner, S. M.; Eaton, W. A.; Austin, R. H. *Proc. Natl. Acad. Sci. U.S.A.* **1999**, *86*, 10115.
(250) Hirai, M.; Kawai-Hirai, R.; Sanada, M.; Iwase, H.; Mitsuya, S. *J. Phys. Chem. B* **1999**, *103*, 9658.
(251) Dobashi, T.; Yeh, F.-J.; Ying, Q.; Ichikawa, K.; Chu, B. *Langmuir* **1995**, *11*, 4278.
(252) Wu, G.; Ying, Q.; Chu, B. *Macromolecules* **1994**, *27*, 5758.
(253) Wu, G.; Zhou, Z.; Chu, B. *J. Polym. Sci., Part B: Polym. Phys.* **1993**, *31*, 2035.
(254) Hirai, M.; Takizawa, T.; Yabuki, S.; Hirai, T.; Hayashi, K. *J. Phys. Chem.* **1995**, *99*, 17456.
(255) Gaponov, Y. A.; Karakchiev, L. G.; Lyakhov, N. Z.; Tolochko, B. P.; Lembke, U.; Bohlmann, K.; Dolbnya, I. P. *Nucl. Instrum. Methods Phys. Res., Sect. A* **1995**, *359*, 170.
(256) Vos, W. L.; Megens, M.; van Kats, C. M.; Boesecke, P. *J. Phys.: Condens. Matter* **1996**, *8*, 9503.
(257) Vos, W. L.; Megens, M.; van Kats, C. M.; Boesecke, P. *Langmuir* **1997**, *13*, 6004.
(258) Megens, M.; van Kats, C. M.; Boesecke, P.; Vos, W. L. *J. Appl. Crystallogr.* **1997**, *30*, 637.
(259) Megens, M.; van Kats, C. M.; Boesecke, P.; Vos, W. L. *Langmuir* **1997**, *13*, 6120.
(260) Diat, O.; Berret, I. F.; Porte, G. *Phys. Rev. B.* **1996**, *54*, 22.
(261) Nojima, S.; Kato, K.; Yamamoto, S.; Ashida, T. *Macromolecules* **1992**, *25*, 2237.
(262) de Moor, P.-P. E. A.; Beelen, T. P. M.; Komanschek, B. U.; Diat, O.; van Santen, R. A. *J. Phys. Chem. B* **1997**, *101*, 11077.
(263) Li, Y.; Gao, T.; Chu, B. *Macromolecules* **1992**, *25*, 1737.
(264) Jinnai, H.; Hashimoto, T.; Lee, D.; Chen, S.-H. *Macromolecules* **1997**, *30*, 130.
(265) Berk, N. F. *Phys. Rev. Lett.* **1987**, *58*, 2718.
(266) Chen, S. H.; Lee, D. D.; Chang, S. L. *J. Mol. Struct.* **1993**, *296*, 259.
(267) Cahn, J. W. *J. Chem. Phys.* **1965**, *42*, 93.
(268) Debye, P.; Anderson, H. R., Jr.; Brumberger, H. *J. Appl. Phys.* **1957**, *28*, 679.
(269) Hirai, T.; Okinaka, T.; Amemiya, Y.; Kobayahsi, K.; Hirai, M.; Hayashi, S. *Angew. Makromol. Chem.* **1996**, *240*, 213.
(270) Izumi, Y.; Takezawa, H.; Kikuta, N.; Uemura, S.; Tsutsumi, A. *Macromolecules* **1998**, *31*, 430.
(271) Liao, G.; Xie, Y.; Ludwig, K. F., Jr.; Bansil, R.; Gallagher, P. *Phys. Rev. E: Stat. Phys., Plasmas, Fluids, Relat. Interdiscip. Top.* **1999**, *60*, 4473.
(272) de Lange, R. S. A.; Hekkink, J. H. A.; Keizer, K.; Burggraaf, A. J. *J. Non-Cryst. Solids* **1995**, *191* (1, 2), 1.
(273) Izumi, Y.; Saito, S.; Soma, K. *Prog. Colloid Polym. Sci.* **1999**, *114* (Physical Chemistry and Industrial Application of Gellan Gum), 48.
(274) Vigild, M. E.; Almdal, K.; Mortensen, K.; Hamley, I. W.; Fairclough, J. P. A.; Ryan, A. J. *Macromolecules* **1998**, *31* (17), 5702.
(275) Zhou, S.; Yeh, F. J.; Burger, C.; Chu, B. *ACS Symp. Ser.* **2000**, *739* (Scattering from Polymers), 244.
(276) Tashiro, K.; Satkowski, M. M.; Stein, R. S.; Li, Y.; Chu, B.; Hsu, S. L. *Macromolecules* **1992**, *25* (6), 1809.
(277) Nojima, S.; Tsutsui, H.; Urushihara, M.; Kosaka, W.; Kato, N.; Ashida, T. *Polym. J.* **1986**, *18* (6), 451.
(278) Nojima, S.; Kato, K.; Ono, M.; Ashida, T. *Macromolecules* **1992**, *25* (7), 1922.
(279) Cheung, Y. W.; Stein, R. S.; Chu, B.; Wu, G. *Macromolecules* **1994**, *27* (13), 3589.
(280) Eersels, K. L. L.; Groeninckx, G.; Koch, M. H. J.; Reynaers, H. *Polymer* **1998**, *39* (17), 3893.
(281) Hsiao, B. S.; Verma, R. K.; Sauer, B. B. *J. Macromol. Sci., Phys.* **1998**, *B37* (3), 365.
(282) Wang, W.; Schultz, J. M.; Hsiao, B. S. *Mater. Res. Soc. Symp. Proc.* **1997**, *461* (Morphological Control in Multiphase Polymer Mixtures), 33.
(283) Liu, L.; Chu, B.; Penning, J. P.; Manley, R. *J. Macromol. Sci., Phys.* **1998**, *B37* (4), 485.
(284) Liu, L.; Chu, B.; Penning, J. P.; Manley, R. *Macromolecules* **1997**, *30* (15), 4398.
(285) Yeh, F.; Hsiao, B. S.; Chu, B.; Sauer, B. B.; Flexman, E. A. *J. Polym. Sci., Part B: Polym. Phys.* **1999**, *37* (21), 3115.
(286) Vandermarliere, M.; Groeninckx, G.; Reynaers, H.; Riekel, C.; Koch, M. H. J. *Morphol. Polym., Proc., Europhys. Conf. Macromol. Phys.* **1986**, 421.
(287) Wilkson, A. N.; Tattum, S. B.; Ryan, A. J. *Polymer* **1997**, *38* (8), 1923.
(288) Okamoto, Y.; Miyagi, H.; Uno, T.; Amemiya, Y. *Polym. Eng. Sci.* **1993**, *33* (24), 1606.
(289) Ying, Q.; Chu, B.; Wu, G.; Linliu, K.; Gao, T.; Nose, T.; Okada, M. *Macromolecules* **1993**, *26* (22), 5890.
(290) Chu, B.; Ying, Q.; Linliu, K.; Xie, P.; Gao, T.; Li, Y. *Polym. Mater. Sci. Eng.* **1991**, *65*, 209.
(291) Chu, B.; Ying, Q.; Linliu, K.; Xie, P.; Gao, T.; Li, Y.; Nose, T.; Okada, M. *Macromolecules* **1992**, *25* (26), 7382.
(292) Rabeony, M.; Shao, H.; Liang, K. S.; Siakali-Kioulafa, E.; Hadjichristidis, N. *Macromolecules* **1997**, *30* (23), 7332.
(293) Hsiao, B. S.; Gardner, K. H.; Wu, D. Q.; Chu, B. *Polymer* **1993**, *34*, 3986
(294) Hsiao, B. S.; Gardner, K. H.; Wu, D. Q.; Chu, B. *Polymer* **1993**, *34*, 3996
(295) Georgiev, G.; Dai, P. S.; Oyebode, E.; Cebe, P.; Capel, M. *NASA Conf. Publ.* **1999**, *209092*, 107.
(296) Fougnies, C.; Damman, P.; Villers, D.; Dosiere, M.; Koch, M. H. J. *Macromolecules* **1997**, *30* (5), 1385.
(297) Jonas, A. M.; Russell, T. P.; Yoon, D. Y. *Macromolecules* **1995**, *28* (25), 8491.
(298) Wang, J. et al. *Macromolecules* **1992**, *25*, 6943.
(299) Krüger, K. N.; Zachmann, H. G. *Macromolecules* **1993**, *26*, 5202.
(300) Hsiao, B. S.; Cheng S. Z. D.; Ho, R. M. *J. Polym. Sci. Polym. Phys.* **1995**, *33* (17), 2439.
(301) Wang, W.; Schultz, J. M.; Hsiao, B. S. *Macromolecules* **1997**, *30* (15), 4544.
(302) Ezquerra, T. A.; Liu, F.; Boyd, R. H.; Hsiao, B. S. *Polymer* **1997**, *38* (23), 5793.
(303) Hsiao, B. S.; Sauer, B. B.; Verma, R. K.; Zachmann, H. G.; Seifert, S.; Chu, B.; Harney, P. *Macromolecules* **1995**, *28* (20), 6931.
(304) Rueda, D. R.; Garcia Gutierrez, M. C.; Ania, F.; Zolotukhin, M. G.; Calleja, F. J. Balta. *Macromolecules* **1998**, *31* (23), 8201.
(305) Brandom, D. K.; Wilkes, G. L. *Polymer* **1994**, *35* (26), 5672.
(306) Liu, J.; Cheng, S. Z. D.; Harris, F. W.; Hsiao B. S.; Gardner, K. H. *Macromolecules* **1994**, *27*, 989.
(307) Jonas, A. M.; Russell, T. P.; Yoon, D. Y. *Colloid Polym. Sci.* **1994**, *272* (11), 1344.
(308) Zachmann, H. G.; Wiswe, D.; Gehrke, R.; Riekel, C. *Makromol. Chem. Suppl.* **1985**, *12*, 175.
(309) Wu, W. L.; Zachmann, H. G.; Rickel, C. *Polym. Commun.* **1984**, *25* (3), 76.
(310) Wang, Z. G.; Hsiao, B. S.; Sauer, B. B.; Kampert, W. G. *Polymer* **1999**, *40*, 4615.
(311) Wang, Z. G.; Hsiao, B. S.; Fu, B. X.; Liu, L.; Yeh, F.; White, H.; Sauer, B. B.; Chang, H.; Schultz, J. M. *Polymer* **1999**, *41*, 1791.
(312) Sauer, B. B.; Hsiao, B. S.; Wang, Z.-G. *Polym. Mater. Sci. Eng.* **1999**, 266.
(313) Lee, C. H.; Saito, H.; Inoue, T.; Nojima, S. *Macromolecules* **1996**, *29* (22), 7034.
(314) Fronk, W.; Heise, B.; Neppert, B.; Schubach, H. R.; Wilke, W. *Colloid Polym. Sci.* **1984**, *262* (2), 99.
(315) Hsiao, B. S.; Wang, Z. G.; Yeh, F. J.; Gao, Y.; Sheth, K. *Polymer* **1999**, *40*, 3515.
(316) Bark, M.; Zachmann, H. G. *Acta Polym.* **1993**, *44* (6), 259.
(317) Mathot, V. B. F.; Scherrenberg, R. L.; Pijpers, M. F. J.; Bras, W. *J. Therm. Anal.* **1996**, *46* (3−4), 681.
(318) Akpalu, Y.; Kielhorn, L.; Hsiao, B. S.; Stein, R. S.; Russell, T. P.; van Egmond, J.; Muthukumar, M. *Macromolecules* **1999**, *32* (3), 765.
(319) Akpalu, Y. A.; Amis, E. J. *J. Chem. Phys.* **1999**, *111* (18), 8686.
(320) Liu, W.; Kim, S.; Lopez, J.; Hsiao, B.; Keating, M. Y.; Lee, I.-H.; Landes, B.; Stein, R. S. *J. Therm. Anal. Calorim.* **2000**, *59* (1−2), 245.
(321) Goderis, B.; Mathot, V. B. F.; Reynaers, H. *Polym. Mater. Sci. Eng.* **1999**, *81*, 344.
(322) Liu, W.; Hsiao, B. S.; Stein, R. S. *Polym. Mater. Sci. Eng.* **1999**, 267.
(323) Chiu, F. C.; Fu, Q.; Leland, M.; Cheng, S. Z. D.; Hsieh, E. T.; Tso, C. C.; Hsiao, B. S. *J. Macromol. Sci., Phys.* **1997**, *B36* (5), 553.

(324) Wang, Z. G.; Hsiao, B. S.; Lopez, J.; Armistead, J. P. *J. Polym. Res.***1999**, *6* (3), 1.
(325) Wang, Z. G.; Hsiao, B. S.; Zong, X.; Yeh, F.; Zhou, J.; Dormier, E. *Polymer* **2000**, *41* (2), 621.
(326) Zong, X. H.; Wang, Z. G.; Hsiao, B. S.; Chu, B.; Zhou, J. J.; Dormier, E.; Jamiolkowski, D. D. *Macromolecules* **1999**, *32*, 8107.
(327) Cheng, S. Z. D.; Wu, S. S.; Chen, J.; Zhuo, Q.; Quirk, R. P.; Von Meewall, E. D.; Hsiao, B. S.; Habenschuss, A.; Zschack, P. R. *Macromolecules* **1993**, *26*, 5105.
(328) Lee, S.; Chen, E.; Zhang, A.; Yoon, Y.; Moon, B. S.; Lee, S.; Harris, F. W.; Cheng, S. Z. D.; von Meerwall, E. D.; Hsiao, B. S.; Verma, R.; Lando, J. B. *Macromolecules* **1996**, *29* (27), 8816.
(329) Chen, E. Q.; Lee, S.-W.; Zhang, A. Q.; Moon, B. S.; Honigfort, P. S.; Mann, I.; Lin, H. M.; Harris, F. W.; Cheng, S. Z. D.; Hsiao, B. S.; Yeh, F. *Polymer* **1999**, *40* (16), 4543.
(330) Chen, E. Q.; Lee, S. W.; Zhang, A.; Moon, B. S.; Mann, I.; Harris, F. W.; Cheng, S. Z. D.; Hsiao, B. S.; Yeh, F.; Von Merrewell, E.; Grubb, D. T. *Macromolecules* **1999**, *32* (15), 4784.
(331) Zhu, L.; Chen, Y.; Zhang, A.; Calhoun, B. H.; Chun, M.; Quirk, R. P.; Cheng, S. Z. D.; Hsiao, B. S.; Yeh, F.; Hashimoto, T. *Phys. Rev. B: Condens. Matter Mater. Phys.* **1999**, *60* (14), 10022.
(332) Chen, E. Q.; Lee, S. W.; Zhang, A.; Moon, B. S.; Mann, I.; Harris, F. W.; Cheng, S. Z. D.; Hsiao, B. S.; Yeh, F.; Von Meerwall, E. D. *ACS Symp. Ser.* **2000**, *739* (Scattering from Polymers), 118.
(333) Fu, Q.; Livengood, B. P.; Shen, C. C.; Lin, F.; Harris, F. W.; Cheng, S. Z. D.; Hsiao, B. S.; Yeh, F. *Macromol. Chem. Phys.* **1998**, *199*, 1107.
(334) Fu, Q.; Livengood, B. P.; Shen, C. C.; Lin, F. L.; Li, W.; Harris, F.; Cheng, S. Z. D.; Hsiao, B. S. *J. Polym. Res.* **1997**, *4* (1), 1.
(335) Wang, Z. G.; Murthy, N. S.; Hsiao, B. S. *J. Appl. Crystallogr.* **2000**, *33* (3), 690.
(336) Ruland, W. *Colloid Polym. Sci.* **1977**, *255*, 417.
(337) Vonk, C. G.; Kortleve, G. *Colloid Polym. Sci.* **1967**, *220*, 19.
(338) Strobl, G. R.; Schneider, M. J. *Polym. Sc., Polym. Phys. Ed.* **1980**, *18*, 1343.
(339) Koberstein, J. T.; Morra, B.; Stein, R. S. *J. Appl. Crystallogr.* **1980**, *13*, 34.
(340) Hsiao, B. S.; Verma, R. K. *J. Synchrotron Radiat.* **1998**, *5* (1), 23.
(341) Zachmann, H. G.; Schmidt, G. F. *Makromol. Chem.* **1962**, *52*, 23.
(342) Keller, A. IUPAC Int. Symp. Macromol. Proc. Florence, Italy, 1980, p 135.
(343) Fischer, E. W.; Schmidt, G. F. *Angew. Chem.* **1962**, *74*, 551.
(344) Imai, M.; Kaji, K.; Kanaya, T. *Macromolecules* **1994**, *27* (24), 7103.
(345) Imai, M.; Kaji, K.; Kanaya, T. *Phys. Rev. Lett.* **1993**, *71* (25), 4162.
(346) Imai, M.; Mori, K.; Mizukami, T.; Kaji, K.; Kanaya, T. *Polymer* **1992**, *33* (21), 4457.
(347) Imai, M.; Mori, K.; Mizukami, T.; Kaji, K.; Kanaya, T. *Polymer* **1992**, *33* (21), 4451.
(348) Ezquerra, T. A.; López-Cabarcos, E.; Hsiao, B. S.; Baltà-Calleja, F. J. *Phys. Rev. E.* **1996**, *54*, 989.
(349) Ryan, A. J.; Terrill, N. J.; Fairclough, P. A. *ACS Symp. Ser.* **2000**, *739* (Scattering from Polymers), 201.
(350) Ryan, A. J.; Fairclough, P. A.; Terrill, N. J.; Olmsted, P. D.; Poon, W. C. K. *Faraday Discuss.* **1999**, *112*, 13.
(351) Olmsted, P. D.; Poon, W. C. K.; McLeish, T. C. B.; Terrill, N. J.; Ryan, A. J. *Phys. Rev. Lett.* **1998**, *81* (2), 373.
(352) Wang, Z. G.; Hsiao, B. S.; Sirota, E. B.; Agarwal, P.; Srinivas, S. *Macromolecules* **2000**, *33* (3), 978.
(353) Wang, Z. G.; Hsiao, B. S.; Sirota, E. B.; Srinivas, S. *Polymer* **2000**, *41* (25), 8825.
(354) Ryan, A. J.; Li, W.; Heeley, E. *Polym. Prepr. (Am. Chem. Soc., Div. Polym. Chem.)* **1999**, 429.
(355) Elwell, M. J.; Ryan, A. J.; Grunbauer, H. J. M.; Van Lieshout, H. C. *Polym. Prepr. (Am. Chem. Soc., Div. Polym. Chem.)* **1996**, *37* (2), 769.
(356) Wilkinson, A. N.; Naylor, S.; Elwell, M. J.; Draper, P.; Komanschek, B. U.; Stanford, J. L.; Ryan, A. J. *Polymer* **1996**, *37* (10), 2021.
(357) Elwell, M. J.; Ryan, A. J.; Gruenbauer, H. J. M.; Van Lieshout, H. C. *Macromolecules* **1996**, *29* (8), 2960.
(358) Ryan, A. J.; Willkomm, W. R.; Bergstrom, T. B.; Macosko, C. W.; Koberstein, J. T.; Yu, C. C.; Russell, T. P. *Macromolecules* **1991**, *24* (10), 2883.
(359) Winans, R. E.; Seifert, S.; Thiyagarajan, P. *Prepr. Symp.−Am. Chem. Soc., Div. Fuel Chem.* **1999**, *44* (3), 576.
(360) Lyakhov, N.; Gaponov, Yu.; Tolochko, B. *Solid State Ionics* **1997**, *101−103* (Pt.2), 1251.
(361) Ogasawara, T.; Izawa, K.; Hattori, N.; Okabayashi, H.; O'Connor, C. J. *Colloid Polym. Sci.* **2000**, *278* (4), 293.
(362) Vaia, R. A.; Lincoln, D.; Wang, Z. G.; Hsiao, B. S.; Krishnamoorti, R. *Polym. Mater. Sci. Eng.* **2000**, *82*, 257.
(363) Barber, G. D.; Carter, C. M.; Moore, R. B. *Annu. Technol. Conf.−Soc. Plast. Eng.* **2000**, *58* (3), 3763.
(364) Chaker, J. A.; Dahmouche, K.; Craievich, A. F.; Santilli, C. V.; Pulcinelli, S. H. *J. Appl. Crystallogr.* **2000**, *33* (3, Pt. 1), 700.
(365) Becker, C.; Kutsch, B.; Krug, H.; Kaddami, H. J. *Sol−Gel Sci. Technol.* **1998**, *13* (1/2/3), 499.
(366) Tan, N. C. Beck; Balogh, L.; Trevino, S. F.; Tomalia, D. A.; Lin, J. S. *Mater. Res. Soc. Symp. Proc.* **1998**, *519* (Organic/Inorganic Hybrid Materials), 143.
(367) Somani, R. H.; Hsiao, B. S.; Stein, R. S. *Physica*, 2001, in press.
(368) Nogales, A.; Hsiao, B. S.; Somani, R. H.; Srinivas, S.; Tsou, A. H.; Balta-Calleja, F. J.; Ezquerra, T. A. *Polymer* **2001**, *42*(12), 5247.
(369) Burghardt, Wesley R.; Ugaz, Victor M.; Cinader, David K., Jr. *ACS Symp. Ser.* **2000**, *739* (Scattering from Polymers), 374.
(370) Cinader, D. K., Jr.; Burghardt, W. R. *J. Polym. Sci., Part B: Polym. Phys.* **1999**, *37* (24), 3411.
(371) Cinader, D. K., Jr.; Burghardt, W. R. *Polymer* **1999**, *40* (15), 4169.
(372) Ugaz, V. M.; Burghardt, W. R. *Macromolecules* **1998**, *31* (24), 8474.
(373) Ugaz, V. M.; Cinader, D. K., Jr.; Burghardt, W. R. *J. Rheol.* **1998**, *42* (2), 379.
(374) Hsiao, B. S.; Leach, R. A.; Kennedy, A. D.; Gardner, K. H.; Gochanour, C.; Biswas, A.; Seifert, S.; Zachmann, H. G. *Polym. Prepr. (Am. Chem. Soc., Div. Polym. Chem.)* **1995**, *36* (1), 321.
(375) Lee, H. S.; Yoo, S. R.; Seo, S. W.n. *J. Polym. Sci., Part B: Polym. Phys.* **1999**, *37* (22), 3233.
(376) Stribeck, N. J. *Polym. Sci., Part B: Polym. Phys.* **1999**, *37* (10), 975.
(377) Stribeck, N.; Fakirov, S.; Sapoundjieva, D. *Macromolecules* **1999**, *32* (10), 3368.
(378) Stribeck, N.; Sapoundjieva, D.; Denchev, Z.; Apostolov, A. A.; Zachmann, H. G.; Stamm, M.; Fakirov, S. *Macromolecules* **1997**, *30* (5), 1329.
(379) Salomons, G. J.; Singh, M. A.; Hiltz, L. G.; Pan, L. H.; Newson, W. R. *Nucl. Instrum. Methods Phys. Res., Sect. B* **1995**, *97* (1−4), 282.
(380) Mills, P. J.; Kramer, E. J.; Brown, H. R. *J. Mater. Sci.* **1985**, *20* (12), 4413.

CR9900376